LUND UNIVERSITY

Time-dependent crack growth and fracture in concrete

Zhou, Fan Ping

1992

[Link to publication]

Total number of authors:
1

Time-dependent Crack Growth

and Fracture in Concrete

Fan Ping Zhou

Time-dependent Crack Growth

and Fracture in Concrete

Fan Ping Zhou

tekn lic

AKADEMISK AVHANDLING

som för avläggande av teknisk doktorsexamen
vid tekniska fakulteten vid Lunds Universitet
kommer att offentligen försvaras vid sektionen
för väg- och vattenbyggnad, John Ericssons väg 1, hörsal V:C,
fredagen den 27 mars 1992, kl 10.15.

Title and subtitle

Time-dependent Crack Growth and Fracture in Concrete

Abstract

The objectives of this thesis are to study time-dependent fracture behaviour in concrete. The thesis consists of an experimental study, constitutive modelling and numerical analysis.

The experimental study was undertaken to investigate the influences of time on material properties for the fracture process zone and on crack growth and fracture in plain concrete structures. The experiments include tensile relaxation tests, bending tests on notched beams to determine fracture energy at varying deflection rates, and sustained bending and compact tensile tests. From the tensile relaxation tests, the envelope of the σ-w relation does not seem to be influenced by holding periods, though some local detrimental effect does occur. Fracture energy seems to decrease as rates become slower. In the sustained loading tests, deformation (deflection or CMOD) growth curves display three stages, as usually observed in a creep rupture test. The secondary stage dominates the whole failure lifetime, and the secondary deformation rate appears to have a good correlation with the failure lifetime.

A crack model for time-dependent fracture is proposed, by applying the idea of the Fictitious Crack Model. In this model, a modified Maxwell model is introduced for the fracture process zone incorporated with the static σ-w curve as a failure criterion, based on the observation of the tensile relaxation tests. The time-dependent σ-w curve is expressed in an incremental law.

The proposed model has been implemented in a finite element program and applied to simulating sustained flexural and compact tensile tests. Numerical analysis includes simulations of crack growth, load-CMOD curves, stress-failure lifetime curves, size effects on failure life etc. The numerical results indicate that the model seems to be able to properly predict the main features of time-dependent fracture behaviour in concrete, as compared with the experimental results.

Key words　　concrete, crack model, creep, creep crack growth, creep rupture, Fictitious Crack Model, finite element method, fracture mechanics, rupture test, sustained loading, tensile fracture, time-dependent fracture, visco-elastic fracture.

Classification system and/or index terms (if any)

Distribution by (name and address)

　　Division of Building Materials, Lund Institute of technology, Box 118, S-221 00 LUND, Sweden

Signature _____Fan Ping Zhou_____　　　　Date _____January 20, 1992_____

Time-dependent Crack Growth

and Fracture in Concrete

Fan Ping Zhou

Acknowledgements

Abstract

The objectives of this thesis are to study time-dependent fracture behaviour in concrete. The thesis consists of an experimental study, constitutive modelling and numerical analysis.

The experimental study was undertaken to investigate the influences of time on material properties for the fracture process zone and on crack growth and fracture in plain concrete structures. The experiments include tensile relaxation tests, bending tests on notched beams to determine fracture energy at varying deflection rates, and sustained bending and compact tensile tests. From the tensile relaxation tests, the envelope of the σ-w relation does not seem to be influenced by holding periods, though some local detrimental effect does occur. Fracture energy seems to decrease as rates become slower. In the sustained loading tests, deformation (deflection or CMOD) growth curves display three stages, as usually observed in a creep rupture test. The secondary stage dominates the whole failure lifetime, and the secondary deformation rate appears to have a good correlation with the failure lifetime.

A crack model for time-dependent fracture is proposed, by applying the idea of the Fictitious Crack Model. In this model, a modified Maxwell model is introduced for the fracture process zone incorporated with the static σ-w curve as a failure criterion, based on the observation of the tensile relaxation tests. The time-dependent σ-w curve is expressed in an incremental law.

The proposed model has been implemented in a finite element program and applied to simulating sustained flexural and compact tensile tests. Numerical analysis includes simulations of crack growth, load-CMOD curves, stress-failure lifetime curves, size effects on failure life etc. The numerical results indicate that the model seems to be able to properly predict the main features of time-dependent fracture behaviour in concrete, as compared with the experimental results.

Keywords: concrete, crack model, creep, creep crack growth, creep rupture, Fictitious Crack Model, finite element method, fracture mechanics, rupture test, sustained loading, tensile fracture, time-dependent fracture, visco-elastic fracture.

Table of Contents

NOTATIONS

Notations and symbols are explained in the text when they first appear. The main notations are listed below.

Latin letters

a	crack length
a_c	critical crack length
a_f	total crack length (= real + fictitious crack length)
b	thickness, width
c	crack mouth opening displacement (CMOD)
CMOD	crack mouth opening displacement
COD	crack tip opening displacement (CTOD)
d	depth, height
E	modulus of elasticity
f_c	compressive strength
f_f	flexural strength
f_{net}	net flexural strength
f_t	tensile strength
FCM	Fictitious Crack Model
g	gravity acceleration (9.8 Kgm/s^2)
G_c	fracture toughness
G_F	fracture energy
h	height
K	stress intensity factor
K_T	tangential stiffness matrix
l_{ch}	characteristic length ($=EG_F/f_t^2$)
L	length
LEFM	linear elastic fracture mechanics

m	mass
max	maximum
Min	minute
min	minimum
P	load
R	relaxation
S	span
s	second
t	time
t_{cr}	failure lifetime in rupture tests
u	deflection
U	potential energy
w	deformation in fracture zone
W	depth
Y	geometry factor

Greek letters

σ	stress
σ_{net}	net section stress
α	relaxation limit constant
τ	relaxation time
ϵ	strain
δ	crack tip opening displacement

Others

.	time differential
I, II, III	basic modes of crack extension

Chapter 1
Introduction

1.1 Background

Cracking appears to be inevitable even in reinforced concrete structures. Due to the low tensile strain capacity of concrete, cracks may readily be initiated by structural deformations, shrinkage, thermal strains and so on. As the need for structures such as marine and nuclear facilities is rapidly growing, a thorough understanding of various failure mechanisms including tensile cracking is crucial to ensure safe and economic designs. Furthermore, crack problems can be of great concern from the aspect of durability.

Application of fracture mechanics to concrete can be traced back to Kaplan (1961). However, classic fracture mechanics, developed mainly from metals, yields quite controversial results when applied to concrete. Because the fracture process zone in front of crack tip developed in a labortary-size concrete specimen is too large. In 1976, Hillerborg, Modeer and Petersson proposed the well-known Fictitious Crack Model (FCM). The model proved to be very consistent with experiments and aroused world-wide interests. Since then, intensive fracture mechanics studies have been producing quite a few fruitful results.

Fracture mechanics studies indicate that structural behaviour depends not only on strength, but also on fracture resistance, and dimension of structures as well. Observed size effects of plain or lightly reinforced concrete structures under bending, shear and torsion confirm theoretical predictions. Similar concepts may be applied to compressive

1

fracture behaviour of high-strength concrete, as a pronounced strain softening has also been observed (Hillerborg, 1989b).

What are the possible practical applications? On one hand, based on theoretical results, it leads to more rational designs than those based on empirical rules. On the other hand, fracture mechanics may serve as a good tool for choosing or improving material to meet various practical needs.

Up to now, attention has mainly been focused on quasi-static fracture problems. In practice, concrete structures might be imposed to both sustained and fatigue loading, and simultaneously against wetting-drying, freezing-thawing etc. Thus time-dependent crack models are necessary in order to lead to more accurate predictions.

1.2 Aim and Scope

The main objectives of this thesis are to study time-dependent fracture behaviour in concrete. The present work includes an experimental study, constitutive modelling and numerical analysis.

The experimental work aims at investigating time effects on the material properties (the σ-w relation and G_F) for the fracture zone and time-dependent fracture behaviour of various concrete specimens subjected to sustained loading.

Based on the experimental observations on tensile relaxation tests, a crack model is proposed for time-dependent fracture by applying the similar idea of the Fictitious Crack Model. In this model, an incremental time-dependent stress-deformation law is employed for describing the behaviour in the fracture zone.

The proposed model is implemented in a finite element program. The Numerical analysis involves simulations of crack growth, creep deformation curve, stress-failure lifetime relation etc. in sustained loading tests.

In the present work, only the time-dependency in the fracture zone is considered while the material behaviour outside the zone is assumed to be time-independent.

1.3 Outline of Contents

Chapter 2 gives a brief overview of fracture mechanics and its application to concrete, especially the Fictitious Crack Model.

Chapter 3 presents a literature review of the influences of time on material parameters and fracture behaviour of concrete. Applications of linear elastic fracture mechanics to describe the time-dependent crack growth and fracture are also discussed.

Chapter 4 describes the experimental work conducted to determine time-dependency of material parameters as well as to investigate creep crack growth and failure behaviour where tensile fracture is relevant.

Chapter 5 presents a model for the analysis of creep crack growth and fracture of concrete by extending the ideas of FCM.

Chapter 6 presents the theoretical predictions of time-dependent fracture. Comparisons with the test results in Chapter 4 are also made.

The concluding remarks are given in Chapter 7.

Chapter 2
Fracture Mechanics Applied to Concrete

2.1 Introduction

The theory of conventional fracture mechanics has mainly been established from studies of metals. During the past two decades, fracture mechanics has been applied to concrete. Thus some basic parameters will be introduced in the first two sections.

The Fictitious Crack Model (FCM) has been successfully used to describe tensile stress-induced fracture behaviour in non-yielding materials like concrete, rock etc. The principle and its applications of the model will be reviewed.

Fracture modes can be divided into mode I, II and III, which are referred to as opening mode, sliding mode and tearing mode respectively. The present study in the thesis mainly concerns fracture of mode I.

2.2 Linear Elastic Fracture Mechanics (LEFM)

2.2.1 Stress intensity factor

In an infinitely large plate of linear elastic solid, Irwin (1958) showed that the stress field at the tip of a crack is characterised by a singularity of the stresses. The stresses are proportional to the inverse square root of the distance from the tip. The singular stress field (Fig. 2.1) can be expressed as:

$$\sigma_{xx} = \frac{K_I}{\sqrt{2\pi r}} \cos\frac{\theta}{2}\left(1 - \sin\frac{\theta}{2}\sin\frac{3\theta}{2}\right) + ...$$

$$\sigma_{yy} = \frac{K_I}{\sqrt{2\pi r}} \cos\frac{\theta}{2}\left(1 + \sin\frac{\theta}{2}\sin\frac{3\theta}{2}\right) + ... \qquad (2.1)$$

$$\tau_{xy} = \frac{K_I}{\sqrt{2\pi r}} \cos\frac{\theta}{2}\sin\frac{\theta}{2}\cos\frac{3\theta}{2} + ...$$
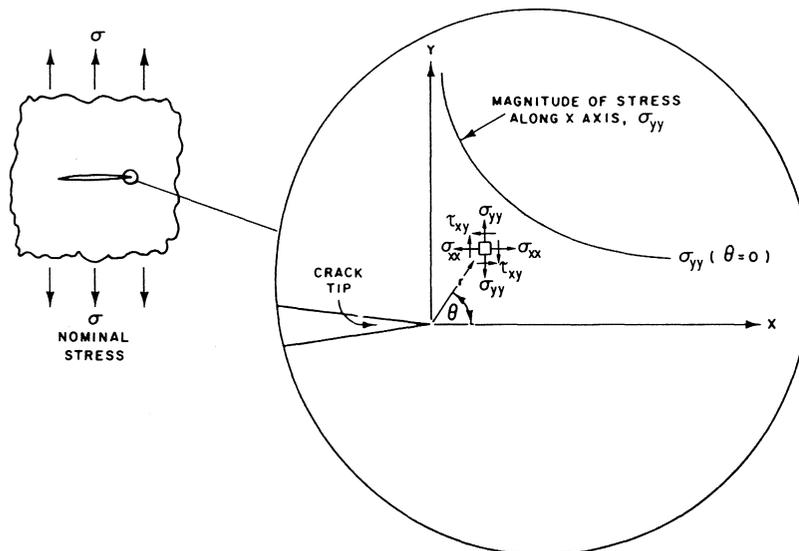
Fig. 2.1 Stress field near crack tip

K_I in the equations above is the so-called stress intensity factor for mode I. K_I can be calculated from the following equation:

$$K_I = Y\sigma\sqrt{\pi a} \qquad (2.2)$$

where σ is usually taken to be the nominal stress if the crack does not exist, and Y is geometry factor.

Since K_I provides a measure of the severity of the crack tip environment, it is logical to characterise the resistance of a material to fracture by the critical value, K_{Ic}. K_{Ic} is called fracture toughness. If the fracture toughness K_{Ic} of a material is know, the critical stress σ_c or crack length a_c can be obtained from the following relationship:

$$\sigma_c\sqrt{a_c} = \frac{K_{Ic}}{Y\sqrt{\pi}} \qquad (2.3)$$

2.2.2 Energy release rate

The original work was carried out by Griffith (1921). The basic idea is that crack growth can occur if the energy required to form a crack increment da can be delivered by the system. The criterion may be expressed as:

$$G_I \equiv -\frac{1}{B}\frac{dU}{da} = G_{Ic} \qquad (2.4)$$

where G_I is the energy release rate, or the crack extension force, U is potential energy, B is thickness, a is crack length, and G_{Ic} stands for the crack resistance.

The energy release rate can be related to the stress intensity by the following:

$$G_I = \frac{K_I^2}{E^*} \qquad (2.5)$$

where $E^* = E$ for plane stress; $= E/(1+v)$ for plane strain.

2.3 Non-linear Fracture Mechanics

2.3.1 J-integral

In analyzing elastic-plastic failure, a widely used approach is the J-integral proposed by Rice (1968). It can be formally expressed as follows:

$$J = \int_{\Gamma} (W dy - T_i \frac{\partial u}{\partial x} ds) \tag{2.6}$$

where W is strain energy density, u_i is the displacement vector, T_i the vector traction and ds an increment along the integral path (Fig. 2.2).
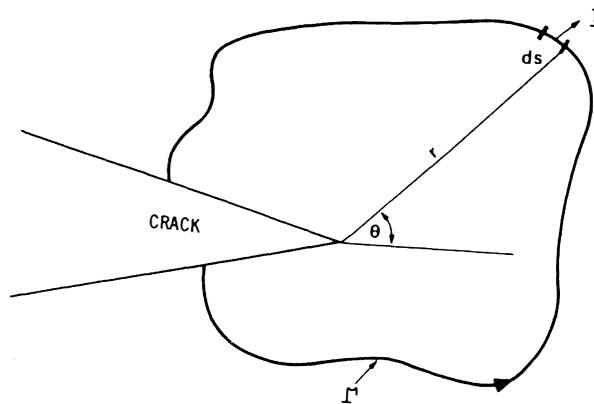
Fig. 2.2 J-integral evaluation path

Strictly speaking, the path independency of the J-integral holds only for linear and non-linear elastic materials where unloading occurs along the same curve as the initial loading. However, it can be approximately applied to elastic-plastic fracture problems provided that no intensive unloading occurs. This may be the reason why the J-integral has been successfully used in elastic-plastic materials.

It is found that when crack growth occurs, the J-integral approaches a critical value which is a material parameter. Thus it is possible to define the initiation of crack

growth as

$$J=J_c \tag{2.7}$$

For linear and non-linear elastic materials, the J-integral can be shown to be equal to G_I, the strain energy release rate. It can be related to the stress intensity factor in mode I by:

$$J=G_I=\frac{K_I^2}{E^*} \tag{2.8}$$

2.3.2 Crack opening displacement (COD)

Another powerful parameter in elastic-plastic fracture mechanics is the crack tip opening displacement (COD), δ. Experimental observations have indicated that there is a critical value δ_c, which can serve as a criterion for crack growth. It can be shown that, for ideal plastic materials, δ_c can be related to J_c by:

$$\delta_c=\frac{J_c}{\sigma_y} \tag{2.9}$$

where σ_y is the yield strength.

2.3.3 Crack models including plastic zone

For an elastic-ideal plastic material, the stress cannot exceed the yield strength σ_y. Thus a plastic zone must exist in front of the crack tip. Irwin estimated the size of the plastic zone (Fig. 2.3) to be $2r_y$ according to

$$2r_y=\frac{1}{\pi}\left(\frac{K_I}{\sigma_y}\right)^2 \tag{2.10}$$
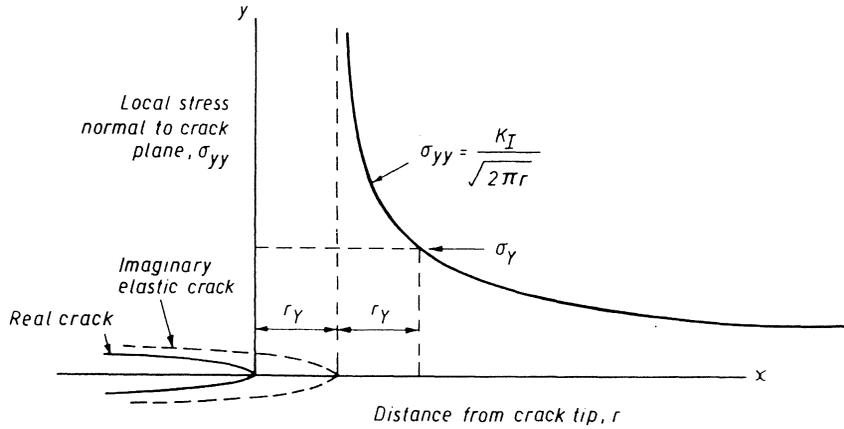
Fig. 2.3 Irwin's imaginary elastic crack and assumed stress field

The analysis can only be applied to a highly localized plastic zone, when the nominal stress σ is much smaller than the yield strength σ_y in small-scale yielding problems. The effective fracture toughness can be calculated from Eq. 2.2 by replacing a with $a+r_y$.

In studying crack problems in a thin sheet of milt steel, Dugdale (1960) set up a model including a plastic zone in front of the crack tip (Fig 2.4). The stresses in this zone should be equal to the yield strength for an elastic-ideal plastic material.
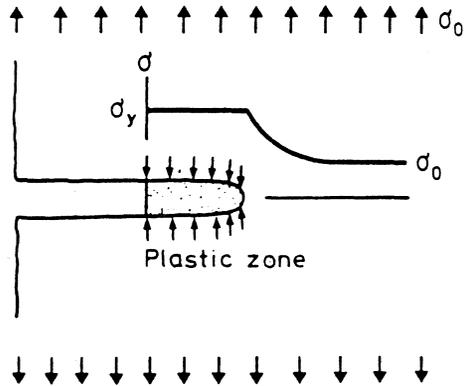
Fig. 2.4 The Dugdale model

2.4 Fracture Mechanics of Concrete

Unlike steel, concrete does not exhibit significant plastic deformations. It seemed that linear elastic fracture mechanics might be readily applicable. However, fracture parameters such as K_c and G_c determined in accordance with LEFM seem to depend on sizes and geometries. Some other approaches such as J_c, critical COD etc. are also found to be of limited use.

According to the stress-strain state, it is possible to define three different zones as linear elastic zone, nonlinear hardening zone and fracture process zone around the crack tip. In the fracture process zone, strain softening takes place. Fig 2.5 illustrates relative sizes of those three zones in brittle materials, metals and concrete.

Brittle materials   Metals   Concrete
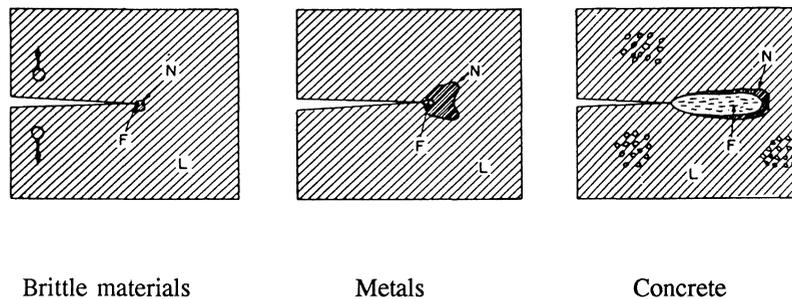
Fig. 2.5 Relative sizes of fracture process zone (F), nonlinear hardening zone (N) and linear elastic zone (L) in different types of materials (Bazant & Oh, 1983)

The fracture process zone in concrete is relatively large so that LEFM cannot be applied to fracture of laboratory-size specimens. Strain softening in the fracture zone results in unloading around the tip. This may be the reason why the J-integral cannot be used either.

Based on tension fracture behaviour, Hillerborg, Modeer & Petersson (1976) proposed the Fictitious Crack Model, which is similar to the Dugdale model. Bazant & Oh (1983) proposed the Crack Band Model. Those models are sometimes referred to as cohesive models, or fracture process models, in the literature.

Another approach to tackling fracture problems in concrete is to modify the linear elastic fracture mechanics by using effective crack length (or equivalent crack length) concept. The Two-Parameter Model (TPM) by Jeng and Shah (1985b) and the Effective Crack Model (ECM) by Karihaloo & Nallathambi (1989a) belong to this category.

Many other models have been introduced to describe fracture of concrete. An evaluation of various models can be found in the article by Elices and Planas (1989). In the following section only the Fictitious Crack Model will be described.

2.5 The Fictitious Crack Model

2.5.1 Principle

In the model, the concept of fictitious crack, introduced into the fracture zone in front of crack tip, is based on the description of fracture behaviour in direct tension tests. A typical tension test is illustrated in Fig 2.6. The complete stress-deformation curve consists of an ascending and a descending part, if a deformation-controlled tensile test is properly performed. Stresses and deformations are uniformly distributed along the length of the specimen before the peak point in the curve. When the peak point is passed, a localized fracture zone starts to develop. The load the specimen can bear will decrease with increasing deformation in the zone. At last the specimen is broken into two halves along the zone. Therefore, it is impossible to find a unified stress-strain relation to describe the whole development in the tension test. In the fracture zone, a softening (σ-w) relation must be used while the rest part can be still described by a stress-strain (σ-ϵ) relation.
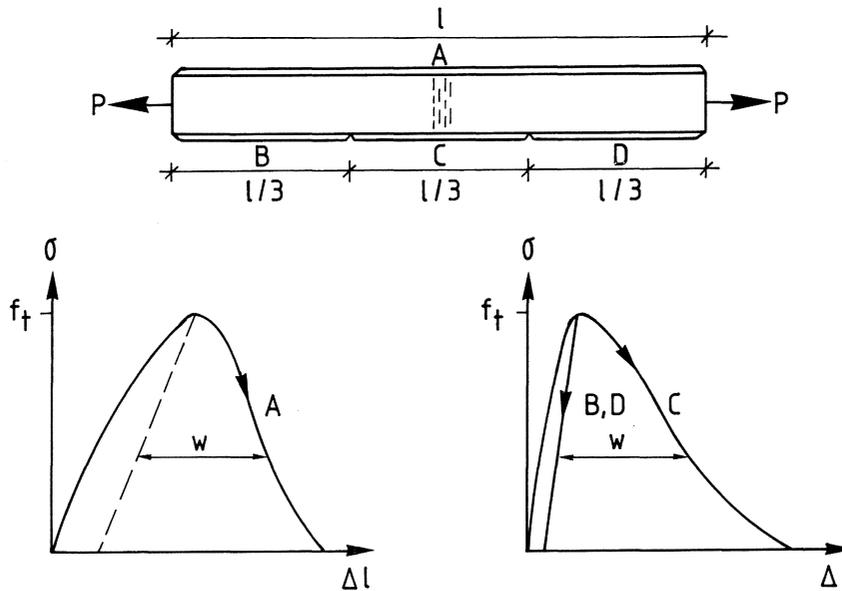
Fig. 2.6 Deformation behaviour in tension (Hillerborg, 1986)

The fracture zone is concentrated within a very thin band. Therefore it may well be represented by a crack which is able to transfer stress. Of course such a crack is not a real crack but a fictitious crack, and it will not develop into a real one until the opening of the fictitious crack reaches a critical value.

The same idea may be applied to modelling the fracture zone in a general stress state. The fictitious crack is assumed to initiate at the point where the maximum principal stress reaches the tensile strength. The stress-deformation curve can be assumed to be a material property provided that the minimum principal stresses are much smaller than the compressive strength. No shear stress is assumed to occur in the fracture zone, as only fracture in Mode I is involved.

2.5.2 Material parameters

The Fictitious Crack Model is described by means of a stress-strain (σ-ϵ) law and a stress-deformation (σ-w) law.

The stress-strain curve for ordinary concrete can well be approximated to be a straight line. The curve can be determined solely by the tensile strength f_t and modulus of elasticity E. Of course a more realistic, non-linear relation might also be used in this model.

The stress-deformation relation is usually simplified as a linear, bilinear or multi-linear curve. Since the shape of this relation is well-known and quite similar for concrete materials, the relation can be determined if tensile strength f_t and fracture energy G_F are known.

Therefore material properties in the FCM model can be represented by tensile strength f_t, modulus of elasticity E and fracture energy G_F. Another useful parameter is characteristic length, a ratio between G_F/f_t and f_t/E:

$$l_{ch} = \frac{EG_F}{f_t^2} \qquad (2.11)$$

It may also be interpreted as the ratio between fracture energy per unit area G_F and strain energy density at failure f_t^2/E. l_{ch} can be regarded as a measure of material brittleness and is probably related to the size of the fracture zone.

It should be pointed out that the shape of the σ-w curve is also very important. As already shown by Modeer (1979) and Petersson (1981), the initial slope of the curve can greatly influence fracture behaviour, even if G_F and f_t are the same. Therefore, if two materials with σ-w curves of quite different shapes are involved, the slope must be taken into account. However, no proper parameter used to measure the effect is available.

The σ-ϵ curve and the σ-w curve may be determined directly from uniaxial tensile tests. However, it usually requires very sophisticated testing machines and arrangements. In addition, proper sizes of specimens must be chosen in order to obtain the real material parameters. Therefore the two curves are often determined indirectly from f_t, E and G_F as the shapes of the curves are known. f_t can be determined from a simple tension test. E can be determined from dynamic method. Fracture energy G_F can be determined from three-point bending tests on notched beams according to the RILEM recommendation (1985) (Fig. 2.7). It can be evaluated using the following formula:

$$G_F = \frac{A_1 + A_2 + A_3}{b(h-a)} = \frac{A_1 + mg\delta_0}{b(h-a)} \tag{2.12}$$

where m is mass of beam and g gravity acceleration. A_1 and δ_0 are shown in Fig. 2.7.
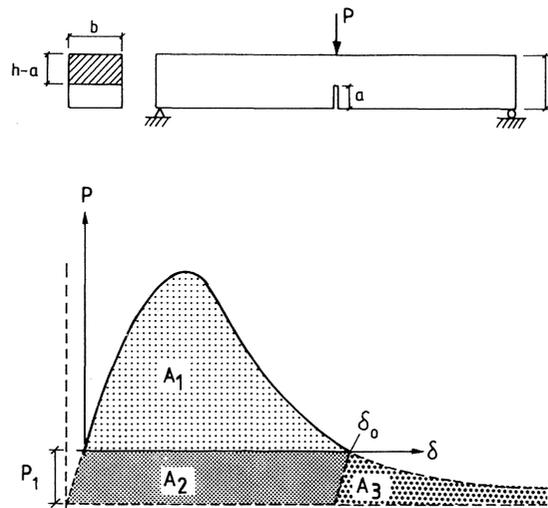
Fig. 2.7 RILEM recommendation for G_F testing. $A2 = A3 = mg\delta_0/2$

2.5.3 Numerical implementation

Except for very few simple cases, generally numerical methods are required in applications of the Fictitious Crack Model. The finite element method, as the most flexible and general numerical method, naturally becomes the first choice. Some other methods, e.g. the boundary element method, have also been used.

The finite element implementation has been discussed extensively by Petersson (1981), Gustafsson (1985). In the following, the basic techniques and calculation procedures will be described.

In a finite element analysis, the crack propagation path is arranged to situate along element boundaries and the fracture zone (fictitious crack) is modelled using negative spring elements (Fig. 2.8). If the maximum principal stress at the node point in front of the fictitious crack tip reaches the tensile strength, this node is split into two nodes and a spring element is inserted. The fictitious crack moves to next node. The carrying load of the spring is evaluated according to the σ-w relation. When the deformation of the spring is equal to w_c, the two nodes are completely disconnected, a fictitious crack transforms to a real crack. The real crack tip moves a step to next node. In this way the formation and propagation of a crack can be simulated.
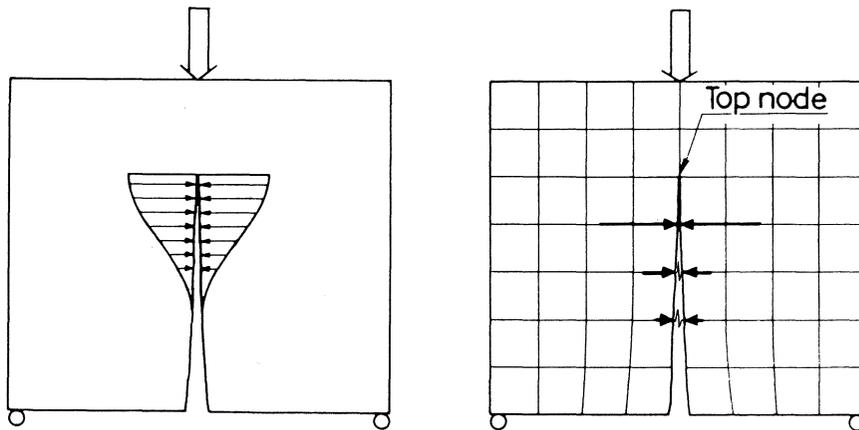
Fig 2.8 Finite element representation of a fictitious crack (Petersson et al., 1980)

Generally in solving nonlinear problems, iterations are necessary to maintain the equilibrium. In FCM analysis, if linear elastic behaviour is assumed outside the fracture zone and the σ-w curve is assumed to be piecewise linear, then the analysis can be performed in increments without iterations. The substructure technique is often used to reduce the computational work.

2.5.4 Main features and applications

The model employs both a strength criterion as in strength theory, and an energy criterion as in fracture mechanics. Therefore, it is able to solve fracture problems in a more general, realistic way, irrespective of whether an initial crack exists or not. It makes it easy to deal with initial stress and strain problems possibly caused by shrinkage and thermal strains.

In principle, the model can be applied to any tensile fracture problem. The model has been employed to predict fracture and strength in bending and shear problems by Modeer (1979), Petersson (1981), Gustafsson (1985). Gylltoft (1983) has extended the model to the analysis of fatigue fracture of concrete.

Chapter 3
Time Effects on Fracture of Concrete

3.1 Introduction

Mechanical behaviour of concrete is highly sensitive to loading rate. It might be expected that the tensile fracture behaviour is also time-dependent. A brief review of this subject will be presented in this chapter.

Firstly, the effects of loading rate on basic material properties used for cracking models, e.g. tensile strength, fracture energy, modulus of elasticity etc. will be reviewed. Secondly, different models to describe time-dependent crack growth and fracture will be discussed.

3.2 Experimental Findings

3.2.1 Effects of loading rate

The rate effect on tensile strength may be expressed as a power law (Reinhardt 1990):

$$\frac{f_t}{f_{t0}} = \left(\frac{\dot{\sigma}}{\dot{\sigma}_0}\right)^b \tag{3.1}$$

where $\dot{\sigma}_0$ = 0.1 MPa/s and the material constant b depends on the composition of concrete, humidity and temperature. According to Reinhardt (1990), b can be calculated from

$$b = \left(10 + \frac{f_{cm}}{2}\right)^{-1} \tag{3.2}$$

where f_{cm} is compressive strength in MPa. With concrete of normal quality, b changes from 0.02 to 0.05.

Modulus of elasticity is less affected by loading rate and can be expressed as:

$$\frac{E}{E_0} = \left(\frac{\dot{\sigma}}{\dot{\sigma}_0}\right)^{0.016} \tag{3.3}$$

where $\dot{\sigma}_0$ = 0.1 MPa/s.

Brühwiler and Wittmann (1990) determined the fracture energy by means of both three-point bending and wedge splitting tests at various loading rates. They found that fracture energy increases with increasing loading rate at high rates. Similar results can be found in the works of Reinhardt (1990) and Wittmann et al. (1987). It seems the rate effect on fracture energy might be attributed to the sensitivity of tensile strength to loading rate. At low loading rates, however, the fracture energy seems to increase slightly as loading rate decreases according to Wittmann et al. (1987).

Assuming a similar shape of the stress-deformation curve, Reinhardt (1990) suggests that fracture energy may be dependent on deformation rate in the same way as tensile strength:

$$\frac{G_F}{G_{F0}} = \left(\frac{\dot{u}}{\dot{u}_0} \right)^b \tag{3.4}$$

where b is given in Eq. 3.2.

Körmeling (1986) performed unuaxial tensile tests at three deformation rates. The average stress-deformation curves are given in Fig. 3.1. The transferring stress in fracture zone increases at high loading rates

	$\dot{\delta}$ (mm/s)	f_t (N/mm^2)	δ_{peak} (10^{-6}m)	G_F (N/m)
——	125 10^{-6}	3.3	13	116
----	250 10^{-3}	4.8	17	172
--·--	150	5.5	17	313

meas. length: 100 mm
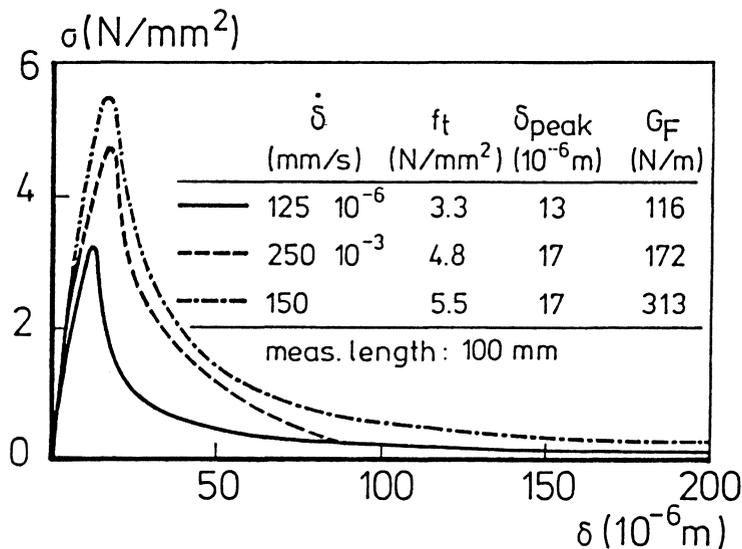
Fig. 3.1 Average stress-deformation curves at different deformation rates (Körmeling, 1986)

Bazant et al. (1989) carried out a extensive series of notched bending tests at various constant rates of crack mouth opening. It was found that the test result for very slow rates is much close to LEFM in the size effect curve.

3.2.2 Creep and creep rupture

The creep-time curve may include three ranges: primary creep, secondary creep and tertiary creep (Fig. 3.2). In the secondary creep range, the creep rate is approximately constant. Thus it is also called stationary creep or steady state creep. The tertiary creep may arise under high applied stresses.
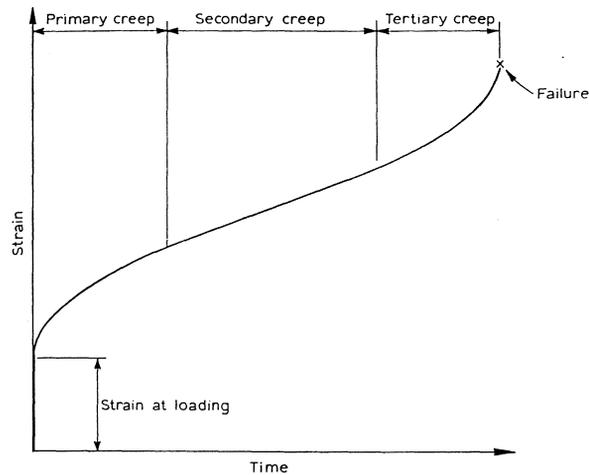
Fig. 3.2 Schematic creep-time curve

The creep-time curve is dependent on the stress-strength ratio. Below stress-strength ratio of about 0.4, creep is proportional to the applied stress. It appears that the initial rate of creep in tension is higher than that in compression under the same stress, at longer time the reverse may be true according to Illston (1965). The effect of stress-strength ratio seems similar to compressive creep, creep is proportional to the applied stress up to 0.5, even higher.

Domone (1974) investigated the effect of humidity on tensile creep. Specimens were cured by either immersed in water or sealed. Creep of specimens immersed in water both during curing and testing is smaller than creep of sealed specimens. If drying is allowed during loading, creep both for immersed and sealed curing specimens seems to be greater than that if the humidity keeps constant. Cyclic drying and wetting results in much higher creep.

Stresses higher than a certain limit produces failure after a certain time, known as static fatigue or creep rupture. It is believed this limit is probably about 75% of the static strength (Domone 1974).

Al-Kubaisy and Young (1975) performed a series of tests under sustained tension at high stress-strength ratio (from 0.6 to 0.95). The loading rate is 0.015 MPa/s and the static strength is 2.5 MPa.

By means of ultrasonic-pulsevelocity equipment to monitor the process of microcracking, they also observed three stages in the stress-strain curve:

(1). A few interfacial cracks are formed before loading, but the majority of cracks of this type do not form until at an applied stress ratio of 0.2 - 0.38.

(2). Up to 0.68 - 0.78, the interfacial cracks stabilize and become dormant.

(3). Rupture range: cracks grow in cement matrix. They grow with time, and eventually macroscopic cracks are formed which bridge the interfacial cracks and produce failure.

They found that the failure strain is approximately constant for creep rupture. A stress-failure lifetime relation is plotted in Fig. 3.3 and is expressed
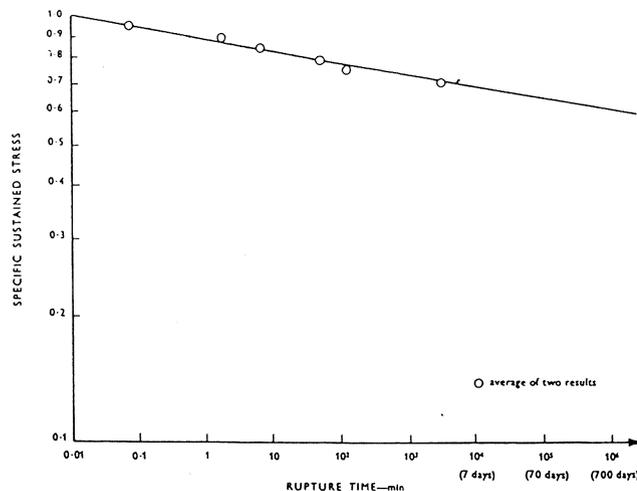
Fig. 3.3 Stress-failure lifetime relation (Al-Kubaisy et al. 1975).

as

$$t_{cr} = 0.016 \cdot (\frac{\sigma}{f_t})^{-34.4}$$ (3.5)

Reinhardt and Cornelissen (1985) recently performed intensive sustained tensile tests. The relation between stress and failure lifetime is as follows (Fig. 3.4):

$$\log t_{cr} = 13.63 - 14.46 \frac{\sigma}{f_t}$$ (3.6)
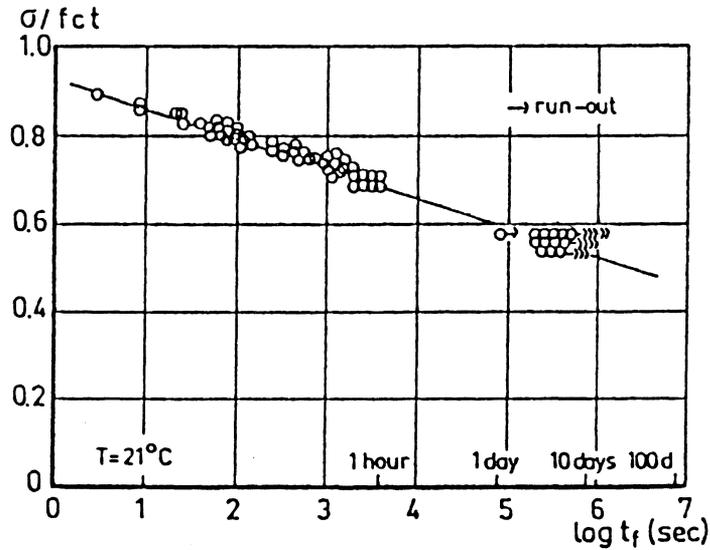
Fig. 3.4 Stress-failure lifetime relation (Reinhardt et al., 1985)

In tensile creep tests on sealed specimens, Cornelissen (1983) proposed a relationship between the secondary creep strain and the failure lifetime as:

$$\log t_{cr} = -4.37 - 0.96 \cdot \log \frac{d\varepsilon_{sec}^{cp}}{dt}$$ (3.7)

He found that the secondary creep rate is a good predictor for the time to failure, irrespective of whether this rate is caused by a constant or a varying stress (Cornelissen, 1984).

They also suggested a stress-strain criterion for fracture:

$$\epsilon = 4.5 * 10^{-5} + \frac{\sigma}{E} \tag{3.8}$$

As shown in Fig. 3.5, this criterion seems to hold for concrete of different compositions under both static and sustained tests. It seems that the effect of a temperature between 4 and 20 C is not significant.
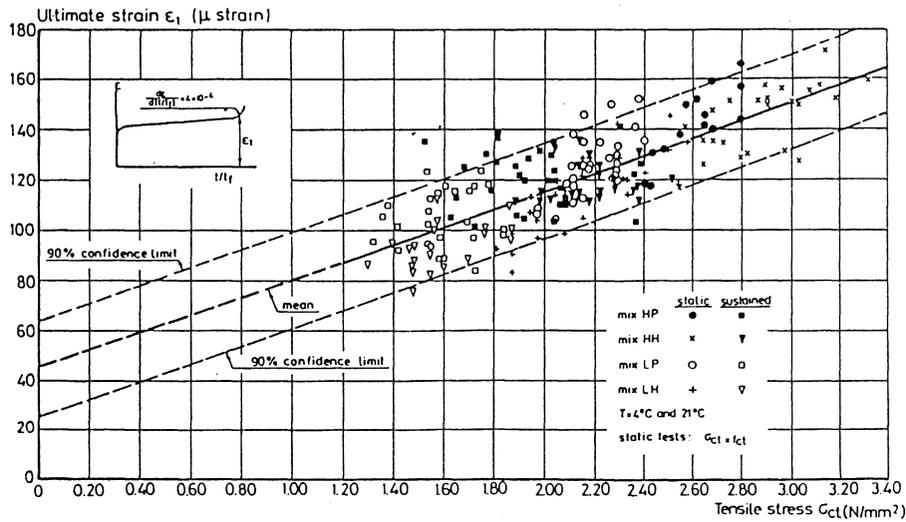
Fig. 3.5 Ultimate strain at failure in tensile creep rupture tests
       (Reinhardt et al., 1985)

Shkoukani (1989) has performed sustained tension tests on both concentric and eccentric loaded specimens. The sustained load level and failure time curves are plotted in Fig. 3.6. As the eccentricity (e/d) increases, the failure time is longer under the same sustained load level. In other words, the decrease of long-term strength is much less.
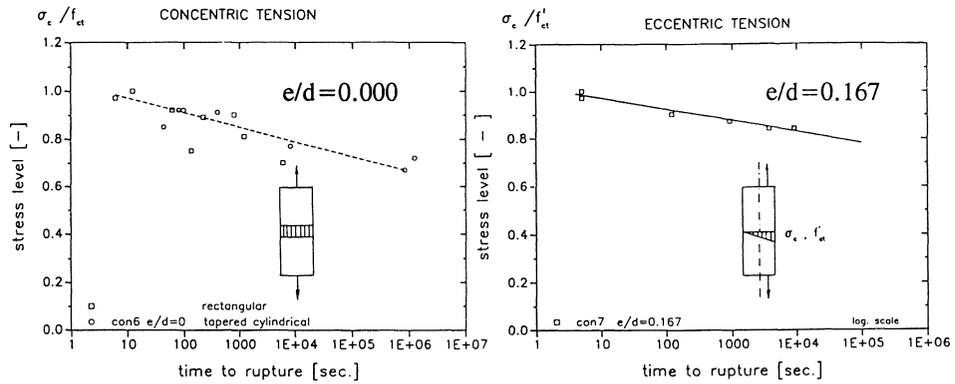
Fig. 3.6 Stress level-failure time curves in concentric and eccentric tension tests (Shkoukani, 1989)

3.2.3 Creep crack growth tests

A few studies have been carried out to determine the relationship between crack growth rate and stress intensity factor for cementitious materials (Mindess et al., 1974, Evans et al., 1976, Tait & Garrett, 1986). Most have used large double torsion specimens. The results are generally presented in a log V versus log K_I curve. These studies show that the slope of the curve, n, is in the order of 30, in the range of crack growth rate from 10^{-6} to 10^{-2} m/s.

Crack growth rate is very sensitive to environment moisture. Tait & Garrett (1986) found the rate in wet specimens is 4 orders higher than that in dry ones (Fig. 3.7) .
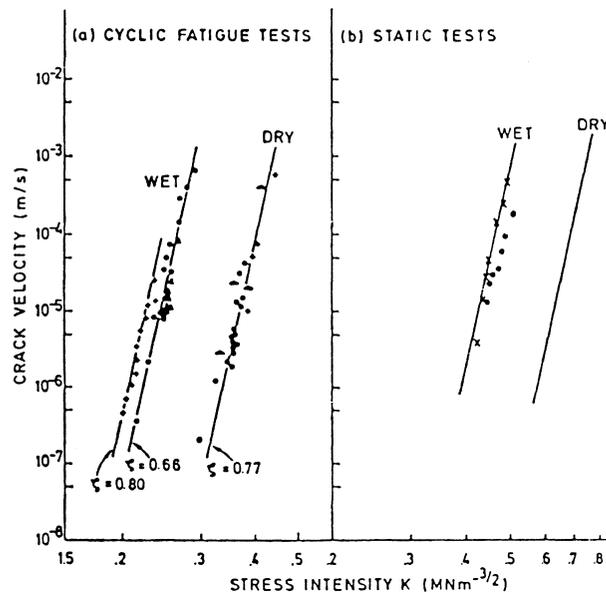
Fig 3.7 Crack velocity as function of stress intensity factor in cyclic and static fatigue tests on wet and dry specimens of cement mortar (Tait & Garrett, 1986)

The mechanisms of time-dependent crack growth in cementitious materials are not yet well understood. However, the presence of water has a significant influence on crack growth, as it is observed that, in completely dry specimens, the rate of crack propagation diminishes to zero (Ruetz, 1968).

The stress corrosion mechanisms dependent on the presence of water, $Ca(OH)_2$ have most often been suggested to explain time-dependent crack growth (Shah & Chandra, 1970, Husak & Krokosky, 1971).

3.3 Modelling of Time-dependent Cracking and Failure

3.3.1 Stress approach

Failure lifetime may be related solely to sustained load level, irrespective of the specimen geometry.

3.3.2 LEFM approach

The time-dependent crack growth is usually related to the stress intensity factor K_I by an empirical relationship:

$$\frac{da}{dt} = A K_I^n \qquad (3.9)$$

where A and n are material constants.

As shown by Nadeau, Bennett and Fuller (1982), the dependency of strength on loading rate or rupture time can be derived from the equation above. The derivatives will given in the following.

In sustained loading, the failure lifetime is related to the load level (σ/σ_0) by

$$t_{cr} = \frac{2 K_{Ic}^{2-n}}{(2-n) A Y^2 \sigma_0^2} \left(\frac{\sigma}{\sigma_0}\right)^{-n} \qquad (3.10)$$

For constant loading rate, the strength depends on the rate as

$$\sigma^{n+1} = \frac{2(n+1) K_{IC}^{2-n}}{(n-2) A Y^2 \sigma_0^{n-2}} \dot{\sigma} \qquad (3.11)$$

3.3.3 Non-linear fracture mechanics approach

Hillerborg (1991) suggested a method to estimate the long-term strength. The structural strength is generally expressed as a function of d/l_{ch}. If the formal modulus $E(t)$ is evaluated as $E/(1+\phi(t))$, where $\phi(t)$ is the creep factor, the time-dependent strength may be evaluated from the relation, provided that tensile strength and fracture energy are not time-dependent.

Hansen (1990) recently proposed a visco-elastic model by extending the Fictitious Crack Model (Fig. 3.8). He took into account the time-dependency of material properties in the fracture zone by employing rheological elements instead of spring elements. However, he used a negative dashpot which seems to lack solid physical meanings.
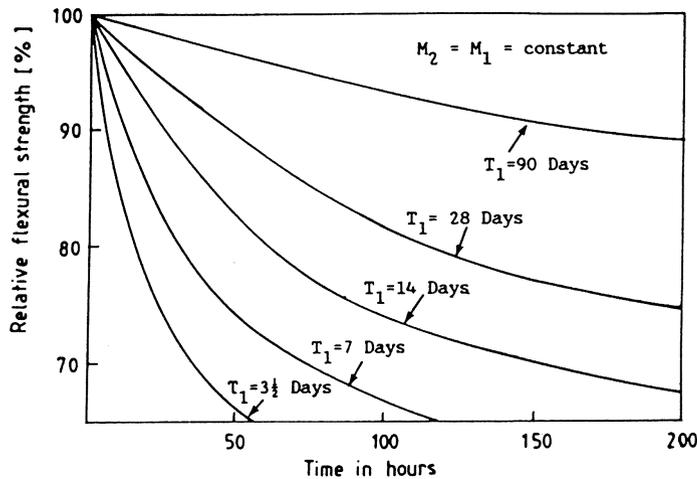
Fig. 3.8 Calculated sustained flexural strength as a function of time and redardation time (Hansen, 1990)

Table 4.1 Experimental program 33

Geometry of specimen (mm)	No of test	Objective
	5	Tensile strength (f_t)
	6	Relaxation
	3	Modulus of elasticity (E)
	14	Rate effect on fracture energy (G_F)
	12	Flexural creep rupture
	6	Fracture energy (G_F)
	14	Flexural creep rupture
	16	Compact tensile creep rupture
	3	Compressive strength
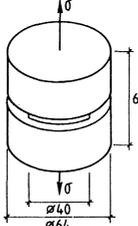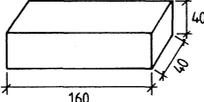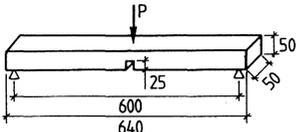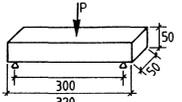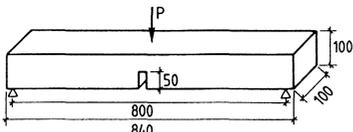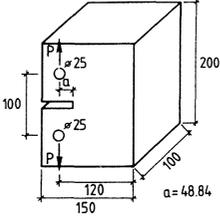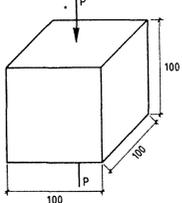
4.2 Research Program

The primary objective of the program was to investigate the time-dependency of tensile softening behaviour (the σ-w curve, G_F) and creep crack growth and fracture in plain concrete structures. The experiments involved determining the basic material properties (f_t, E and G_F), time-dependency of G_F and σ-w curve, flexural and compact tensile creep rupture. All the tests are given in Table 4.1

4.2.1 Basic material tests

The basic material parameters for FCM are tensile strength, f_t, fracture energy, G_F, and modulus of elasticity, E. Tensile strength was determined from direct tensile tests on notched cylinders. Fracture energy was obtained according to the RILEM recommendation (1985). The dimension of specimens was 100*100*840 mm and the span was 800 mm. Beams (40*40*160 mm) were used to measure the dynamic modulus E by the resonance frequency method (Vinkeloe, 1962). The 28-day compressive strength of the concrete was determined from cubes with the dimensions 100*100*100 mm.

4.2.2 Rate effect on the σ-w curve and G_F

To investigate the rate effect on the σ-w curve, relaxation tests of notched cylinders in tension were carried out. The tests were carried out by keeping the crack opening constant and registering the relaxation load.

The rate effect on G_F was studied by means of three-point bending tests of notched beams (50*50*640 mm). The span was 600 mm and the notch length was 25 mm. The deflection rates varied from 0.05 um to 50 um/s.

4.2.3 Creep rupture tests

In order to study time-dependent fracture behaviour, flexural and compact tensile creep rupture tests were performed. Both notched beams (840*100*100 mm, span = 800 mm, notch depth = 50 mm) and unnotched beams (320*50*50 mm, span = 300 mm) were used in the flexural tests. The dimensions of specimens used in the compact tensile tests are given in Table 4.1. The notch ratio a/W was 0.4 and 0.7.

4.4 Experimental Methods and Set-ups

4.4.1 Testing machine

All the tests were carried out in an electro-hydraulic, closed-loop materials testing machine (MTS-810). It is possible to perform tests in three different control modes: stroke control, load control and deformation control. Under stroke control, the displacement of the loading head is used as the feedback. Most of the flexural tests were performed in this control mode. Under load control, the amount of load serves as the primary feedback. Creep rupture tests were carried out in this mode. The deformation control mode uses the crack opening measured from clipgauges. In direct tension tests, the stress-deformation curves are obtained under deformation control.

4.4.2 Tension tests

In determining the stress-deformation curve from tension tests, two kinds of stability problems might arise. The first one is to ensure a stable development of the fracture zone and being able to follow the complete softening curve. With modern closed-loop testing machines, it is no longer difficult to follow the softening part in tension tests.

The second is to maintain an even distribution of stresses and deformations in the fracture zone. Due to possible initial stresses, material defects in concrete and the possible eccentricity of tests, the fracture zone is apt to start from one side of the specimens. It is similar to a bending test rather than a tension one. Consequently the curve measured does not represent the real material behaviour in tension. To counteract the rotation effect, the testing arrangement must have a sufficient rotational stiffness.

Therefore a special arrangement (Fig. 4.1), which was designed by Hassanzadeh (1987, 1990) and can reduce possible rotation, was used in order to obtain a real material relation.
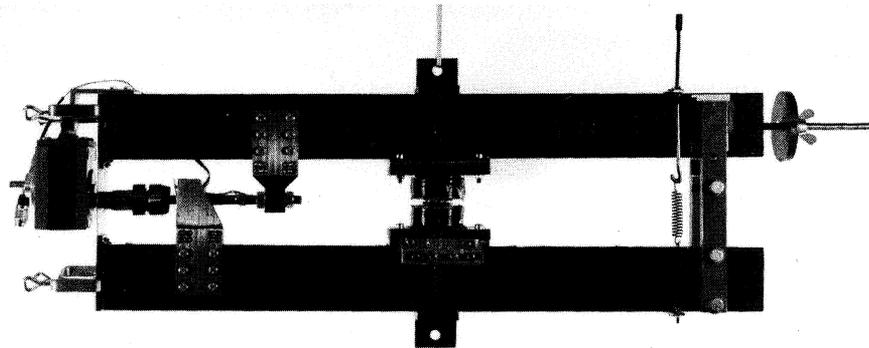
(a) Photograph
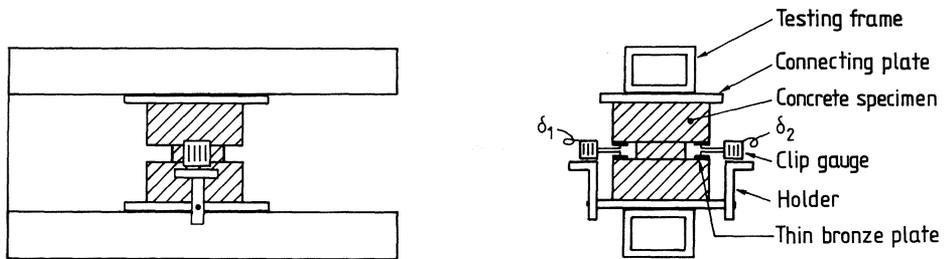
(b) Schematic illustration

Fig. 4.1 Experimental set-up for stable tension tests
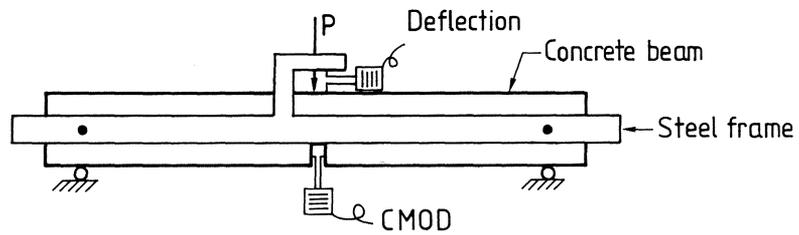
Fig. 4.2 Set-up for bending tests

This arrangement was designed for mix mode I and II tests, although the tests presented in this thesis involve only mode I fracture. The arrangement mainly consists of two steel frames connected with a thin steel plate and specimens are glued to steel plates which are attached to the arrangement (Fig 4.1 b). Two clip gauges are inserted between notched surfaces on both sides. In order to prevent clip gauges from moving or dropping out, clip gauge holders are used and thin bronze plates are glued to the places where clip gauges are set.

The deformation for fracture zone is the average value of the deformations measured by clip gauges. The stress is calculated from load divided by fracture section area.

In tension tests, the ends of each specimen were ground and washed and allowed to dry in about 4 hours while the rest part was wrapped with wet cloth. Then the specimen was glued to steel plates using 5-minute epoxy. Testing was performed in at least 4 hours after gluing.

4.4.3 Bending tests

To measure deflections accurately, a stiff steel frame was fastened at both ends of a beam. The deflection was measured between the upper edge and the frame (Fig. 4.2) by means of clip gauges. CMOD was also measured using clip gauges. A number of bending tests with beams (840*100*100) were carried out with this set-up.

4.5 Test Results and Discussions

In all the tests, specimens were wrapped in plastic foil and notches were covered with wet cloth to avoid drying-induced stresses and cracks.

4.5.1 Basic material parameters

The basic parameters, i.e tensile strength, f_t, fracture energy, G_F, and modulus of elasticity, E, are given in Table 4.3. All specimens used to obtain those parameters were about 4 months old at testing. The 28-day compressive strength is 38 MPa.

Table 4.3 Material parameters

Tensile strength f_t (MPa)	Fracture energy G_F (Nm/m^2)	Modulus of elasticity E (GPa)	Characteristic length l_{ch} (m)
2.8 (0.2)	82 (9)	36 (2)	0.38

* Standard deviations are given in parentheses

The tensile strength was determined from notched cylinders. The effect of a notch on the tensile strength and the σ-w curve has been analyzed theoretically by the author (Zhou, 1988).

A uniaxial tension test on a double notched prisms (Fig. 4.3 a) was simulated by means of the Fictitious Crack Model. The input σ-w curve was assumed to be bilinear with f_t = 4 MPa, E = 35 GPa and G_F=80 Nm/m^2 (Fig 4.3 b). The net section stress was calculated from the total load divided by the cross-section area along the notches. The deformation was the average value of deformations measured on both sides in a 10-mm length.

The stress distribution across the fracture cross-section is uneven up to the peak point (Fig. 4.3 d). The measured strength is smaller than the input one (Fig. 4.3 c). The difference between them depends on brittleness number (d/l_{ch}) (Fig. 4.4).
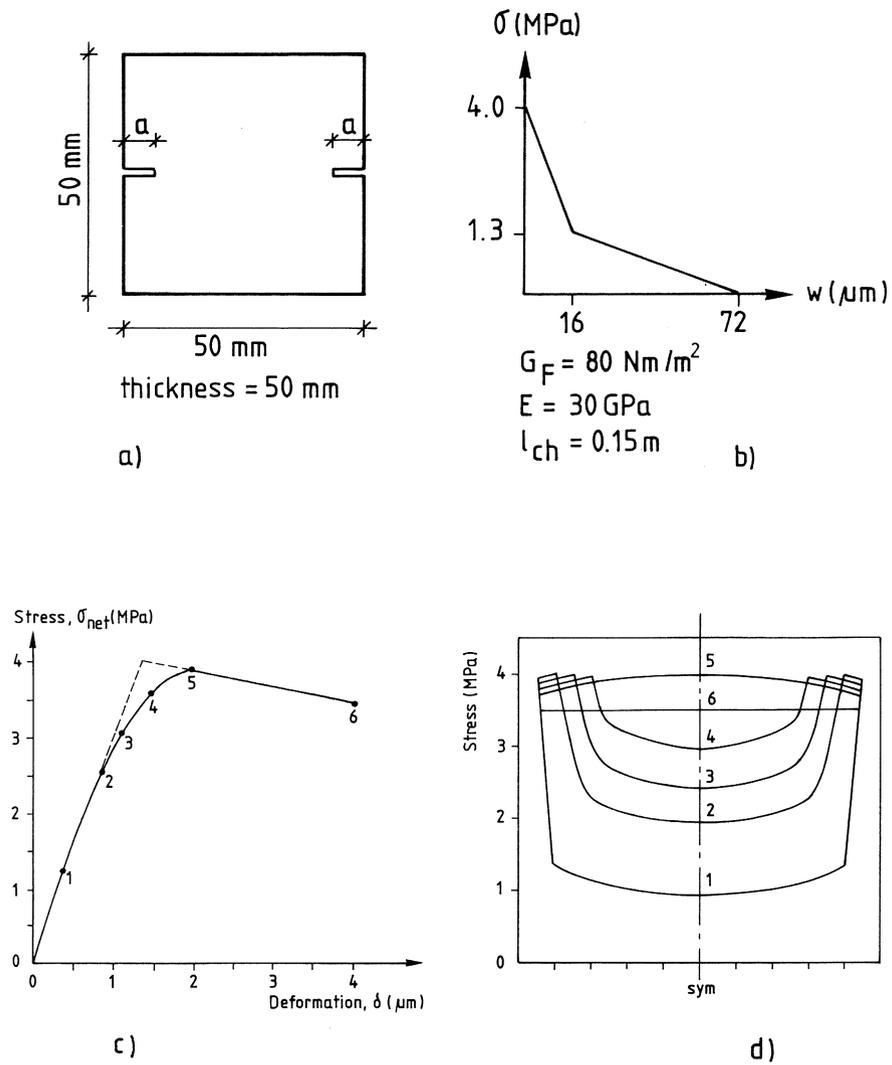
Fig. 4.3 Simulated uniaxial tension test of a double notched prism according to Zhou (1988).

    (a) Specimen geometry;

    (b) Input material properties;

    (c) Comparison between simulated and input curves;

    (d) Stress distributions across the fracture zone.

For notched cylinders, the effect of a notch might be expected to be similar. d/l_{ch} is about 0.2 and $2a/d$ is 0.3. According to Fig. 4.4 the error might be less than 3%. With regard to the all-round notched cylinders used in the present study, the error might be estimated to be double. In that case it is still less than 6% and acceptable.

σ_{net} / f_t

1.00

0.98 $d / l_{ch} = 0.33$

0.96 $d / l_{ch} = 0.67$

0.90

0.92

0.90

0   0.2   0.4   0.6 $2a/d$
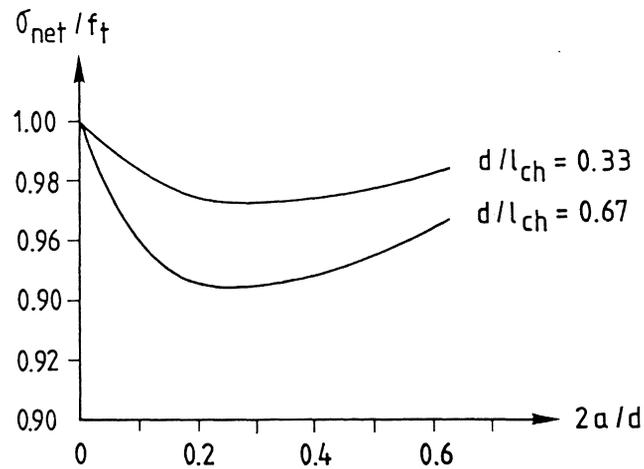
Fig. 4.4 Notch sensitivity of tensile strength

4.5.2 Relaxation tests

In order to get some insight into rate effect on the σ-w curve, a few direct tension tests on notched cylinders were carried out. After maximum load points were reached, the deformation was held constant for a certain period of time and the stress relaxation were registered. One typical test is shown in Fig. 4.5. In this test, the holding period of time was about 60, 30, 30 Min, when the net section stress (total load divided by fracture area) was 2.65, 1.75, 0.90 MPa respectively.

The stress decreases quickly at first but then slows down at each holding period (Fig 4.5 b). When the deformation increases again, the stress increases but does not regain the initial value (Fig 4.5 a). It seems that some damage occurs in the fracture zone during the holding time and results in a decrease in the load carrying capacity of the zone. However, such a damage seems to impose only a local disturbance on the σ-w curve but does not seem to influence the latter part of the curve. It might imply that the σ-w curve could be unique for the same loading rate, irrespective of previous loading history.

To check whether a holding period can influence the envelope of the σ-w curve, the stress-deformation relations evaluated from monotonic static tension tests and relaxation tests are compared at w=5, 10, 20, 30 and 50 μm. The result is shown in Table 4.4. There is no significant difference between the two types of tests.

Table 4.4 Stress ratio (σ/f_t) versus deformation relations evaluated from monotonic static tension and relaxation tests. Coefficient of variation is given in parenthesis.

w (μm)	5	10	20	30	50
static	0.75 (6%)	0.58 (13%)	0.27 (18%)	0.19 (26%)	0.10 (30%)
Relaxation	0.76 (6%)	0.57 (10%)	0.30 (21%)	0.20 (19%)	0.11 (24%)
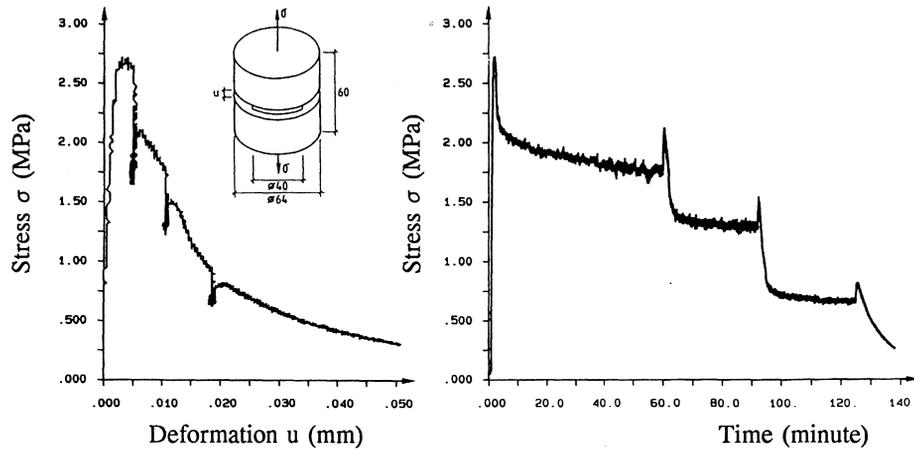
(a) Stress-deformation curve
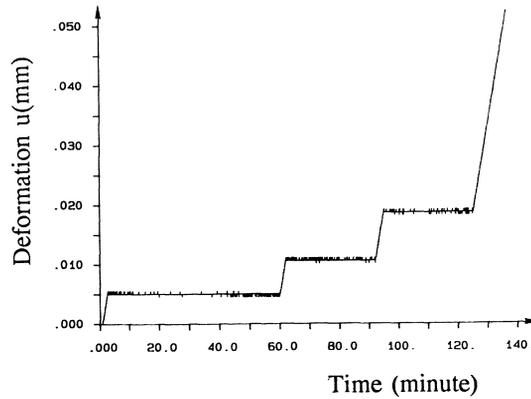
(b) Stress-time curve

(c) Deformation-time curve

Fig. 4.5 A typical relaxation test on a notched cylinder. The deformation was held constant at stress σ=2.65, 1.75 and 0.90 MPa in about 60, 30 and 30 minute respectively.

If the loading rate changes, the fracture zone may follow another σ-w curve. But if the rate changes back, the fracture zone may continue along the same σ-w curve as before the change occurs. A possible rate-dependency of the σ-w curve is schematically illustrated in Fig. 4.6.
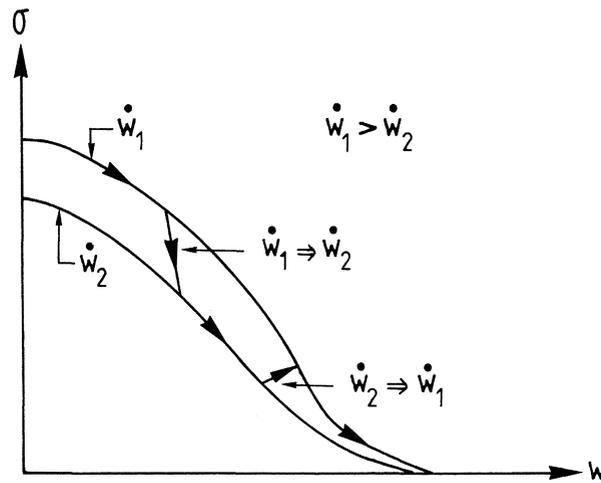
Fig. 4.6 Schematic illustration of rate-dependency of the σ-w curve

Great care was taken to reduce the drift of clip-gauges as small as 1 um/30 Min. To check whether other factors such as clip-gauge drift and creep outside the fracture zone can influence the tests, relaxation tests hade been also made before the load reached the maximum value. The load-time curve of a test is shown in Fig. 4.7. The load changes very little. Therefore the effect observed in Fig. 4.5 seems mainly to be related to the sensitivity of the fracture zone to time effect, at least for the first 20 minutes of the holding period.
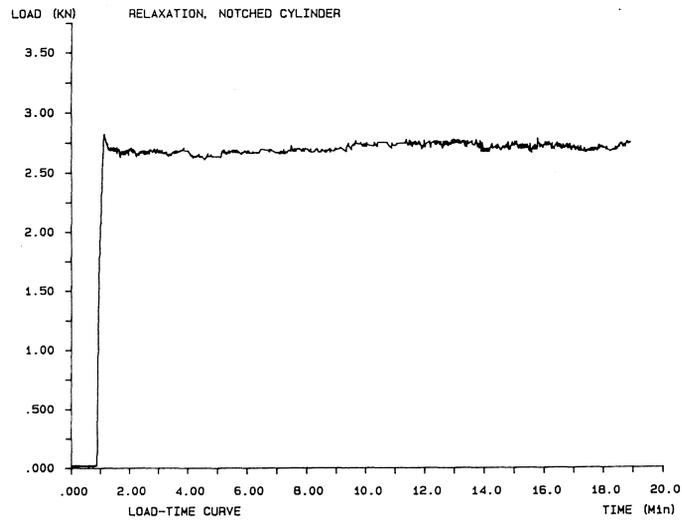
Fig. 4.7 Relaxation test before load reaches the maximum value

Since the stress seems to change very little after about 20 minutes, the load decrease in the first 20 minutes may be used as an estimation of the ultimate stress relaxation. The ratio between the relaxation stress σ^{rl}_m at t=20 minutes and the stress σ_0 at the beginning of the holding period is plotted for all the tests in Fig.4.8 (see also Table A.1, Appendix A). The ratio may be taken to be 0.7. However, there are large scatters in load decrease rates in relaxation curves. Therefore accurate relaxation relations cannot be established on the basis of the tests.
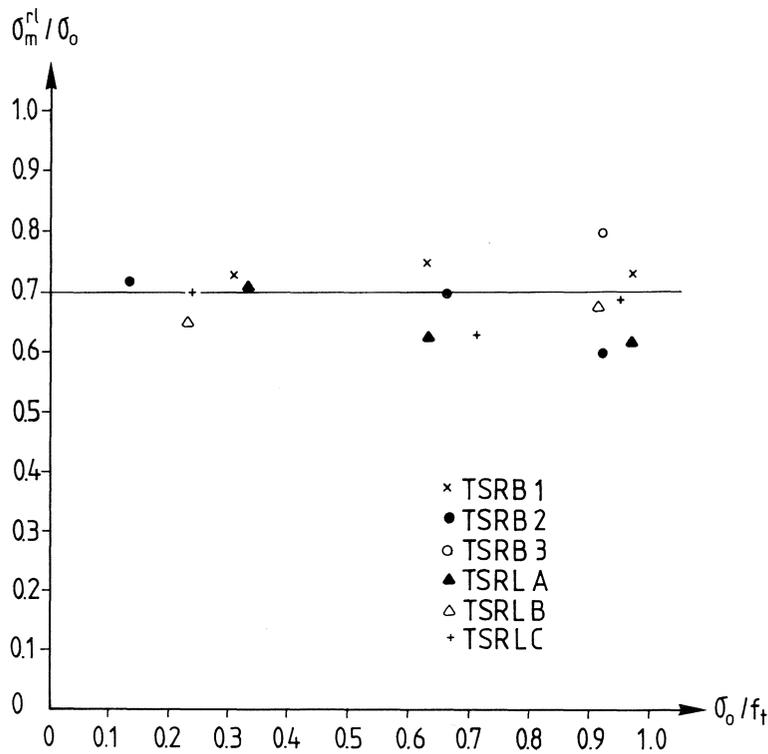
Fig. 4.8 Ultimate relaxation stress related to initial stress

4.5.3 Rate effect on fracture energy

The time-dependency of the σ-w curve can be investigated indirectly by studying the effect of the loading rate on fracture energy, as fracture energy is equal to the area below the σ-w curve. Fracture energy is usually determined from bending tests of notched beams, which are much easier to carry out than tension tests.

A series of tests has been carried out with varying deflection rates from 0.05 to 50 um/s. The corresponding time to reach the maximum load ranged from about 5 to 5000 seconds. The mean curves of four deflection rates are depicted in Fig. 4.9. The CMOD rate is about 0.1 of the deflection rate for the specimens.
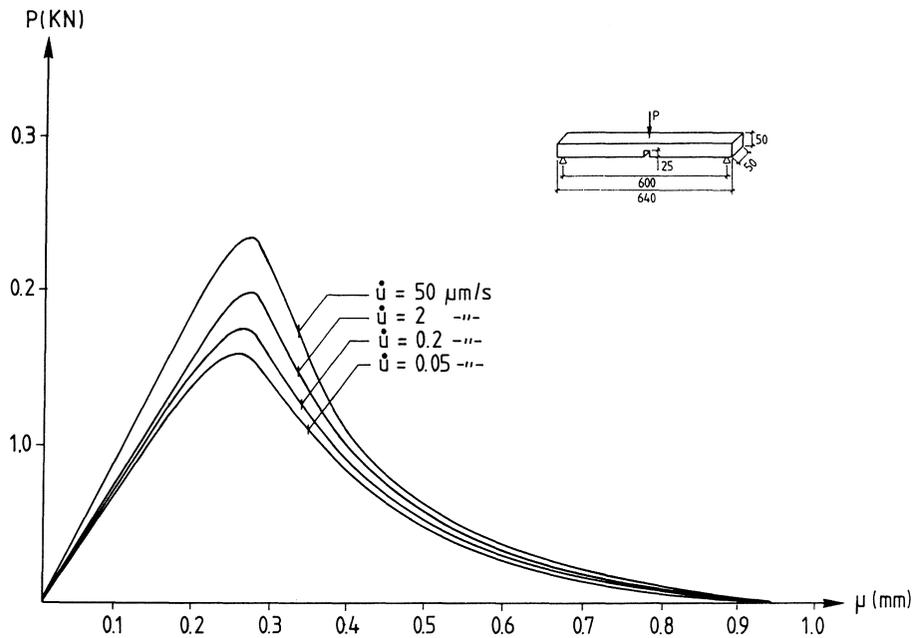
Fig. 4.9 Load-deflection curves of various deflection rates

Fracture energy is evaluated according to the RILEM recommendation for different rates and is given in Table A.2, Appendix A. The result is also plotted in a double logarithm in Fig. 4.10.
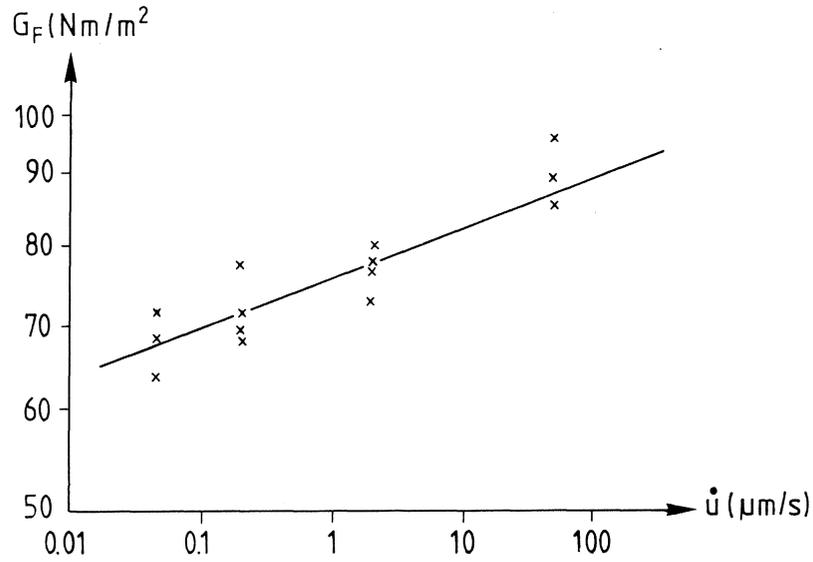
Fig. 4.10 Rate effect on G_F

In the present tests, fracture energy seems to decrease as loading rate decreases. Fracture energy may be related to deflection rate in a power law as

$$\frac{G_F}{G_{F0}} = (\frac{\dot{u}}{\dot{u}_0})^{0.04} \qquad (4.1)$$

where $\dot{u}$ = deflection rate and $\dot{u}_0$ = 2 um/s.

At loading rates higher than the static one, fracture energy seems to decrease with loading rates (Reinhardt 1990, Brühwiler et al. 1990). Nevertheless, few tests have been done on the influence of very slow rate on fracture energy. Wittmann et al. have carried out three-point bending tests at varying deflection rates (from 0.001 mm/Min to 10 mm/Min) to determine rate effect on fracture energy. The result is shown in Fig. 4.11. At higher loading rates, fracture energy decreases as the rate gets slower. For much slower loading than static loading (0.1 mm/Min), however, fracture energy seems to increase as the rate decreases.
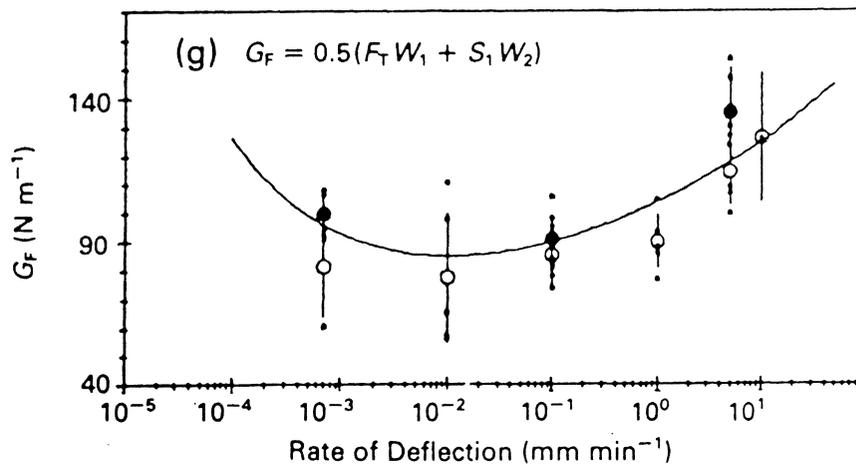
Fig. 4.11 Rate effect on G_F according to Wittmann et al. (1987)

Bazant et al. (1989) have investigated the rate effect on G_F indirectly derived from Bazant's size effect law. They found that fracture energy decreases as the loading rate decreases.

By data-fitting load-deflection curves in different loading rates, Wittmann et al. (1987) have derived the corresponding rate effect on the σ-w curve, as illustrated in Fig. 4.12. On the other hand, it is quite difficult to determine to what extent non-elastic energy due to creep outside the fracture zone may contribute to fracture energy in a very slow loading. It may be reasonable to assume that fracture energy decrease with loading as Eq. 4.1.
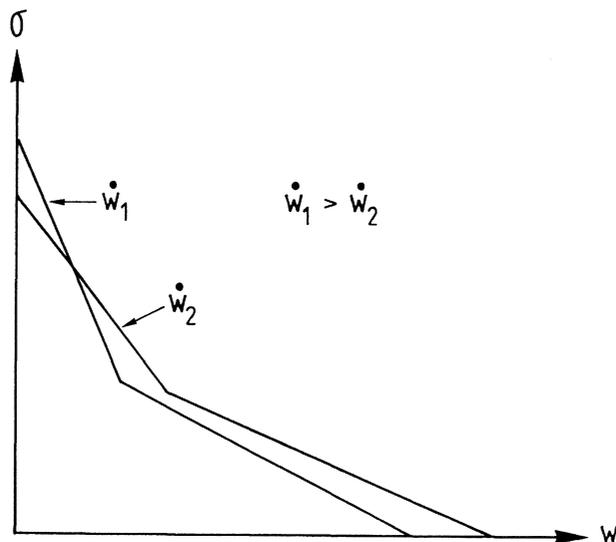
Fig. 4.12 Illustrated rate effect on σ-w curve according to the results of Wittmann et al. (1987)

4.5.4 Flexural creep rupture

Unnotched beams

All the tests were performed under load control, and the load rate was 50 N/s. Four specimens were loaded to failure in about 40 seconds, the ultimate load P_{max} and f_f (= $3P_{max}S/2bh^2$) were determined. Then 8 beams were tested under sustained load levels $\sigma/f_f = P/P_{max}$ from 0.67 to 0.95, and failure times (measured from beginning of sustained loading) were registered. The experimental results (Table A.3, Appendix A) are plotted in Fig. 4.13.
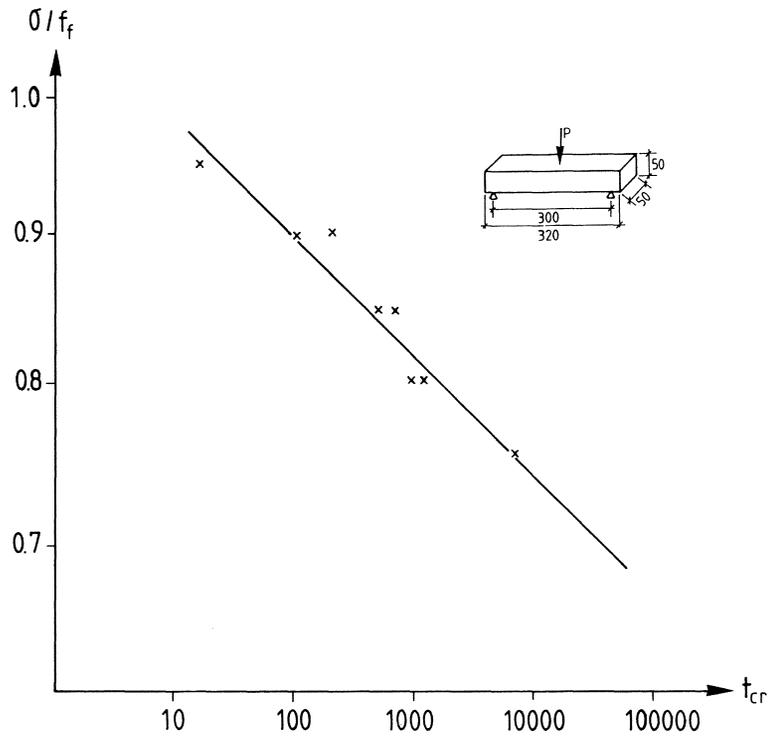
Fig. 4.13 Flexural creep rupture

The regression relationship between stress and failure time can be given in a power law:

$$t_{cr} = 7.2 \left(\frac{\sigma}{f_f} \right)^{-24} \tag{4.2}$$

The exponent is 24 and is comparable to 20-30 for flexural rupture tests (Mindess, 1984).

Notched beams

The ultimate load P_{max} was determined by means of deflection control (5 um/s). It took about 60 seconds to reach the maximum load. The net flexural strength, f_{net}, was calculated from the ultimate load by $3P_{max}S/2b(h-a)^2$. Then 11 rupture tests were carried out under various load ratios (σ_{net}/f_{net}). Failure times were measured from the beginning of sustained loading. In addition to deflection and load, the crack mouth opening displacement (CMOD) was also registered by a pair of clipgauges.

The stress-failure time curve is shown in Fig. 4.14. A regression relation can be expressed as:

$$t_{cr} = 6\left(\frac{\sigma_{net}}{f_{net}}\right)^{-22} \qquad\qquad (4.3)$$
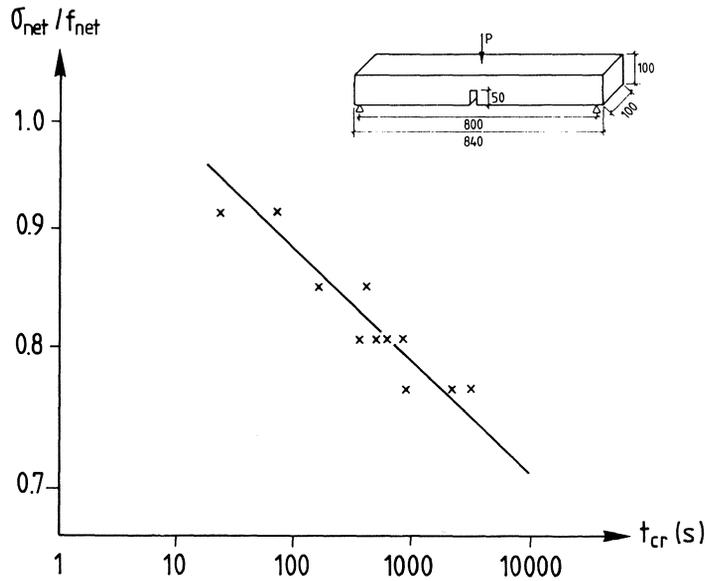
Fig. 4.14 Stress-failure time curve from flexural rupture tests

Figs. 4.15-18 show CMOD-time curves at load ratios of 0.92, 0.85 0.8 and 0.76 respectively. CMOD grows in three stages as usually observed in a creep rupture test. CMOD increases rapidly in the primary stage, but the growth rate gradually slows down. In the secondary stage, the rate of CMOD is constant. In the last stage, CMOD grows increasingly rapidly.

The secondary stage dominates the whole course of creep failure life and CMOD grows considerably in the last stage. The degree of CMOD growth in the primary stage seems to diminish under higher stress level, as observed in a creep test in low loading (less than 40% ultimate load).
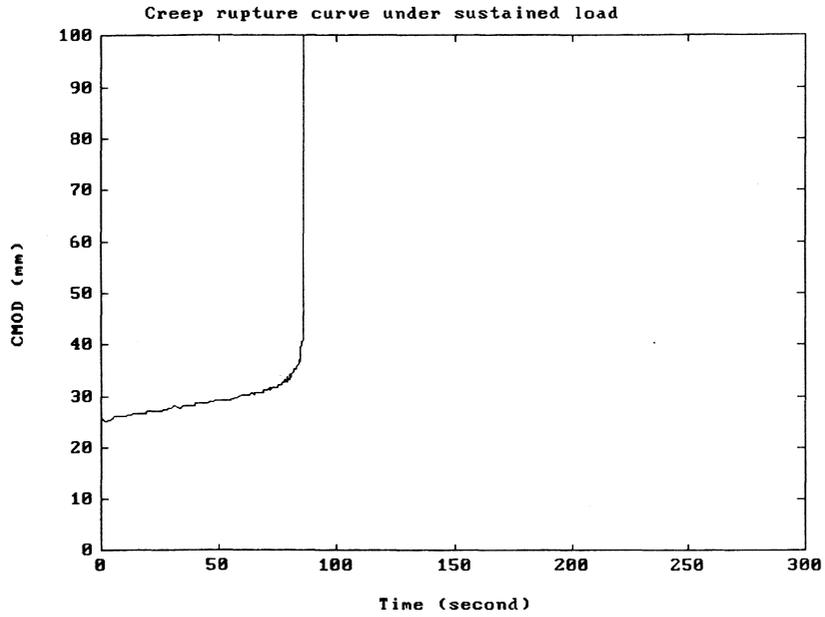
Fig. 4.15 CMOD-time curve under sustained load level $\sigma_{net}/f_{net}=0.92$
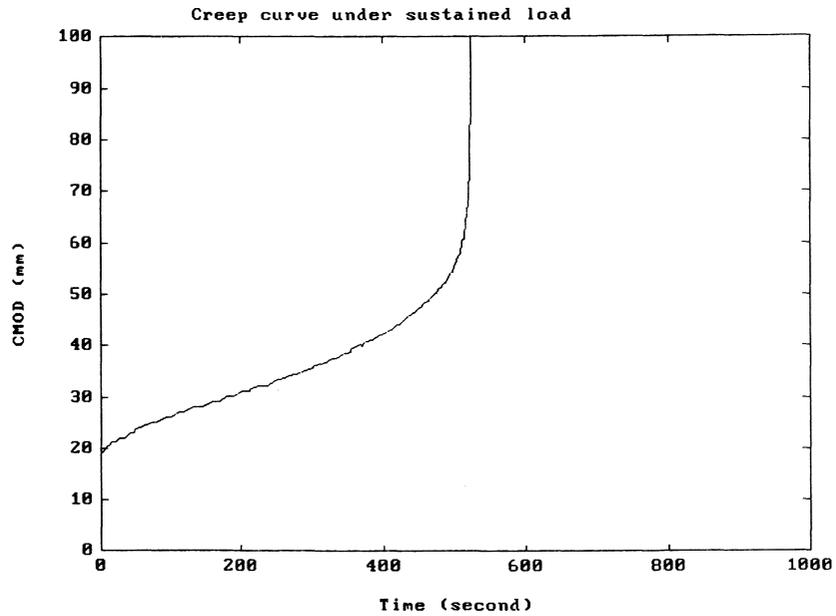
Fig. 4.16 CMOD-time curve under sustained load level $\sigma_{net}/f_{net}=0.85$
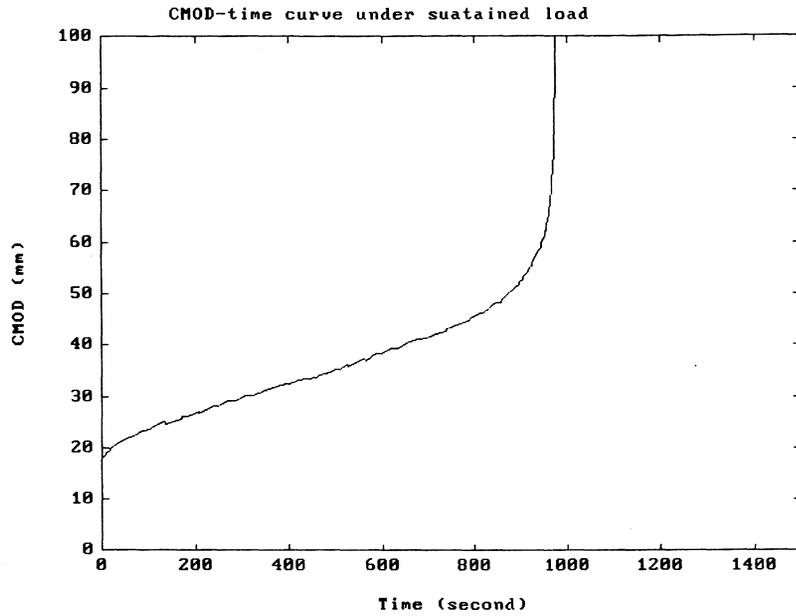
Fig. 4.17 CMOD-time curve under sustained load level $\sigma_{net}/f_{net}=0.80$
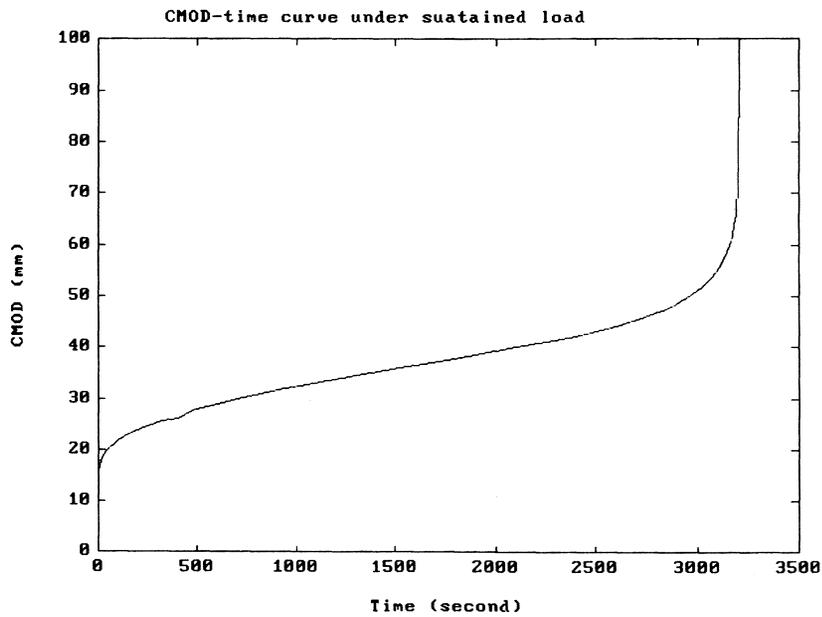
Fig. 4.18 CMOD-time curve under sustained load level $\sigma_{net}/f_{net}=0.76$

Experiments (Cornelissen, 1984) show that the relationship between the creep strain rate in the secondary stage and failure time is more consistent and less scattered than the stress-failure time relation in tensile tests, both under cyclic and sustained loading. The secondary creep strain can be used to predict rupture and fatigue life.

The rates of CMOD in the secondary stage are given in Table A.4, Appendix A. Fig. 4.19 represents the CMOD rate-failure time curve. It yields a much more consistent curve, compared to the stress-failure lifetime curve in Fig 4.14. A regression relation can be given as:

$$\log \dot{c} = 1.22 - 0.95 \log t_{cr} \qquad (4.4)$$
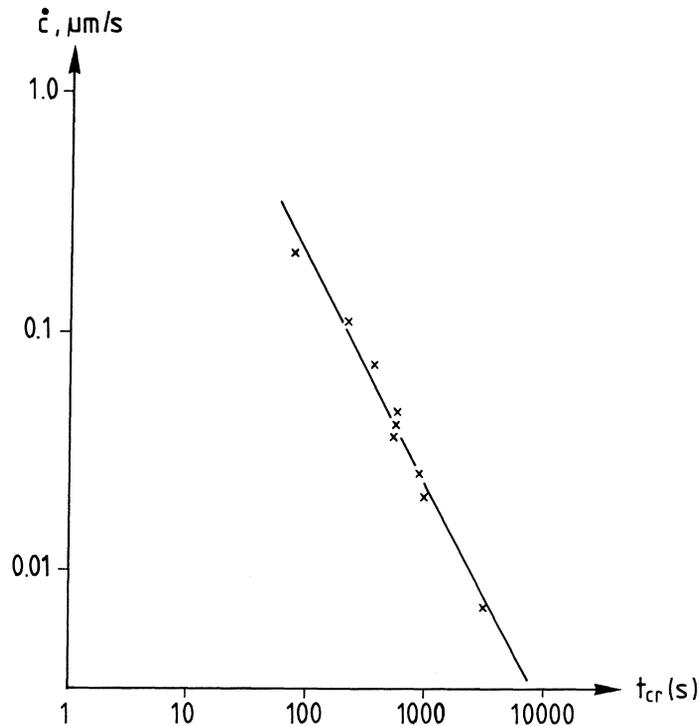
Fig. 4.19 Secondary CMOD rate-failure time curve

In compressive tests, the descending branch of a stress-strain curve from monotonic loading seems to serve as a failure criterion for cyclic loading tests (Karsan et al., 1969). To check if such an assumption can also be made for sustained loading, values of CMOD at initial and failure points for all tests are given in Table A.4. Although there is some uncertainty in determining the failure values of CMOD, CMOD at failure under sustained loading seems to approach the corresponding value in the static load-CMOD curve. Therefore the descending part of the static load-CMOD curve may serve as a criterion for failure in sustained loading (Fig. 4.20)
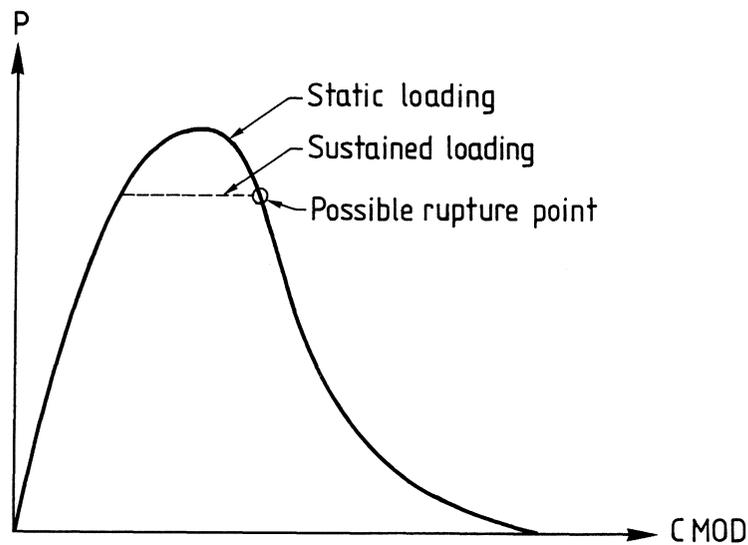
Fig. 4.20 Illustrated relation between the load-CMOD curves
in static and sustained loading

4.5.5 Compact tensile creep rupture

In order to investigate the creep fracture behaviour of different geometries, compact tensile tests with notch ratios a/W as 0.4 and 0.7 were performed. The number of specimens subjected to sustained loading was 6 for a/W=0.4 and 4 for a/W=0.7. The ultimate loads (P_{max}) were determined in deformation control and it took about 1 Min to reach the peak-point in tests. Net strength, f_{net}, was calculated from P_{max}/b(W-a). Rupture tests under various σ_{net}/f_{net} were performed to determine stress-failure time relations. The results are depicted in Fig. 4.21.

Regression relations can be derived from curves for a/W=0.7 and 0.4 as:

$$t_{cr} = 3\left(\frac{\sigma_{net}}{f_{net}}\right)^{-29} \qquad\qquad\qquad (4.5)$$

and

$$t_{cr} = 10\left(\frac{\sigma_{net}}{f_{net}}\right)^{-29} \qquad\qquad\qquad (4.6)$$

respectively.

Compared to flexural rupture tests, the failure time becomes longer under the same stress level (σ_{net}/f_{net}) and the long-time strength may be higher in compact tension. The exponent in the stress-failure time relation may vary for different geometries.
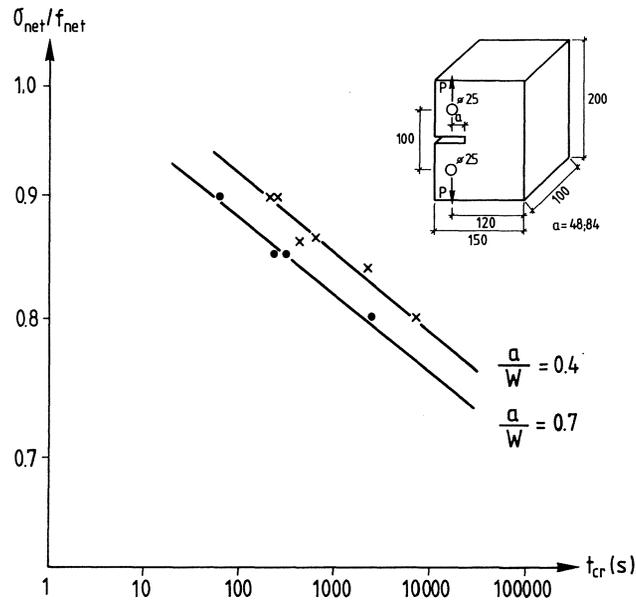
Fig. 4.21 Creep rupture in compact tension tests

Fig. 4.22 shows pictures of specimen and fracture surfaces. Since only fine aggregate was used in the cast specimen, the fracture surface looks quite smooth.
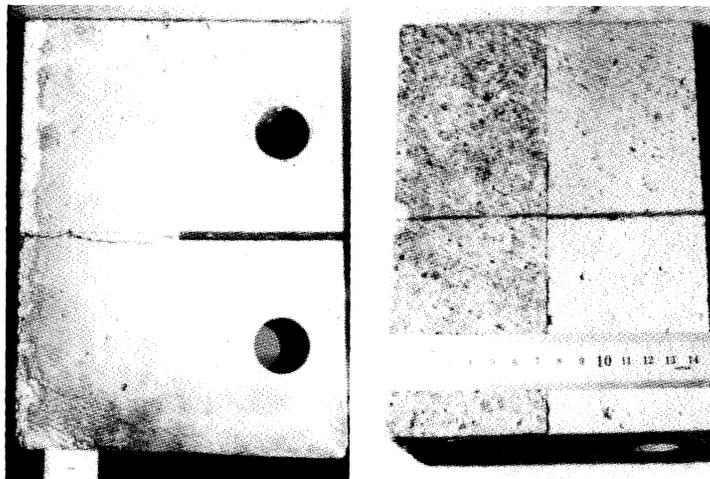
Fig. 4.22 Specimen and fracture surfaces

CMOD-failure time curves under stress levels $\sigma_{net}/f_{net}=0.9$, 0.8 are depicted in Figs. 4.23 and 4.24 for notch ratio a/W = 0.4 and Figs. 4.25 and 4.26 for a/W = 0.7. Three stages can be observed in the CMOD-time curves, similar to the flexural rupture tests. The secondary stage constitutes a large part of the failure life, and the rate of CMOD in this stage may be expected to determine failure time.

Under the same stress level, a specimen with a high notch ratio can withstand a shorter time. This may partly be due to the decrease in fracture cross-section and partly to notch sensitivity.
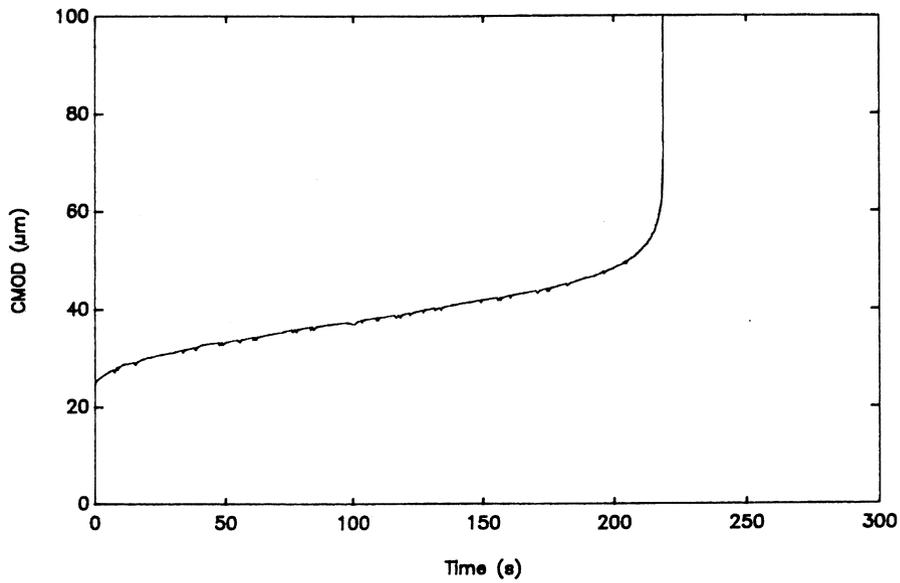
Fig. 4.23 CMOD-failure lifetime curve (a/W=0.4, $\sigma_{net}/f_{net}=0.9$)
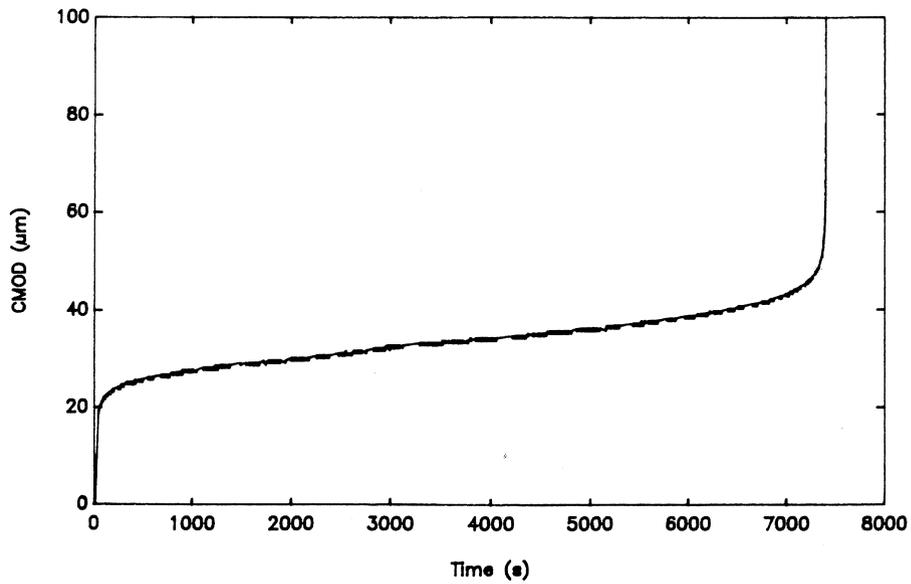
Fig. 4.24 CMOD-failure lifetime curve (a/W=0.4, $\sigma_{net}/f_{net}=0.8$)
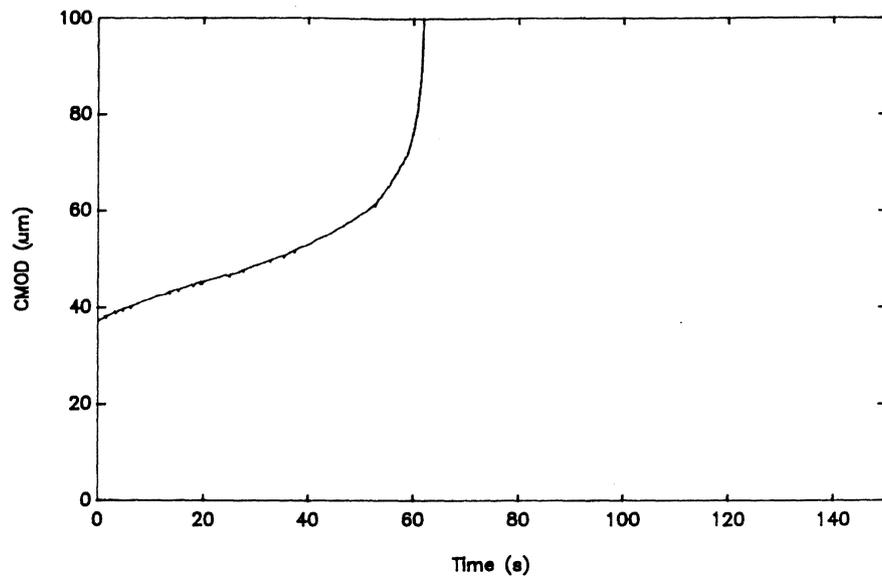
Fig. 4.25 CMOD-failure lifetime curve (a/W=0.7, $\sigma_{net}/f_{net}=0.9$)
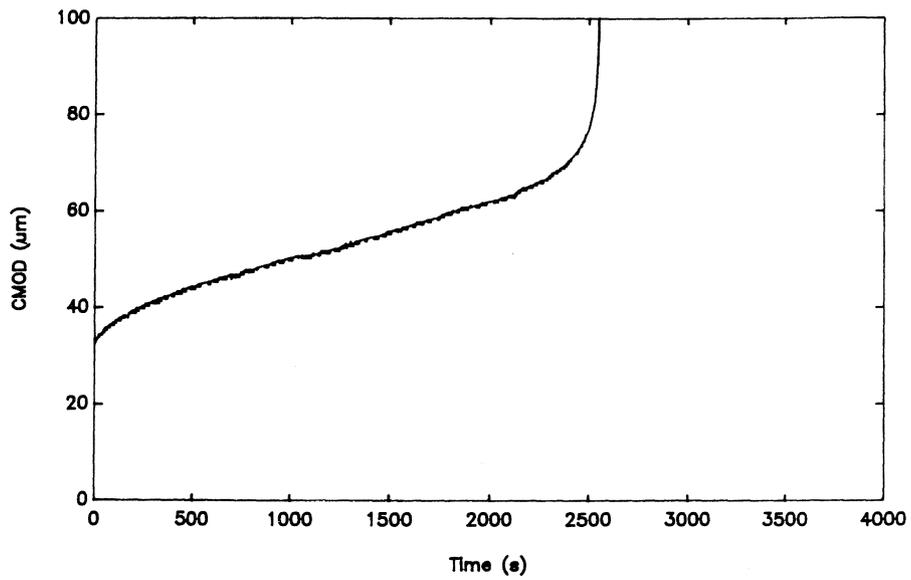
Fig. 4.26 CMOD-failure lifetime curve (a/W=0.7, $\sigma_{net}/f_{net}=0.8$)

4.6 Summary and Conclusions

A series of experimental tests has been carried out to gain information about the influence of time on the fracture parameters and to investigate the time-dependent fracture behaviour of various concrete structures subjected to high sustained loading.

According to direct tensile tests, the σ-w curve seems sensitive to the deformation rate. When the deformation is held constant (zero deformation rate) for a period of time, a loss in load-carrying capacity will result. However, the damage does not seem to have a significant influence on the latter part of the σ-w curve. It seems that the σ-w curve may be unique for the same loading rate.

The influence of time on fracture energy is studied by means of bending tests on notched beams with various loading rates. Fracture energy tends to decrease with loading rates even at slower rates than static one.

Flexural rupture tests of both notched and unnotched beams with the same height display no significant differences in stress-failure time curves. This may be true only for small specimens. For compact tensile tests it seems that failure time is longer than that for flexural tests at the same stress level.

In rupture tests, deformations gradually develop in three stages. In the primary stage, the deformation rate decreases, and becomes constant in the secondary stage. The rate increases rapidly until failure in the tertiary stage. The deformation rate in the secondary stage seems to be a very good predictor for rupture life. It seems that the descending branch of the load-deformation curve in static loading might serve as a failure criterion for rupture tests.

Chapter 5
A Model for Creep Fracture

5.1 Introduction

The Fictitious Crack Model has been successfully applied to simulating tensile fracture under static loading conditions. Similar models have also been incorporated in creep and shrinkage analyses (de Borst and van den Berg 1986, Dahlblom 1987). However, no time effect has been considered within the fracture zone in those crack models.

It might be expected that the Fictitious Crack Model can be applied to creep crack growth as well. Surely proper modifications must be made with regard to time effects on softening behaviour. In the following sections, a crack model with regard to time effects on the fracture zone will be presented. Creep outside the fracture zone has not been included in the model. The static tensile strength serves as a criterion for crack initiation and is considered to be time-independent. The Necessary numerical implementation will be presented in the last section.

5.2 Visco-elasticity theory

Time-dependent behaviour is usually investigated by creep or relaxation tests. In a uniaxial creep test, the stress history $\sigma(t)$ is prescribed by

$$\sigma(t) = \sigma_0 H(t) \qquad\qquad (5.1)$$

where σ_0 is constant stress applied at time $t=0$, $H(t)$ is the Heavyside unit step function defined as

$$
\begin{aligned}
H(t) &= 0 \qquad t < 0 \\
&= 1 \qquad t \geq 0
\end{aligned}
\qquad\qquad (5.2)
$$

The creep strain $\epsilon(t)$

$$\epsilon(t) = J(t)\sigma_0 \qquad\qquad (5.3)$$

where $J(t)$ is creep compliance.

On the contrary, a uniaxial relaxation test is characterized by a prescribed strain history $\epsilon(t)$

$$\epsilon(t) = \epsilon_0 H(t) \qquad\qquad (5.4)$$

In the equations above, and ϵ_0 are constant stress and strain values applied at time $t=0$. The corresponding relaxation stress $\sigma(t)$ is given by

$$\sigma(t) = G(t)\epsilon_0 \qquad\qquad (5.5)$$

where $G(t)$ is called relaxation modulus.

A simple way to describe viscoelastic behaviour is to use rheological models. Those model are assemblages of linear (Hookean) springs and linear (Newtonian) dashpots. A spring element can be described by Hooken's law as

$$\sigma = E\varepsilon \qquad (5.6)$$

and a dashpot is an ideal viscous element and can be described by

$$\dot{\varepsilon} = \frac{\sigma}{\eta} \qquad (5.7)$$

where η is the coefficient of viscosity of the dashpot.

The Maxwell element consists of a spring and a dashpot in series, while the Kelvin element is a parallel coupling of a spring and a dashpot (Fig. 5.1). The compliance for a Maxwell element is given by

$$J(t) = J_0 H(t) + \frac{t}{\eta} \qquad (t>0) \qquad (5.8)$$

The relaxation modulus is

$$G(t) = E\exp(-t/\tau) \qquad (t>0) \qquad (5.9)$$

(a) Maxwell   (b) Kelvin
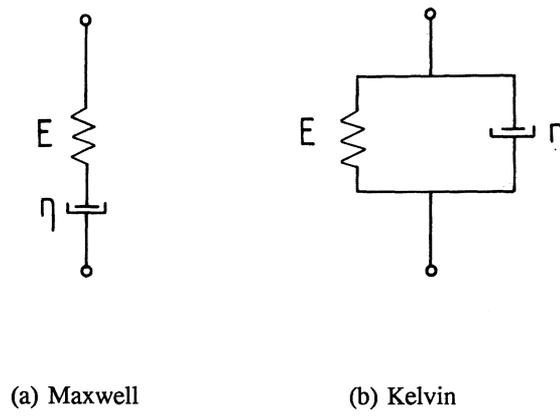
Fig. 5.1 Simple rheological elements
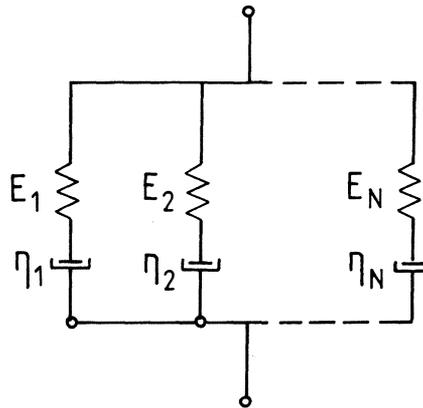
Fig 5.2 Generalized Maxwell model

The simple Maxwell and Kelvin models generally do not predict accurately the behaviour of most materials. Therefore a number of Maxwell or Kelvin elements are usually coupled in series or parallel to fit experimental data. A generalized Kelvin model is well suited to fit creep tests whereas a generalized Maxwell model is more convenient when relaxation data are available.

For the generalized Maxwell model (Fig. 5.2), the relaxation modulus is given by

$$G(t) = \sum_{n=1}^{N} E_n \exp(-\frac{t}{\tau_n}) \qquad (5.10)$$

where $\tau_n = \eta/E_n$ is relaxation time of element n.

For a prescribed strain history $\epsilon(t)$, the corresponding stress can be evaluated from the following integral:

$$\sigma(t) = \int_{-\infty}^{t} G(t-t^*) d\epsilon(t^*) = \sum_{n=1}^{N} E_n \exp(-\frac{t}{\tau_n}) \int_{-\infty}^{t} \exp(\frac{t^*}{\tau_n}) d\epsilon(t^*) \qquad (5.11)$$

According to the trapezoidal rule, the stress increment $d\sigma$ for a small time step dt can be approximately evaluated as

$$d\sigma = \sigma(t+dt) - \sigma(t)$$
$$= \sum_{n=1}^{N} \sigma_n \left(\exp(-\frac{dt}{\tau_n}) - 1 \right) + d\epsilon \cdot \sum_{n=1}^{N} \frac{E_n}{2} \left(\exp(-\frac{dt}{\tau_n}) + 1 \right) \qquad (5.12)$$

where

$$\sigma_n = E_n \exp(-\frac{t}{\tau_n}) \int_{-\infty}^{t} \exp(\frac{t^*}{\tau_n}) d\varepsilon(t^*) \qquad\qquad (5.13)$$

Eq. 5.12 gives the linear viscoelastic constitutive equation on incremental form, which is convenient in numerical analysis.

5.3 The Proposed Time-dependent Crack Model

5.3.1 General considerations

Under long-time loading, time-dependent behaviour may include the time effect both in the fracture zone and outside the zone.

In the part far from the fictitious crack tip, stresses are low and linear visco-elasticity theory can be used. In the high stress zone around the tip, a non-linear creep law should be utilized.

In the Fictitious Crack Model, the static tensile strength serves as criterion for initiation of fictitious crack. Under long-term loading, creep in the high stress zone around the fictitious crack tip may be great enough to reach the tensile strain capacity, so that crack formation can occur below static tensile strength. Therefore the criterion should be adjusted to account for time effect. The time effect on crack criterion may be taken into account by assuming a time-dependent strength criterion for crack initiation. The stress-failure lifetime relation has been used to guide against creep rupture, it seems natural to use such a criterion. Another alternative way may be to use a stress-strain criterion. Reinhardt et al. (1985) has suggested a combined stress-strain criterion both for static and sustained loading. Nevertheless, if a fracture zone already exists, such a time-dependent criterion for crack initiation may not be very important. Therefore in all the theoretical analyses, the static tensile strength is used as criterion.

As far as creep rupture during a short period of a few minutes to a couple of days is concerned, the creep effect outside the fracture zone may be small and neglected. Hence the time effect on softening behaviour in the fracture zone is probably the main source of creep crack growth under creep rupture where tensile fracture behaviour dominates. One possible mechanism may be that stresses transmitted in the fracture zone decrease with time. As a result, the region at the rim of the fracture zone unloads, and the released load drives the fracture zone to progress further.

Time-dependent problems are often solved in increments by dividing time into small steps. Under sustained loading it is usual to evaluate incremental creep strains from stresses at the beginning of the time step and structural responses in the time increment can be obtained by imposing a pseudo load from the creep strains. Obviously this

approach cannot be used in the fracture zone, as the fracture zone should be deforma-tion-controlled. Therefore, an alternative way is chosen in the present modelling . At the beginning of each time step, stress relaxations are computed instead, and consequently a pseudo load can be evaluated from the relaxation stresses. In the next section, a time-dependent constitutive relation for the fracture zone will be proposed based on relaxation tests in uniaxial tension.

5.3.2 Constitutive modelling

The time-dependent σ-w relation may be expressed in the following incremental form:

$$d\sigma = d\sigma^R + d\sigma^I \qquad (5.14)$$

where $d\sigma^R$ and $d\sigma^I$ are stress changes due to relaxation and deformation increment dw respectively during time increment dt.

Since it is quite difficult to perform relaxation tests during a long period of time, accurate stress-time function in relaxation cannot be obtained from the tests. Therefore simple functions based on experimental evidences are proposed in the model to illustrate the main features of time effect in the fracture zone.

Fig 5.3 illustrates the proposed model. During the time increment $dt = t_{i+1} - t_i$, the deformation is first held at w_i and the stress decrease $d\sigma^R$ due to relaxation is $\sigma_A - \sigma_i$; Then, when the deformation increases from w_i to w_{i+1}, the stress can increase until it reaches the envelop of the static σ-w curve at Point B along the path A-B and follow the curve until Point i+1. The stress change $d\sigma^I$ is $\sigma_{i+1} - \sigma_A$. Of course, if the deformat-ion increment dw is small, then Point i+1 may not reach Point B and will instead locate at a point somewhere between A and B.
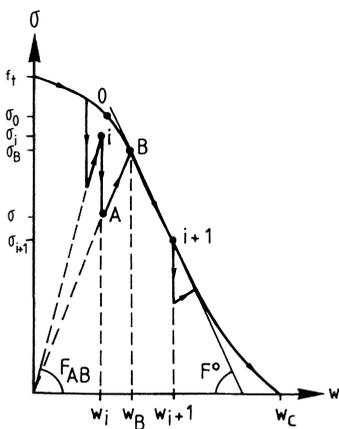
(a) Stress-deformation curve
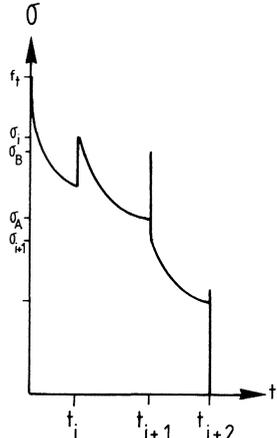
(b) Stress-time curve
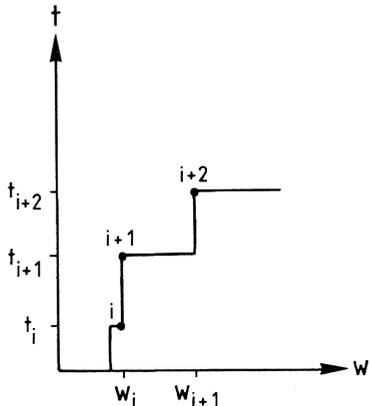
(c) Time-deformation curve

Fig. 5.3 Illustration of the proposed model

The relaxation function of a modified Maxwell model is chosen. Since this is a preliminary study, it is attempted to use a simple rheological element to illustrate the main features of the problems concerned.

The stress relaxation within time increment dt is assumed to be given by

$$d\sigma^R = (\sigma_i - \alpha \sigma_0)\left(\exp(-\frac{dt}{\tau}) - 1\right) \quad \sigma_i > \alpha \sigma_0$$
$$d\sigma^R = 0 \quad \sigma_i \leq \alpha \sigma_0 \tag{5.15}$$

where α is a constant, σ_0 is the stress corresponding to w_i in the static σ-w relation and τ is relaxation time. The relaxation tests in tension show that stress relaxation seems to reach a limit value which is proposed to equal $\alpha\sigma_0$. Therefore in the equation above the term $\alpha\sigma_0$ has been introduced as a relaxation limit. Stress relaxation below the limit is assumed to be zero.

The stress change $d\sigma^I$ is proposed as:

$$d\sigma^I = F*(w_{i+1} - w_i) \quad w_{i+1} \leq w_B$$
$$d\sigma^I = F*(w_B - w_i) + F^0*(w_{i+1} - w_B) \quad w_{i+1} > w_B \tag{5.16}$$

where

$$F = F_{AB}(\exp(-dt/\tau) + 1)/2$$
$$F_{AB} = \frac{\sigma_A}{w_i} = \frac{\sigma_i + d\sigma^R}{w_i} \tag{5.17}$$
$$F^0 = \frac{\partial \sigma^0}{\partial w}(w_B)$$

and $\sigma^0(w)$ represents the static σ-w curve.

   The experimental loading-reloading curve is complicated (see Fig. 4.5). Thus in the model a linear stiffness is proposed in the model to make a simple and proper description of the curve possible.

   In Fig. 5.4 the model is applied to simulate stress-deformation curves in different deformation rates. If the rate is high (close to static loading rate), the stress-deformation curve is near the static one. Meanwhile, the curve deviates more from the static one for slow rate, and the transmitting stress in fracture zone becomes lower than the static one for the same deformation.
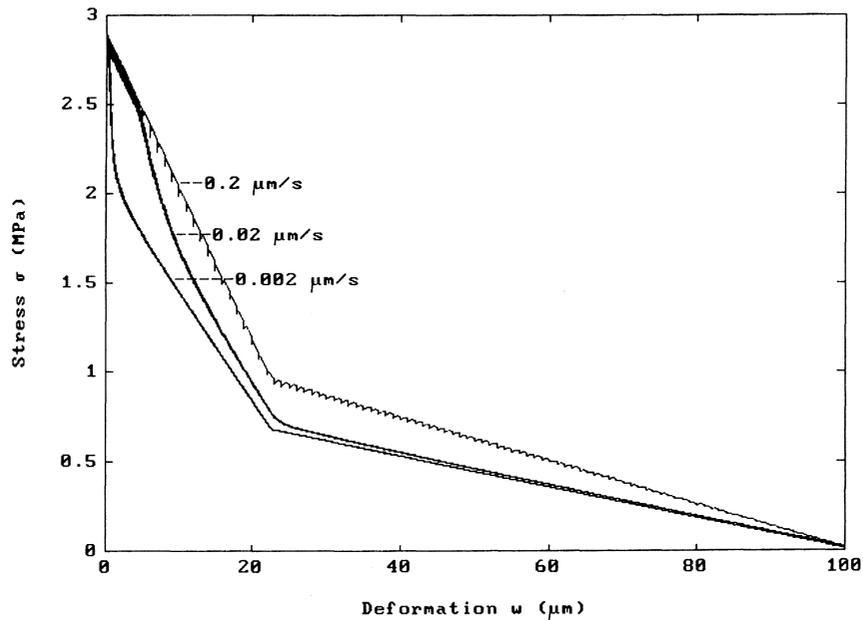
Fig. 5.4 Simulated tensile σ-w curves at different rates according to the model
   $\alpha = 0.7$, $\tau = 25$ second

5.4 Finite Element Implementation

Generally numerical methods are necessary in the application of the Fictitious Crack Model. The finite element method has been used in this thesis. In modelling of the fracture zone, the discrete approach is chosen. No special singular crack elements or very fine meshes are necessary in FCM analysis. A small special program was developed and used in all the calculations.

5.4.1 Finite element formulation

In analyses, the fracture zone is usually modelled by means of springs whose stiffness are calculated according to σ-w curve. The crack propagation path is assumed to be known in advance and is chosen to coincide with the inter-element boundary. Material outside the fracture zone is modelled as linear elastic by using 4-node isoparametric elements or rectangular elements of the Turner and Clough types.

The creep effect is incorporated simply by adding the pseudo load caused by creep to the load vector in the equilibrium equation as:

$$K_T du = dP = dP^{ext} + dP^R \qquad (5.18)$$

where K_T is the tangential stiffness matrix, dP, dP^{ext} and dP^R represent the total load, external load and pseudo load increments respectively. Under sustained loading, the external load increment dP^{ext} is zero.

The incremental pseudo load vector dP^R includes equivalent nodal forces due to stress relaxation in the fracture process zone for the time increment dt. For element e in fracture process zone, the nodal forces due to stress relaxation can be calculated from the following relationship:

$$dP_e^R = -A_e * d\sigma_e^R * \begin{pmatrix} -1 \\ 1 \end{pmatrix} \tag{5.19}$$

where A_e is fracture area represented by the element and $d\sigma_e^R$ is evaluated according to Eq. 5.15.

5.4.2 Numerical solution algorithm

In solving nonlinear problems, an iterative solution procedure is often required. In the standard Newton-Raphson procedure, the stiffness matrix is updated in every single iteration step. Although this procedure needs less iteration, updating of stiffness matrix in each iteration is more expensive. Therefore a modified procedure is used to reduce computational work. In the modified Newton-Raphson method, the stiffness matrix is only updated at the beginning of an increment and then keep constant in all iterations.

In FCM analysis the nonlinear behaviour is caused mainly by the softening of material in FPZ. If the stress-deformation curve is approximated into step-wise linear segments, the global response is able to reproduce by changing material properties in FPZ step-wisely. This approach is simple and able to properly reproduce nonlinear response caused by tensile fracturing in static cases.

In the present analysis of creep fracture, however, the standard Newton-Raphson iteration has been used. At the end of each increment, the residual forces, the differences between external loads and nodal forces from element stresses, are used as a pseudo load to carry out computation. Iterations are carried out until the residual forces are acceptably small according to a given criterion.

5.4.3 Computational procedure

In numerical analysis of creep rupture, the following steps are performed:

Step 1. Perform a static analysis up to the onset of sustained loading, evaluate stresses and deformations and update stiffness matrix K_T.

Step 2. Compute relaxation stresses in the fracture zone for time increment dt according to Eq. 5.15 and evaluate the incremental pseudo load vector dP^R according to Eq. 5.19. Set $dP^{ext} = 0$ and $dP = dP^R$.

Step 3. Solve the system equations and determine displacement increments from

$$du = K_T^{-1} dP \qquad\qquad (5.20)$$

Step 4. Check deformations at certain points to determine if creep rupture of the loading structure has been achieved, for instance if CMOD increment becomes negative. If so, go to Step 8.

Step 5. Find the minimum stress increment $d\sigma_{min}$ for crack initiation at the fictitious crack tip node and calculate the load reduction factor $f = d\sigma_{min}/d\sigma$, where $d\sigma$ is stress increment at the crack tip node corresponding to dP. If $f < 1$, set $f*du \rightarrow du$.

Step 6. Evaluate incremental and total deformations and stresses in the fracture zone, incremental and total element strains and stresses outside the fracture zone, and average stresses at nodes which are located on the crack propagation path. Update stiffness matrix. If $f < 1$, set $(1-f)*dP \rightarrow dP$ and go to Step 3.

Step 7. Find residual forces dP^{re} from difference between nodal forces calculated from element stresses and total external loads. If the following criterion

$$\sqrt{\frac{\sum (dP^{re})^2}{\sum P^2}} < 10^{-6} \qquad\qquad (5.21)$$

is not fulfilled, set dP=dP^{re}, go back to Step 3 and perform iteration until the equilibrium is fulfilled.

Step 8. If creep rupture occurs, perform static computation with deformation-controlled loading until the carrying load of the structure is about zero and then stop. Otherwise return to Step 2 for next new time increment until total loading time is finished.

5.4.4 Program structure

In the present study, a special finite element program was developed to perform the numerical analysis. This program can be used for fracture analysis under both static and sustained loadings. The computational flow chart for the program is shown in Fig. 5.5.

In numerical analysis, the element mesh and topology are created after data input. Then stiffness matrix is established and equivalent loads from gravity loadings are evaluated. According to prescribed loading factor, a time increment and an external load increment are determined. The pseudo load vector due to stress relaxation in the fracture process zone can be calculated for the time increment. The total incremental load vector in turn can be determined. The equation system is solved by the Gauss elimination method.

Check deformations at certain points to see if ultimate load-carrying capacity or creep rupture is reached. For example, if CMOD increment becomes negative, reverse loading directions under static loading if the whole deformation process will be simulated. Under sustained loading creep rupture is achieved when CMOD increment changes sign. The calculation can stop or a static FCM analysis is followed.

Evaluate the stress increment $d\sigma$ and the minimum stress increment $d\sigma_{min}$ to make the maximum principal stress at the fictitious crack tip node reaches the tensile strength, the criterion for crack initiation. Find the load reduction factor $f = d\sigma_{min}/d\sigma$. If $f < 1$, the incremental deformations should be multiplied by the factor f and evaluate the incremental and total strains and stresses, and update stiffness matrix and apply the rest load increments $(1-f)dP$ to perform calculations until the total increment load vector has been applied for the time increment. If $f \geq 1$, evaluate incremental and total strains and stresses. At the end of each increment the residual forces are calculated from the differences between the nodal forces contributed from the external forces and the nodal forces evaluated from element stresses. If the residual forces exceed the given criterion (Eq. 5.21), an iterative loop starts. Otherwise a new step is followed until loading is finished.

```
                        ┌──────────────────────┐
                        │        START         │
                        └──────────────────────┘
                                   │
                    ┌──────────────────────────────────┐
                    │             INPUT                 │
                    │  Input data defining geometry, boundary │
                    │ conditions, loadings and material properties │
                    └──────────────────────────────────┘
                                   │
                    ┌──────────────────────────────────┐
                    │             INIKP                 │
                    │ Create mesh and topology, establish initial stiff- │
                    │ ness matrix, evaluate equivalent load vector for │
                    │ gravity loading and condense stiffness matrix │
                    └──────────────────────────────────┘
                                   │
                    ┌──────────────────────────────────┐
                    │             INCRM                 │
                    │ Evaluate incremental loads dPᵉˣᵗ, dPᴿ and dP │
                    └──────────────────────────────────┘
                                   │
                    ┌──────────────────────────────────┐
                    │             SOLVE                 │
                    │       Solve the equation system   │
                    └──────────────────────────────────┘
```

START

INPUT
Input data defining geometry, boundary conditions, loadings and material properties

INIKP
Create mesh and topology, establish initial stiffness matrix, evaluate equivalent load vector for gravity loading and condense stiffness matrix

INCRM
Evaluate incremental loads dP^{ext}, dP^R and dP

SOLVE
Solve the equation system

CRITER
Ultimate load-carrying capacity or creep rupture is achieved?   **Yes**

No

LOADRF
Find minimum load increment for crack initiation at crack tip node and calculate load reduction factor f.
If $f < 1$, set $f*du \rightarrow du$

$f < 1$

EVALU
Evaluate incremental, total deformations and stresses, residual forces and renew stiffness matrix. If $f < 1$, set $(1-f)*dP \rightarrow dP$

$f \geq 1$

No
ITERCR
Equilibrium criterion satisfied?
Yes

RESULT
Store results in data files

No
FINISH
Loading finished?
Yes

END

Incremental loop

Iterative loop

Fig. 5.5   Flow chart of the computational program developed for fracture analysis

5.5 Summary

A crack model for creep fracture has been proposed. The numerical solution algorithm, computational procedure and program have also been presented.

Chapter 6
Theoretical Analyses and Comparisons

6.1 Introduction

In this chapter, theoretical analyses of creep failure by means of stress-strength approach, linear elastic fracture mechanics and the proposed model will be presented.

6.2 Stress Approach

If creep behaviour of notched structures is essentially ductile, it is possible to use net section stress to predict the failure lifetime. Rupture lifetime is solely related to net section stress as

$$t_{cr} = C * \left(\frac{\sigma_{net}}{f_{net}} \right)^n \qquad (6.1)$$

where C and n are constants, and do not depend on size and geometry of specimens.

For norm concrete, the stress-strength approach may be expected to be true only for structures of very small size.

6.3 LEFM Approach

According to LEFM-based theory of creep fracture (see Appendix B), failure time t_{cr} under creep rupture can be related to stress σ by

$$t_{cr} = \frac{2K_{Ic}^{2-n}}{A(n-2)Y^2\sigma_0^2} \left(\frac{\sigma}{\sigma_0} \right)^{-n} \qquad (6.2)$$

where σ_0 is nominal strength in static fracture.

In three-point bending of notched beams, σ and σ_0 are given in the expressions:

$$\sigma = \frac{3PL}{2Bh^2} = \frac{3PL}{2B(h-a_0)^2} \left(\frac{h-a_0}{h} \right)^2 = \sigma_{net} \left(\frac{h-a_0}{h} \right)^2 \qquad (6.3)$$

and

$$\sigma_0 = \frac{3P_{max}L}{2Bh^2} = \frac{3P_{max}L}{2B(h-a_0)^2} \left(\frac{h-a_0}{h} \right)^2 = f_{net} \left(\frac{h-a_0}{h} \right)^2 \qquad (6.4)$$

In accordance with LEFM, the net flexural strength can be related to the tensile strength (Hillerborg, 1986) by:

$$f_{net} = \frac{1}{Y}\left(\frac{h}{h-a_0}\right)^2 \left(\frac{h-a_0}{a}\right)^{\frac{1}{2}} \left(\frac{h-a_0}{l_{ch}}\right)^{-\frac{1}{2}} f_t \tag{6.5}$$

Combining the equations above, we can obtain the following formula:

$$t_{cr} = \frac{2K_{Ic}^{2-n}}{A(n-2)f_t^2} \frac{a_0}{h-a_0}\left(\frac{h-a_0}{h}\right)^4 \frac{h-a_0}{l_{ch}}\left(\frac{\sigma_{net}}{f_{net}}\right)^{-n} \tag{6.6}$$

or

$$t_{cr} = \frac{2K_{Ic}^{2-n}}{A(n-2)f_t^2}\left(\frac{a_0}{h-a_0}\right)^{1-\frac{n}{2}}\left(\frac{h-a_0}{h}\right)^{4-2n}\left(\frac{h-a_0}{l_{ch}}\right)^{1-\frac{n}{2}}\left(\frac{\sigma_{net}}{f_t}\right)^{-n} \tag{6.7}$$

From the above equations, the failure lifetime is proportional to the dimension for geometrically similar specimens if the stress level (σ_{net}/f_{net}) is the same:

$$t_{cr} \propto h - a_0 \propto h \tag{6.8}$$

However, under the same stress, σ_{net}, the failure time decreases as the dimension increases as follows:

$$t_{cr} \propto \left(\frac{1}{h-a_0}\right)^{\frac{n}{2}-1} \propto \left(\frac{1}{h}\right)^{\frac{n}{2}-1} \tag{6.9}$$

For the same lifetime, strength (σ_{net}) depends on dimension h by

$$\sigma_{net} \propto \left(\frac{1}{h-a_0}\right)^{\frac{1}{n}-\frac{1}{2}} \approx \left(\frac{1}{h-a_0}\right)^{-\frac{1}{2}} \propto \left(\frac{1}{h}\right)^{-\frac{1}{2}} \tag{6.10}$$

1/n-1/2 is approximated as 1/2 since the exponent n for concrete materials is somewhere between 15 and 30 according to Mindess (1984).

The conclusions above can be shown to be also valid for other geometries.
It is known that LEFM is not applicable to fracture behaviour in a concrete structure
of laboratory size. It may be expected that there is a similar limit to the application of
LEFM-based theories to creep crack growth and fracture in concrete.

6.4 The Proposed Model

6.4.1 Flexural creep rupture

The Fictitious Crack Model has proven to be able to predict tensile fracture
behaviour very well. To check if the material properties obtained from the experiments
(see Chapter 4) can be used in the model to describe structural behaviour, numerical
simulations of three-point bending tests are made. The specimen dimension is
840*100*100 mm, and the span is 800 mm. The notch ratio is 0.5. The element mesh
and material data are given in Fig. 6.1. The bilinear σ-w relation proposed by Petersson
(1981) is used, and material properties are taken from Table 4.3 in Chapter 4.

$f_t = 2.8$ MPa
$E = 36$ GPa
$G_F = 82$ Nm/m^2
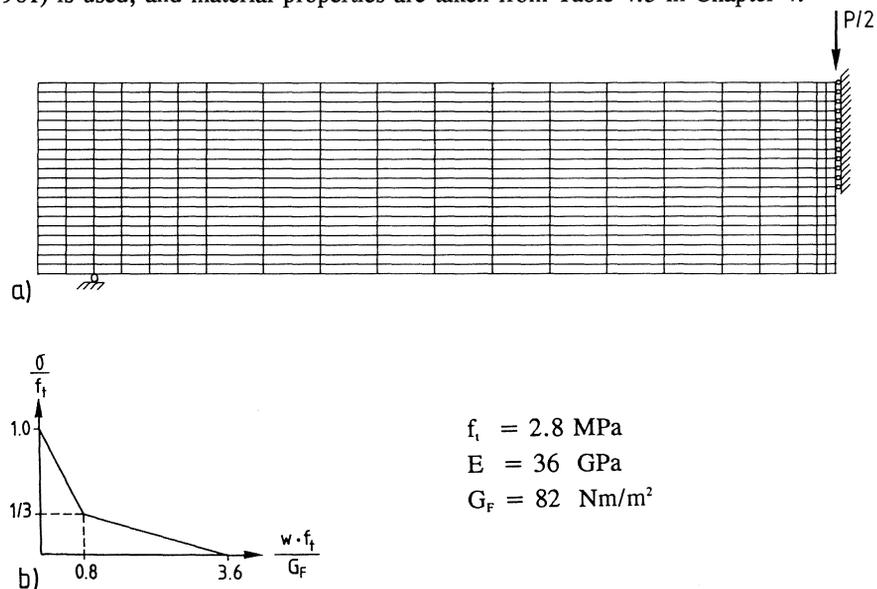
Fig. 6.1 The element mesh and material data for FCM analysis

In determining fracture energy according to RILEM recommendation (1985), the effect of self-weight of beam has been taken into account. To simulate more accurate flexural tests, self-weight has been included in the numerical calculations as an initial load. Fig. 6.2 shows the simulated load-deflection curves with and without self-weight. If the self-weight is not accounted for, the net flexural strength is about 10% lower than the real one and fracture energy G_F is 56 Nm/m^2 and is about 31% less than the input value (82 Nm/m^2). Note that if the self-weight is considered, the calculated fracture energy is about 78 Nm/m^2, which is still less than the input value (82 Nm/m^2). This is because that the last node in the compressive zone is not broken at failure.
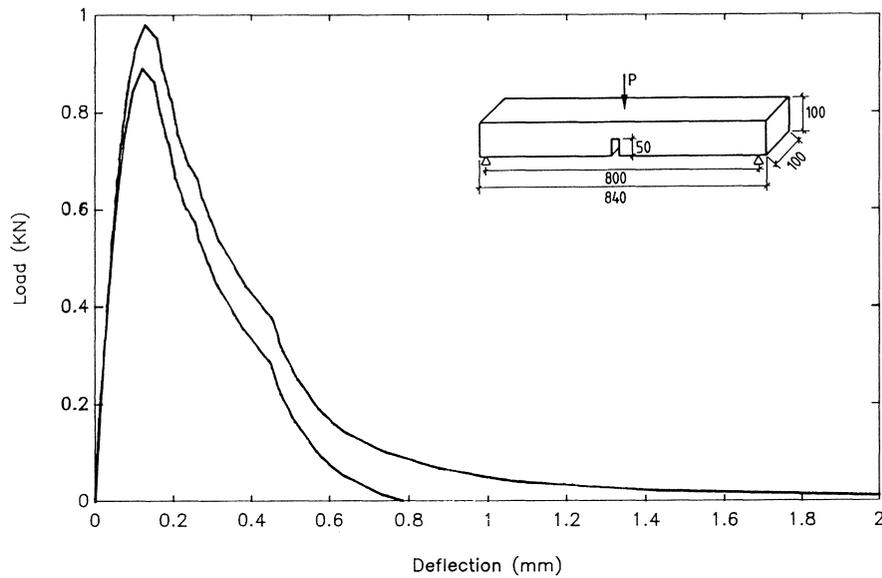
Fig. 6.2 Static load-deflection curves in three-point bending of a notched beam with and without regard to the self-weight

In Fig. 6.2, the simulated curves are not very smooth, which is due to the small number of FCM elements in the fracture zone. To check if a coarse mesh such as the one in Fig. 6.1 can give a fair result, a simulation is made with a fine mesh (the number of elements in the fracture zone is double), as in Fig. 6.3 a. The material law is same as in Fig. 6.1. The comparison is shown in Fig. 6.3 b. The difference is small, and indeed the coarse mesh is able to give a proper result. Therefore the coarse mesh is used in most of the calculations.
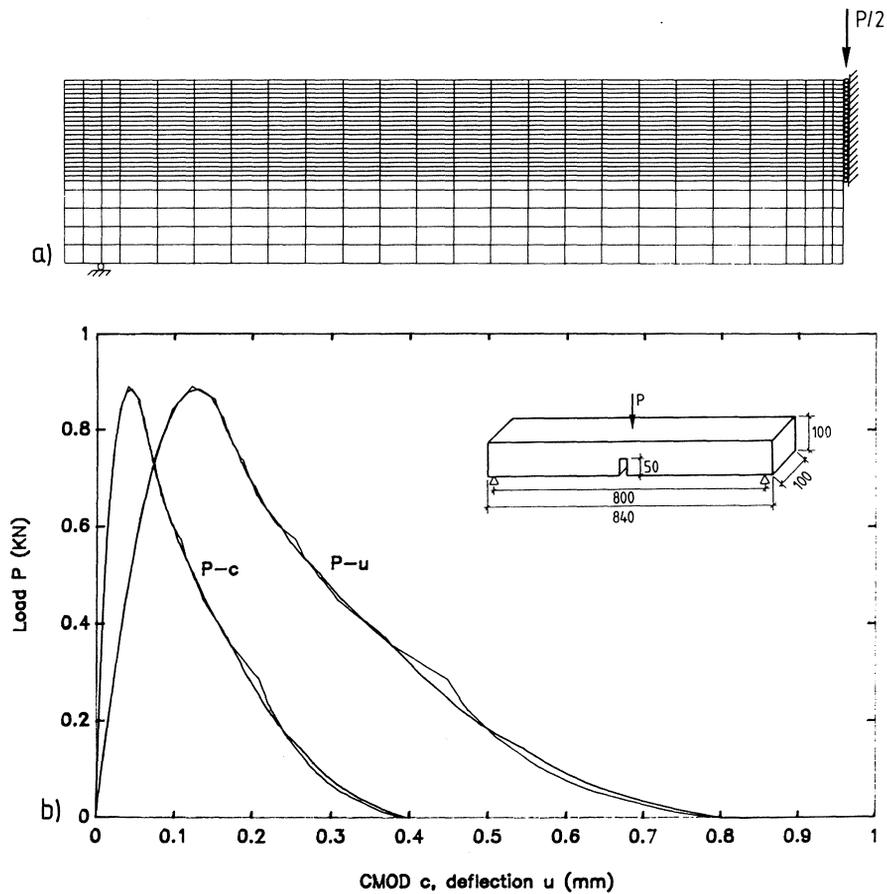
Fig. 6.3   Effect of mesh on simulation of bending

Fig. 6.4 shows the comparison between the static bending tests and the theoretical results. The load-CMOD curves from tests can be simulated quite well.
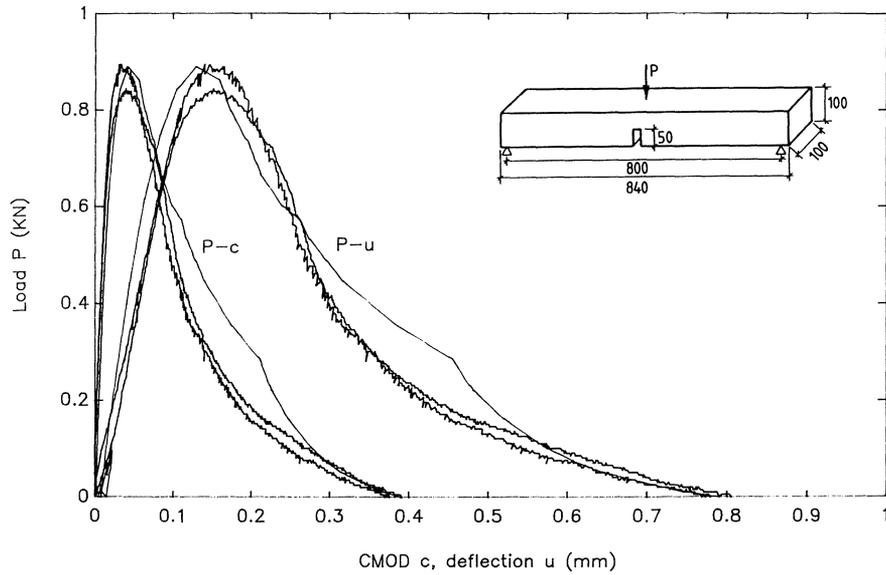
Fig. 6.4   The experimental and theoretical load-deflection and load-CMOD curves in three-point bending

Influence of model parameters

In the proposed model for creep fracture, two material parameters are required in addition to the basic material parameters in FCM. One is limit constant α, and the other is relaxation time τ. According to the relaxation tests (see Fig. 4.8), α is chosen to be 0.7.

If α increases, failure life predicted will be longer. If τ increases, the failure life will increase proportionally since a linear relaxation function is chosen in the model. Table 6.1 shows the influence of α and τ on failure time for bending rupture of a notched beam (Fig. 6.1) is shown.

In order to obtain good correlations with both the tensile relaxation tests and flexural creep rupture tests (Figs. 6.7 and 6.8), τ is chosen to be 25 second in all the remaining calculations.

Table 6.1 Influence of α and τ on failure time

Stress level σ_{net}/f_{net}	Constant α	Relaxation time τ (s)	Failure time t_{cr}(s)
0.76	0.70	50	3328
0.76	0.65	50	1610
0.76	0.60	50	1150
0.76	0.60	100	2230
0.76	0.60	200	4470

Load-CMOD curves in static and sustained loadings

Fig. 6.5 shows the theoretical load-deflection and load-CMOD curves both in static loading and sustained loading. The specimen dimension, element mesh and material law are the same as shown in Fig. 6.1. Four different sustained tests at load levels $P/P_{max}=0.92$, 0.85, 0.8 and 0.76 are simulated. P_{max} is the maximum load from the theoretical simulation of a three-point bending test under static loading.
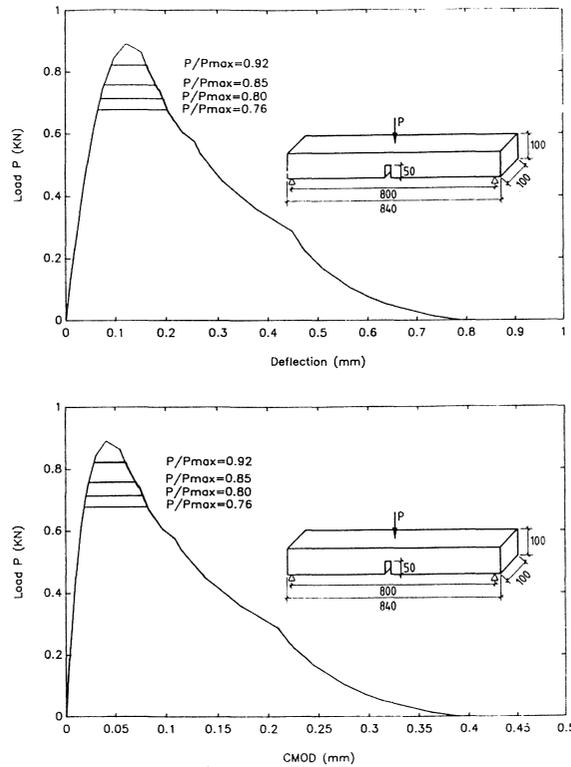
Fig. 6.5   Theoretical load-deflection and load-CMOD curves under static and sustained loading

For each load level, the following computation procedure is carried out. First a static calculation is performed, until the prescribed sustained load is reached. Then the creep fracture analysis starts in time increments which are small enough to allow stable and accurate numerical calculations. In each time step, relaxation stresses are evaluated

according to the relation given in the preceding chapter. At the end of the time step, a pseudo load evaluated from the relaxation stresses is imposed and a static calculation is made to determine displacements and deformations. The calculation continues in this way up to the failure point where the equilibrium cannot be maintained under the pre-scribed sustained load. Subsequently a static calculation without creep is performed again with a decreasing load till the load is about zero.

Under each sustained load, CMOD increases until failure occurs when it almost reach the descending branch of the static load-CMOD curve. It is consistent with experimental results of flexural rupture tests which seem to indicate such a trend.

It is interesting that the static load-CMOD curve is followed after sustained loading if a deformation control test is made possible. This is similar phenomenon observed in fatigue tests. In deformation-controlled fatigue tests, failure will occur when the deformation reaches the descending part of the static load-deformation curve and then follow the rest of the curve. It is believed that a similar effect will occur in creep rupture tests if tests can be performed by deformation control.

Table 6.2 gives fracture energy as evaluated from the area under load-deflection curves for both static and sustained loadings. Fracture energy decreases to just 95.4% when the sustained loading P/P_{max} is as low as 0.76. Hence sustained loading at a high load level does not seem to have a significant effect on fracture energy according to the model. Hansen (1991) performed three-bending tests subjected to constant loads by regulating deflections. It was found that sustained tests at high load levels does not influence so much fracture energy, compared to fracture energy determined from static bending tests.

Table 6.2 Calculated fracture energy under sustained loading

Load level	Fracture energy (Nm/m²)	Percentage (%)
1.00	77.9	100.0
0.92	77.3	99.2
0.85	76.2	97.8
0.80	75.2	96.5
0.76	74.3	95.4

Creep curves

Figs. 6.6 to 6.9 show the simulated CMOD-time curves for stress levels σ_{net}/f_{net} = 0.92, 0.85, 0.8 and 0.76 respectively. The experimental creep curves are also plotted to facilitate comparisons.

The theoretical creep curves seem to be quite similar to the experimental ones. The creep curves display three stages. CMOD grows rapidly at the beginning and then slows down to keep increasing at a constant rate. At the third stage CMOD increases very rapidly to failure.

The third stage seems to start somewhere when CMOD becomes greater than the value (44 um; see Fig. 6.4) at the peak point in the static load-CMOD curve. In fatigue pull-out tests (Balazs, 1986), the deformation at the peak point in the static load-deformation curve is proposed as a criterion for fatigue failure. If a similar criterion is used for creep rupture, it may lead to a safer criterion since the time to reach this criterion is about 70-80% of the total failure life from both the theoretical and experimental results.

It may be observe that the CMOD values are higher than the experimental ones. This is due to the difference in the static load-CMOD curves, as the simulated load-CMOD curve differs a bit from the experimental one.
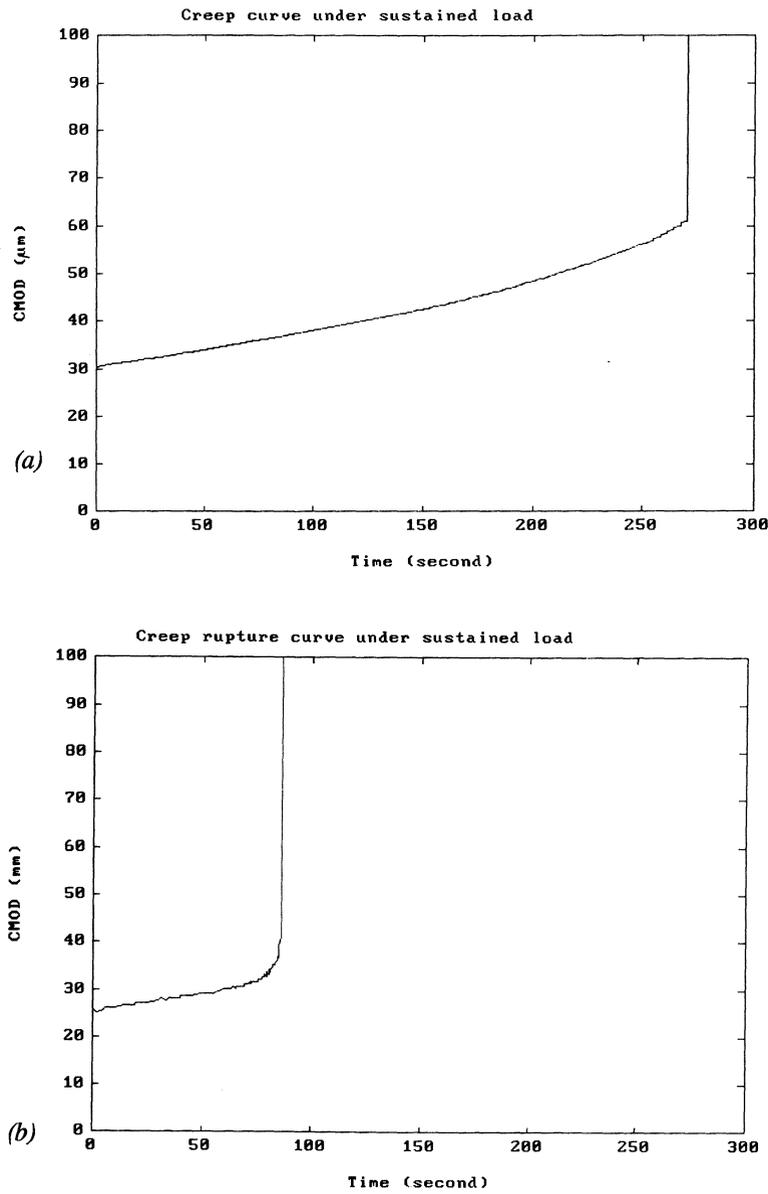
Fig. 6.6 Sustained load level $\sigma_{net}/f_{net} = 0.92$.
        (a) Theoretical CMOD-time curve;
        (b) Experimental CMOD-time curve.
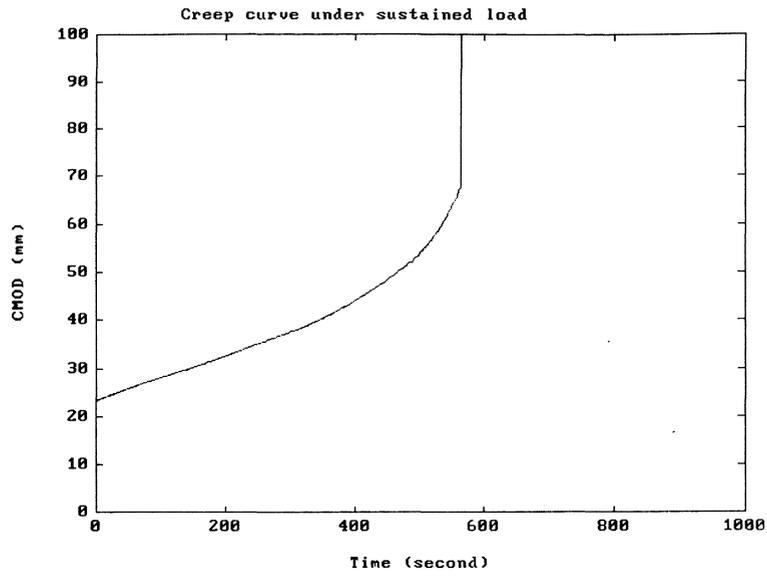
(a)
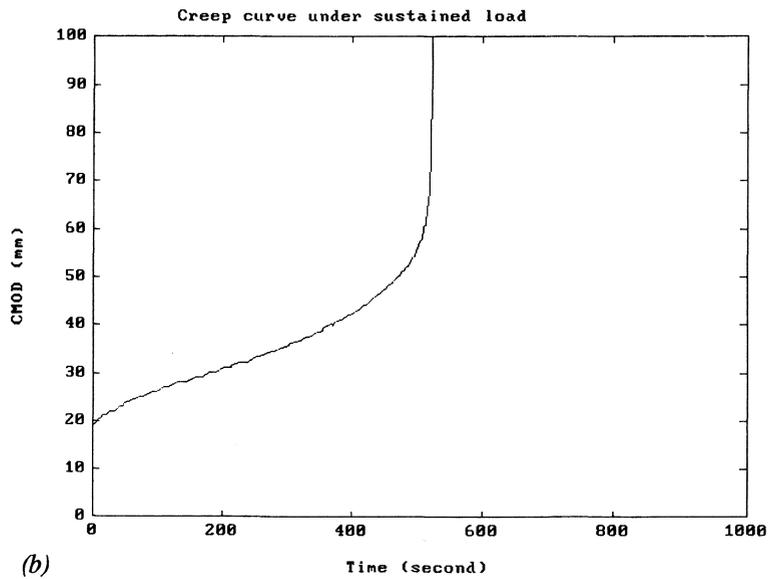
(b)

Fig. 6.7 Sustained load level $\sigma_{net}/f_{net} = 0.85$.
(a) Theoretical CMOD-time curve;
(b) Experimental CMOD-time curve.
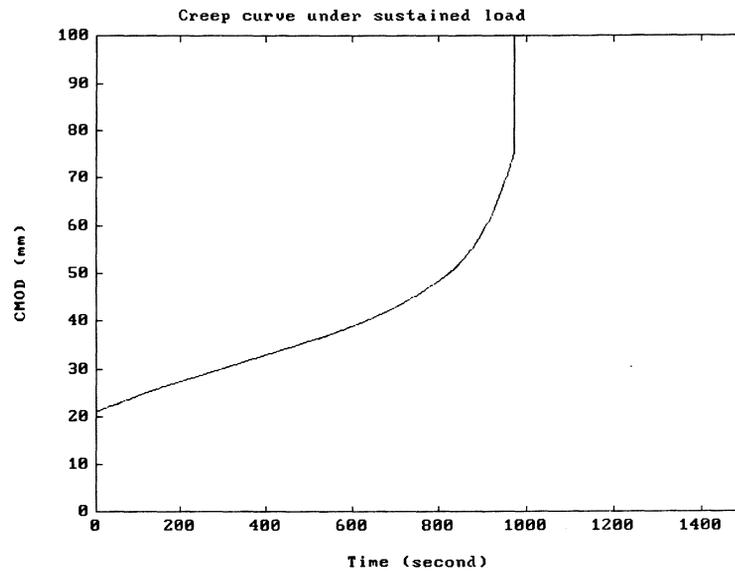
(a)
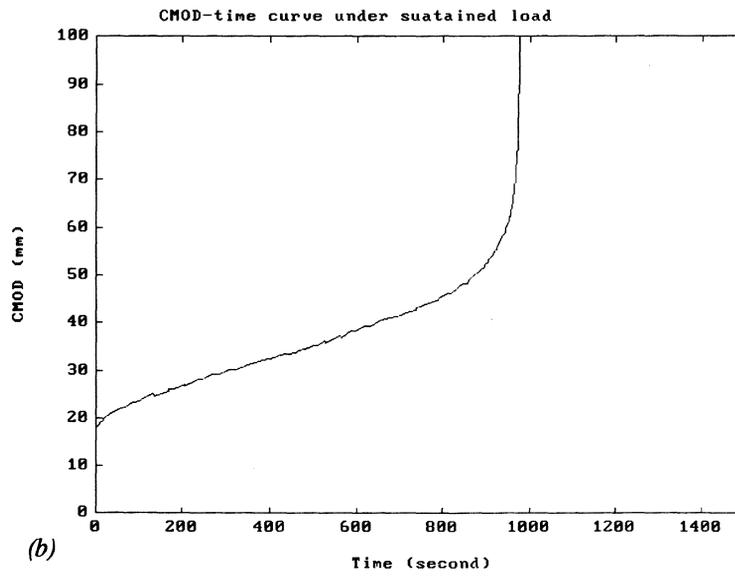
(b)

Fig. 6.8 Sustained load level σ_{net}/f_{net} = 0.80.
(a) Theoretical CMOD-time curve;
(b) Experimental CMOD-time curve.
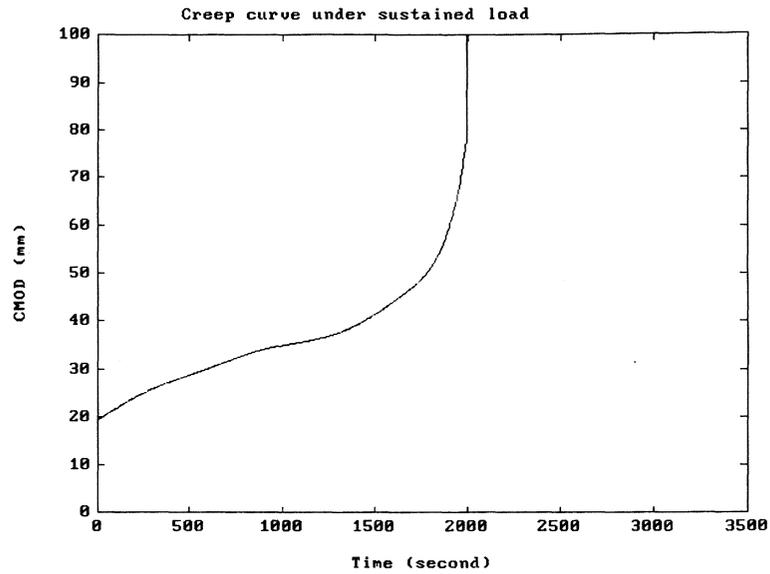
(a)
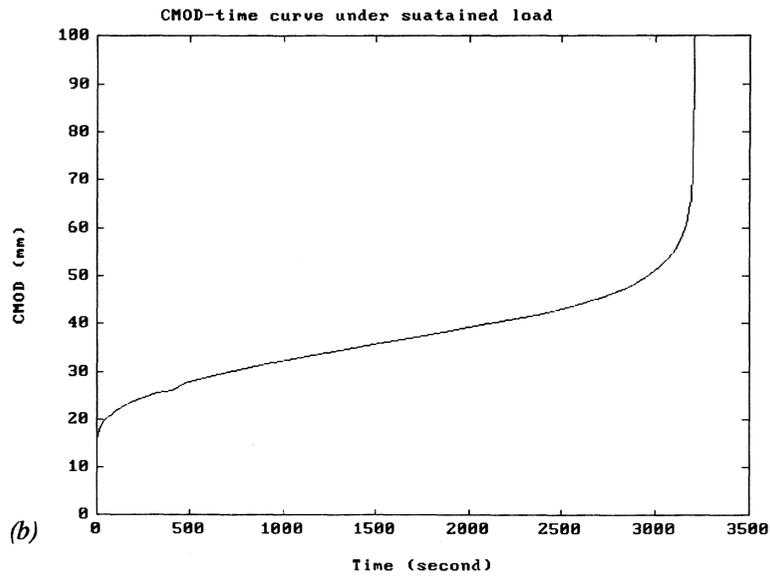
(b)

Fig 6.9 Sustained load level $\sigma_{net}/f_{net} = 0.76$.
    (a) Theoretical CMOD-time curve;
    (b) Experimental CMOD-time curve.

Stress distributions and creep crack growth

The stress distributions within the fracture zone at different stages are plotted in Fig. 6.10. The stress level σ_{net}/f_{net} is 0.80. the fine mesh (Fig. 6.3 a) is used.

Fig. 6.11 shows the growth of fictitious crack with time. a_f is the total crack length measured from crack mouth to fictitious crack tip. The fictitious crack tip moves quickly in the beginning and then smoothly and very rapidly in the last stage.
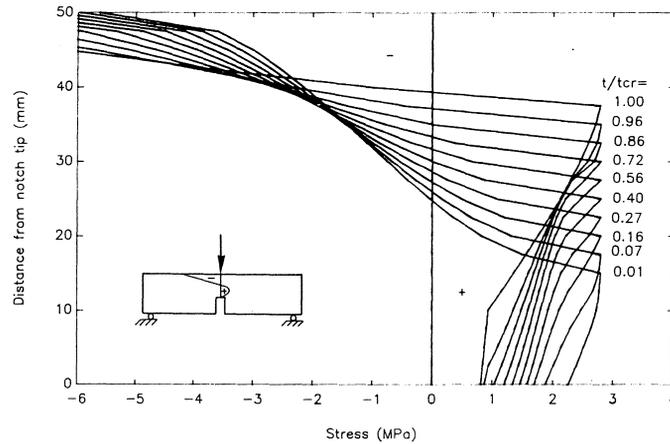
Fig. 6.10 Stress distributions In fracture zone, sustained load $\sigma_{net}/f_{net} = 0.80$
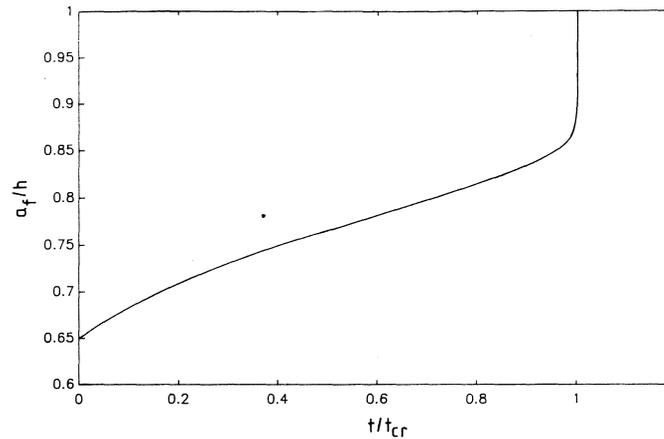
Fig 6.11 Propagation of the fictitious crack tip. a_f is the total crack length measured from crack mouth to fictitious crack tip.

Stress-failure lifetime curve

The theoretical stress-failure lifetime curve is depicted in a double logarithm in Fig. 6.12. Compared with the experiments (Fig. 4.14), it has a steep slope and predicts a longer failure time at higher stress levels. This is because a simple relaxation relation is used, and relaxation rate is proportional to stress. In fact, a non-linear relaxation function may predict the creep behaviour in the fracture zone much better since the stress-deformation σ-w curve seems more sensitive to time effect in the initial, high-stress stage. Nevertheless the model seems to predict the stress-failure time reasonably well with regard to a simple relaxation function employed in the analysis.
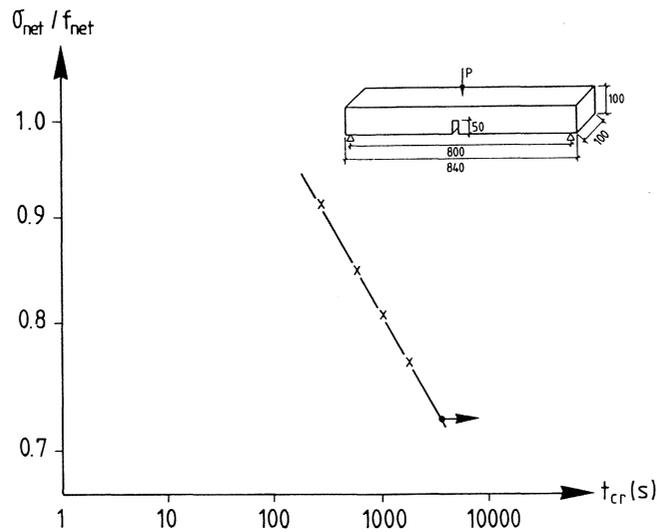
Fig. 6.12 Theoretical stress-failure lifetime curve

Size effect

In static loading, fracture behaviour exhibits size-dependency. As the size of a geometry similar specimen increases, the fracture behaviour changes from ductile to brittle, the structural strength become lower. It might be expect size effect exists in creep fracture.

Fig. 6.13 shows the theoretical size effects on rupture life of sustained bending beams at two stress levels σ_{net}/f_{net} = 0.9 and 0.85. Both length and height of beams increases or decreases proportionally and the same mesh as in Fig 6.1 a is used in each calculation. No self-wight has been accounted. The rupture life does not seems to change very much for small beams and increases more for larger ones. It is more remarkable for lower sustained loading (σ_{net}/f_{net}=0.85) than higher one. From LEFM the failure life seems to increase proportional with increasing size. The size effect may be explained as follows. For small beams fracture zone is large compared to dimension of specimen, and fracture behaviour is more ductile, the failure lifetime is determined solely by stress level. While for a large size specimen fracture behaviour is still dominated by the stress intensity factor K, thus LEFM should be applicable, failure lifetime depends not only on stress level, but also on specimen size.
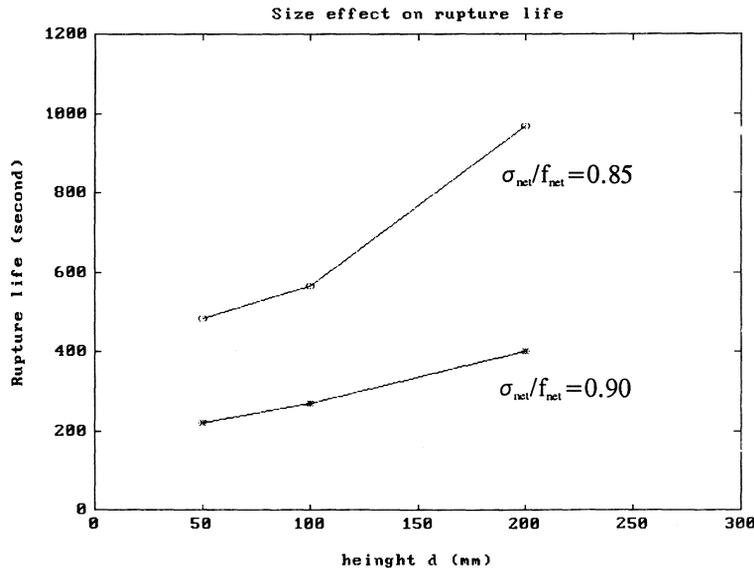
Fig. 6.13 Size effect on failure lifetime in sustained bending of notched beams

Influence of shrinkage

Experiments available in the literature (Mindess et al., 1974) suggest that the failure time for dry specimens is 5-order higher than that for wet ones. One factor may be initial stresses induced by dry shrinkage. Therefore sustained bending of unnotched beams with initial stresses is simulated. The initial shrinkage stress distribution is assumed to be parabolic within the fracture cross-section at the beginning (Fig. 6.14). Such an assumption has been used in analysis of bending tests on dry beams and produces best agreement with tests (Petersson, 1981).

The net flexural strength of the dry specimen decreases to 0.84 of the wet one. At the same sustained load level (sustained stress/static flexural strength), the rupture life for the dry one does show an increase over the wet one, but only about 1.5 times that of the wet one. It seems that the initial stress caused by shrinkage can only partly explain the difference in failure lifetime. Probably the properties of a fracture zone in dry concrete differ quite a lot from those in a wet specimen, especially as far as the time-dependent behaviour is concerned.

$$\sigma_s = f_t \qquad \sigma_s = 0.5\, f_t$$
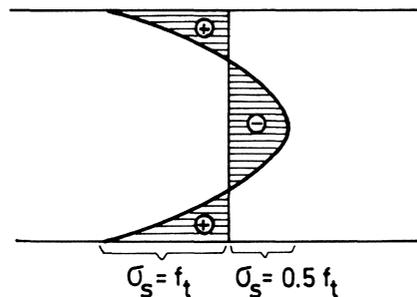
Fig. 6.14 Assumed parabolic distribution of shrinkage stresses across fracture cross-section (Petersson, 1981)

6.4.2 Compact tensile creep rupture

Compact tension tests have been simulated numerically. The sizes of the specimens are given in Table 4.1, and material properties are the same as those used for simulations of bending tests (Fig. 6.1 b). The element meshes are showed in Fig. 6.15. Four-node isoparametric elements are used.

a)

$$\frac{a}{W} = 0.4$$

b)
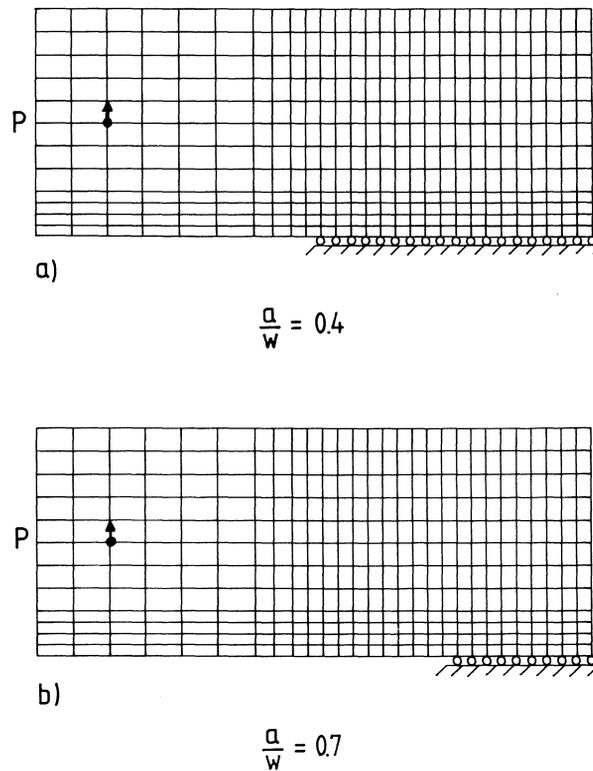
$$\frac{a}{W} = 0.7$$

Fig. 6.15 Element meshes for simulation of compact tension tests
       (a) a/W = 0.4;
       (b) a/W = 0.7.

Load-CMOD curve in static loading

Numerical simulations of load-CMOD curves in static loading are plotted in Fig. 6.16. Compared to experimental results, the numerical results agree fairly well both for notch ratios a/W = 0.4 and 0.7. The differences become greater in the descending parts of the load-CMOD curves. Probably because fracture energy determined from three-point bending tests is slightly greater than that from compact tension tests, since fracture energy from bending of notched beams was used in numerical modelling.
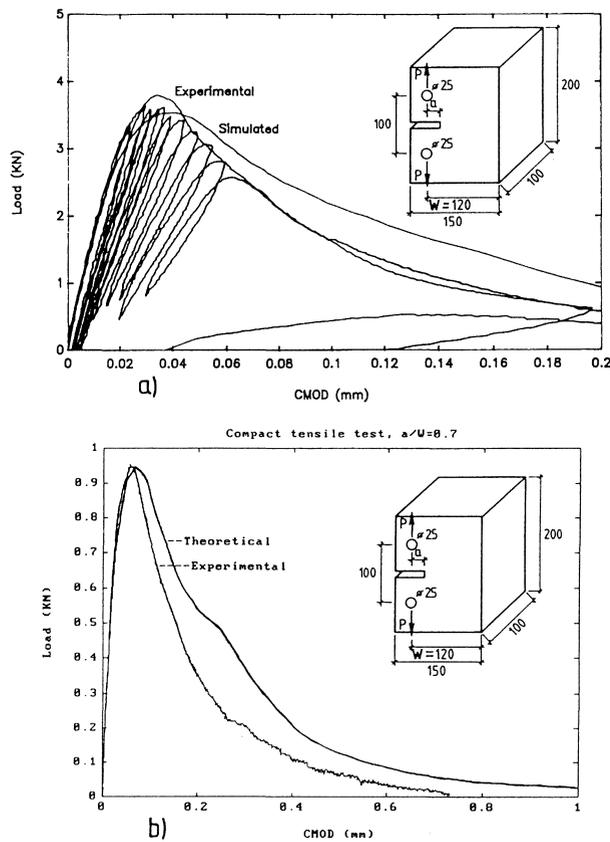
Fig. 6.16 Comparison between the simulated and experimental Load-CMOD curves
in static compact tension
(a) a/W = 0.4;
(b) a/W = 0.7.

Load-CMOD curves in sustained loading

Load-CMOD curves at sustained load levels (P/P_{max}=0.80 and 0.90) are depicted in Fig. 6.17. According to the model, failure occurs when the total CMOD (=elastic + creep CMOD) is equal to the deformation in the descending part of static load-CMOD curve corresponding to the sustained load P.
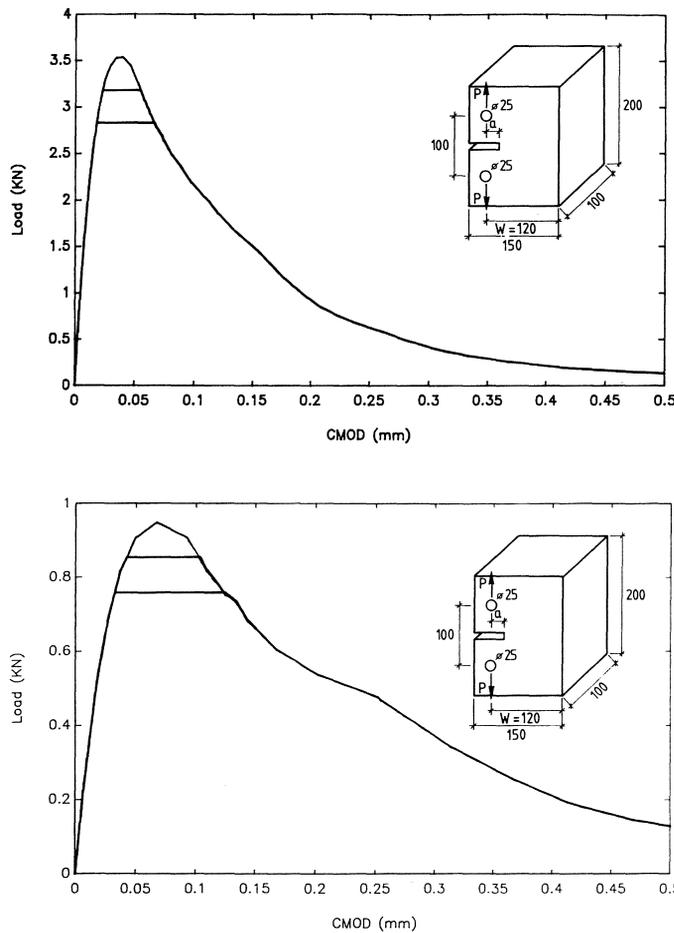
Fig. 6.17 Load-CMOD curves in compact tension subjected to sustained loading
        (a) a/W = 0.4;
        (b) a/W = 0.7.

Creep curves

Creep CMOD-time curves for a/W = 0.4 and 0.7 are shown in Figs. 6.18 and 6.19 respectively. Sustained load levels (P/P$_{max}$) are 0.80 and 0.90.

a)

b)
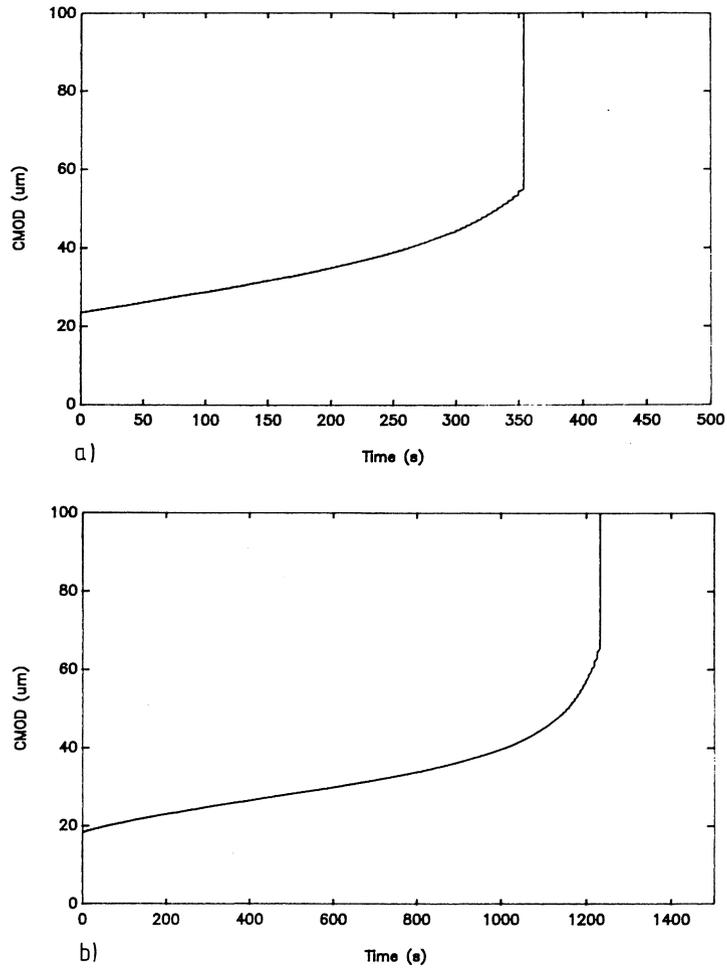
Fig. 6.18 Creep CMOD-time curves in compact tension subjected to sustained load
(a) a/W = 0.4, P/P$_{max}$ = 0.90;
(b) a/W = 0.4, P/P$_{max}$ = 0.80.
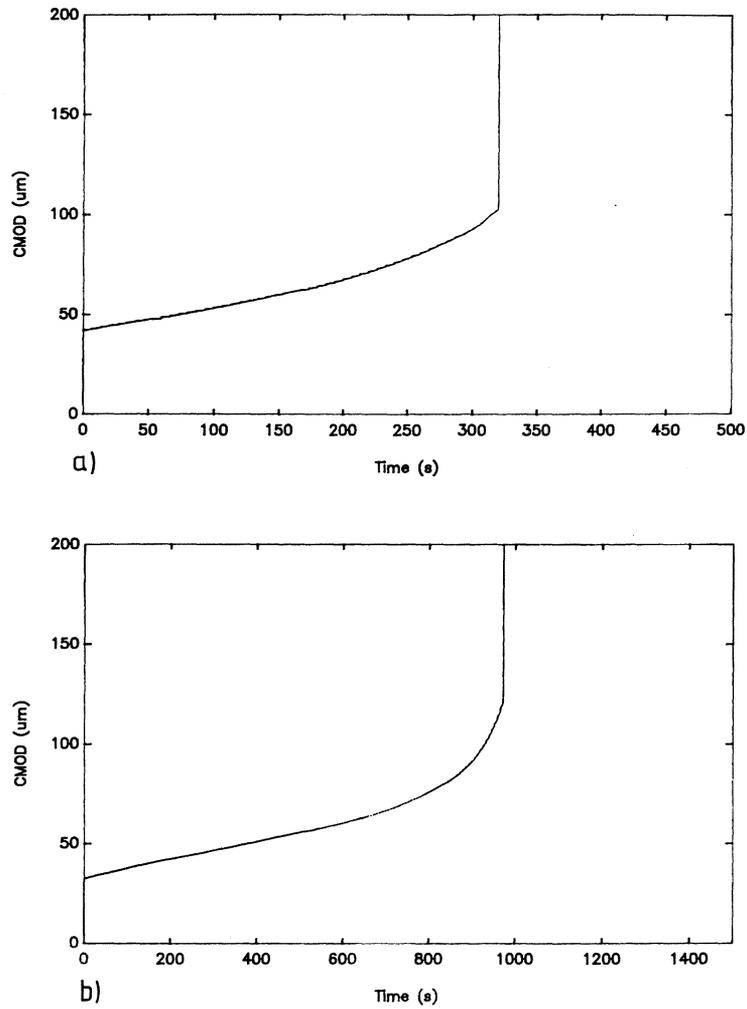
Fig. 6.19 Creep CMOD-time curves in compact tension subjected to sustained load
          (a) a/W = 0.7, P/P$_{max}$ = 0.90;
          (b) a/W = 0.7, P/P$_{max}$ = 0.80.

Stress-failure lifetime relation

Fig. 6.20 shows the theoretical prediction of stress-failure lifetime for compact tension creep rupture for both a/W = 0.4 and 0.7.
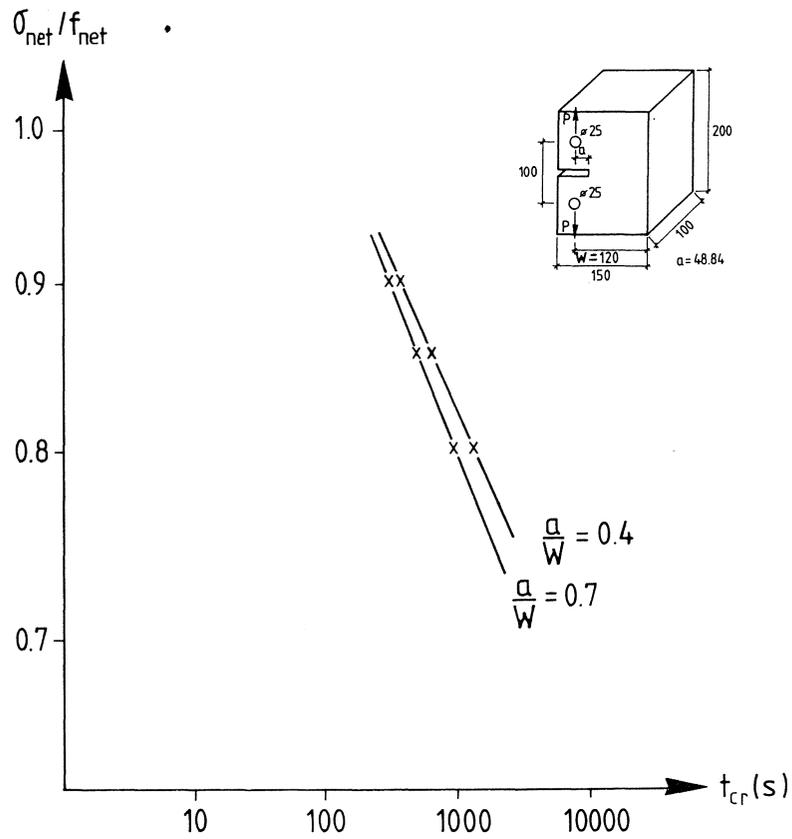
Fig. 6.20 Theoretical stress-failure lifetime relations
in compact tension creep rupture

6.5 Discussions and Conclusions

Application analyses of LEFM and the proposed model for creep fracture have been made. For normal sized laboratory specimens, LEFM-based approaches might not be directly applicable for creep fracture. To predict real fracture behaviour, the proposed model has taken creep effect in the fracture zone into account.

The model has been employed to predict the creep curves, load-deformation relations, stress-rupture life curves and size effect etc. Although simple assumptions are made for the creep effect in a fracture zone, the model seems to predict creep fracture behaviour fairly well, when compared with the experimental results.

Chapter 7
Concluding Remarks

7.1 Summary

The thesis aims at developing a crack model for time-dependent fracture behaviour in concrete by applying the Fictitious Crack Model (FCM). Both experimental (see Chapter 4) and theoretical (Chapters 5 and 6) studies have been carried out.

Time effects on material properties (the σ-w curve, G_F) in the fracture zone are necessary to construct a time-dependent crack model in concrete. Thus tensile relaxation tests on notched cylinders were performed to investigate the sensitivity of properties in the fracture zone to loading time. Rate effect on fracture energy has been investigate by determining fracture energy from bending tests on notched beams at varying deformation rates.

Another type of test is rupture test. It is attempted to investigate time-dependent crack growth and fracture under sustained loading. In addition, the results provided a comparison basis for the theoretical model. Flexural and compact tensile rupture tests were carried out on specimens of various notch ratios.

By applying the basic idea of FCM, a time-dependent crack model is proposed. The descending stress-deformation (σ-w) relation is used to describe the softening behaviour of the fracture process zone, while linear elastic behaviour is assumed outside the zone.

111

Time-dependency of the σ-w relation in the fracture zone has been taken into account by introducing a relaxation function of modified Maxwell type.

The model has been applied to analyze crack growth and failure life both for flexural rupture and compac tension rupture of plain concrete specimens subjected to sustained loads.

In the present studies creep outside the fracture zone has not been considered, since the main attention is focused on the time effect in the fracture zone. On the other hand, as rupture tests with wet specimens last only several hours, creep outside fracture zone is probably quite small. Static tensile strength is used as the criterion for crack initiation.

7.2 Conclusions

From the present work, the following main conclusions may be drawn.

The stress-deformation relation seems sensitive to loading rate. In relaxation tests when the deformation is held constant for a period and then continue to increase, the stress does not regain the value at the beginning of the holding time. However, such damage seems to have no significant effect on the later part of the σ-w curve. It seems a stress-deformation relation may be unique for a loading rate.

Fracture energy seems to decrease as loading rates become slower.

Under rupture tests of both flexure and compact tension, deformations (LPD or CMOD) increase with time in three stages. In the primary stage the deformation rate decreases and become constant in the secondary stage. In the tertiary stage the deformation rate increases rapidly until failure. The secondary stage dominates the entire failure lifetime, and the secondary deformation rate appears to have a good correlation with the failure life.

The proposed model seems to be able to properly predict time-dependent fracture behaviour in concrete, when compared with the experimental results presented in Chapter 4.

7.3 Further developments

Some further development may be suggested as in the following.

* To include creep effect outside the fracture zone.

* To include the time-dependent criterion for crack initiation, i.e. tensile strength is function of time.

* To investigate the time-dependent softening behaviour for varying concrete materials.

* To study the influence of moisture on time-dependency of stress-deformation relations.

Appendix A
EXPERIMENTAL DATA

Table A.1 Tensile relaxation

Test No.	σ_0/f_t	σ^{rl}_m/σ_0	Holding time t (minute)
TSRB1	0.97	0.63	60
	0.63	0.75	30
	0.33	0.73	30
TRRB2	0.92	0.60	50
	0.62	0.70	40
	0.13	0.72	30
TSRB3	0.92	0.80	60
TSRLA	0.91	0.68	25
	0.23	0.65	25
TSRLB	0.97	0.62	40
	0.63	0.63	35
	0.33	0.71	25
TSRLC	0.95	0.69	40
	0.71	0.63	40
	0.24	0.71	30

Note: (1) σ_0/f_t is the initial stress level at the beginning of holding period;

(2) σ^{rl}_m/σ_0 is the stress relaxation level at time t=20 minute.

Table A.2 Rate effect on fracture energy

Deflection rate (um/s)	No. of specimen	Fracture energy (Nm/m²)
0.05	3	68
0.2	4	71
2	4	76
50	3	90

Table A.3 Flexural rupture tests of unnotched beams

Test No.	Stress level σ/f_f	Failure time t_{cr} (s)
BULC8	0.95	15
BULC4	0.90	105
BULC7	0.90	210
BULD4	0.85	540
BULD5	0.85	600
BULD7	0.80	960
BULB4	0.80	1200
BULD6	0.76	7200
BULC6	0.70	> 10000
BULD3	0.67	> 10000

Table A.4 Flexural rupture tests of notched beams

Test No.	σ/f_{net}	t_{cr} (s)	$d\tau/dt$ (um/s)	Rupture $CMOD_{cr}$ (um)	Static $CMOD_{cr}$ (um)
92A	0.92	20		50	50
92B	0.92	70	0.2233	46	50
85A	0.85	190	0.1102	55	62
85B	0.85	530	0.0474	58	62
80A	0.80	550	0.0380	65	70
80B	0.80	580	0.0427	72	70
80C	0.80	360	0.0747	73	70
80D	0.80	980	0.0202	69	70
76A	0.76	930	0.0262	73	77
76B	0.76	3200	0.0071	81	77
76C	0.76	2400			

Notes: (1) $d\tau/dt$ is the rate of CMOD in the secondary stage in creep curves.
(2) CMOD in Column 5 is the value at rupture failure while CMOD in Column 6 is the value taken from the descending part of static curves at the same stress level.

Table A.5 Compact tensile rupture tests

Test No.	Notch ratio a/W	Stress level σ/f_{net}	Failure time t_{cr} (s)
CTC4B1	0.4	0.90	240
CTC4B2	0.4	0.90	220
CTC4C3	0.4	0.86	360
CTCFB1	0.4	0.86	520
CTCFB4	0.4	0.84	2100
CTCFC2	0.4	0.80	7200
CTC7B1	0.7	0.90	60
CTC7C1	0.7	0.85	330
CTC7C3	0.7	0.85	250
CTC7C2	0.7	0.80	2580

Appendix B
LEFM Theory for Creep Fracture

The time-dependent crack growth in brittle materials is usually related to the stress intensity factor K_I by an empirical relationship:

$$\frac{da}{dt} = AK_I^n \qquad (B.1)$$

where A and n are material constants.

As shown by Nadeau, Bennett and Fuller (1982), the dependency of strength on loading rate or rupture time can be derived from the equation above. The derivatives will given in the following.

B.1 Constant load

The stress intensity factor K_I is usually expressed as

$$K_I = Y\sigma\sqrt{a} \qquad (B.2)$$

where Y is geometry factor, σ is nominal stress and a is crack length.

Inserting K_I into Eq. B.1 and integrating it, assuming that Y is not dependent on actual crack length a, we can obtain:

119

$$\int_{a_0}^{a_c} a^{-\frac{n}{2}} Y^{-n} da = A\sigma^n \int_{t_0}^{t_{cr}} dt \qquad\qquad (B.3)$$

where a_0 is the initial crack length, a_c the crack length at failure under constant load σ, t_0 is failure time under stress σ_0 and can be assumed to be zero, t_{cr} is failure time under stress σ (less than σ_0).

Suppose that fracture toughness K_{Ic} is the same both in static and creep fracture:

$$K_{Ic} = Y\sigma_0\sqrt{a_0} = Y\sigma\sqrt{a_c} \qquad\qquad (B.4)$$

Eq. B.3 becomes:

$$t_{cr} - t_0 = \frac{2K_{Ic}^{2-n}}{(2-n)AY^2\sigma^2}\left((\frac{\sigma_0}{\sigma})^{n-2} - 1\right) \qquad\qquad (B.5)$$

Since n is large enough, the equation can be simplified as

$$t_{cr} = \frac{2K_{Ic}^{2-n}}{(2-n)AY^2\sigma_0^2}(\frac{\sigma}{\sigma_0})^{-n} \qquad\qquad (B.6)$$

Thus a logarithmic plot of applied stress σ versus rupture time will give a slope of -1/n.

B.2 Constant loading rate

For a constant loading rate $\dot{\sigma}$, we can similarly obtain:

$$\sigma^{n+1} = -\frac{2(n+1)K_{IC}^{2-n}}{(n-2)AY^2\sigma_0^{n-2}}\left((\frac{\sigma}{\sigma_0})^{n-2}-1\right)\dot{\sigma} \qquad (B.7)$$

If n is large, the equation can be simplified as:

$$\sigma^{n+1} = \frac{2(n+1)K_{IC}^{2-n}}{(n-2)AY^2\sigma_0^{n-2}}\dot{\sigma} \qquad (B.8)$$

If failure stress σ is plotted versus loading rate $\dot{\sigma}$ in a double logarithm, the slope of the curve will be $1/(n+1)$.

REFERENCES

50 FMC Draft Recommendation (1985): "Determination of the fracture energy of mortar and concrete by means of three-point bending testing on notched beams". *Materials and Structures, RILEM, Vol. 18, No 106, pp. 287-290.*

Akutagawa, S., F.L. Jeung, N.M. Hawkins, B.M. Liaw, Du Jiaji & A.S. Kobayashi (1991): "Effects of loading history on fracture properties of concrete". *ACI Materials Journal*, Vol. 88, No. 2, March-April 1991, pp. 170-180.

Alfaiate, J., E.B. Pires & J.A.C. Martins (1991): "The influence of the nonlinear bulk behaviour of concrete on the size-dependency of G_F". In *Proceedings of the International RILEM/ESIS Conference*, Eds. J.G.M. van Mier, J.G. Rots and A. Bakker, E & FN Spon, 1991, p. 966.

Al-kubaisy, M.A. & A.G. Young (1975): "Failure of concrete under sustained tension". *Magazine of Concrete Research,* Sept 1975, Vol. 27, No. 92, pp. 171-178.

Anderson, H. & H. Bergkvist (1970): "Analysis of a non-linear crack model". *J. Mech. Phys. Solids,* Vol. 18, pp.1-28.

Ansari, F. (1989): "Mechanism of microcrack formation in concrete". *ACI Materials Journal,* Vol. 86, No. 5, Sept.-Oct. 1989, pp. 459-464.

Balazs, G.L. (1986): "Bond behaviour under repeated loads". In *Studi e Ricerche, 8,* pp. 395-430.

Barenblatt, G.J. (1962): "The mathematical theory of equilibrium crack in the brittle fracture". *Advance in Applied Mechanics,* Vol. 7, pp. 55-125.

Bathe, K. J. (1982): *Finite Element Procedures in Engineering Analysis,* Englewood Cliffs, Prentice-Hall.

124

Bazant, Z. P. & B.H. Oh (1983): "Crack Band Theory for Fracture of Concrete". *Materials and Structures, RILEM,* Vol. 16, No. 33, pp. 155-177.

Bazant, Z.P. and J.-C. Chern (1985): "Strain softening with creep and exponential algorithm". *J. Eng. Mech. Div., ASCE,* Vol. 111, No. 3, pp. 391-415.

Bazant, Z.P (1986): "Mechanics of distributed cracking". *Applied Mechanics Review, ASME,* Vol. 39, No. 5, pp. 675-705.

Bazant, Z.P. & R. Gettu (1989): "Determination of nonlinear fracture characteristic and its time dependency from size effect". In *Fracture Mechanics of Concrete and Rock. Recent developments*, Eds. S.P. Shah, E.E. Swarts and B. Barr, Elsevier Science Publishers, London/New York, 1989, pp. 549-565.

Bazant, Z.P. (1990): "Recent advances in failure localization and nonlocal models". In *Micromechanics of Failure of Quasi-brittle Materials,* eds. S.P. Shah, S.E. Swartz and M.L. Wang, Elsevier Applied Science, pp. 12-32.

Bazant, Z.P. (1991): "Size effects on fracture and localization: apercu of recent advances and their extension to simultaneous fatigue and rate-sensitivity". In *Fracture Processes in Concrete, Rock and Ceramics,* Proceedings of the International RILEM/ESIS Conference, eds. J.G.M. von Mier, J.G. Rots and A. Bakker. E & FN SPON.

Brameshuber, W. & H.K. Hilsdorf (1990): "Influence of ligament length and stress state on fracture energy of concrete". *Engineering Fracture Mechanics,* Vol. 35, No. 1/2/3, pp. 95-106.

Brühwiler, E. & F.H. Wittmann (1990): "Failure of dam concrete subjected to seismic loading conditions". *Engineering Fracture Mechanics,* Vol. 35, No. 1/2/3, pp. 565-571.

Carol, J. & J. Murcia (1989): "A model for the non-linear time-dependent behaviour of concrete in compression based on a Maxwell chain with exponential algorithm". *Materials and Structures, RILEM,* Vol. 22, pp. 176-184.

Carpinteri, A. (1989): "Fracture mechanics and post-peak structural behaviour of plain

and reinforced concrete". In *Fracture Toughness and Fracture Energy,* eds. Mihashi et al. A.A. Balkema, Rotterdam, pp. 13-28.

Castro-Montero, A., S.P. Shah & R.A. Miller (1990): "Strain field measurement in fracture process zone". *Journal of Engineering Mechanics,* Vol. 116, No. 11, Nov. 1990, pp. 2463-2483.

Chen, W.F. (1982): *Plasticity in Reinforced Concrete.* McGraw-Hill Book Company.

Cook, R.D. (1981): *Concepts and Applications of Finite element Analysis.* John Wiley & Sons.

Cornelissen, H.A.W. (1983): *Tensile creep properties of plain concrete.* Stevin Laboratory, University of Technology, Delft, the Netherlands.

Cornelissen, H.A.W. (1984): *Constant-amplitude tests on plain concrete in uniaxial tension and tension-compression.* Report 5-84-1, Stevin Laboratory, Delft, the Netherlands.

Cornelissen, H.A.W. & H.W. Reinhardt (1984): "Uniaxial tensile fatigue failure of concrete under constant-amplitude and programme loading". *Magazine of Concrete Research, Vol. 36, No. 129, pp. 216-226.*

Dahlblom, O. (1987): *Constitutive modelling and finite element analysis of concrete structures with regard to environmental influence.* Doctoral thesis TVSM-1004, Division of Structural Mechanics, University of Lund, Sweden.

De Borst, R. & P. Van de Berg (1986): "Analysis of creep and cracking in concrete members". In *Fourth RILEM International Symposium on Creep and Shrinkage of Concrete : Mathematical Modelling,* Ed. Z.P. Bazant, 1986, pp. 527-528.

Domone, P.L. (1974): "Uniaxial tensile creep and failure of concrete". *Magazine of Concrete Research,* Vol. 26, No. 88, pp.144-152.

Duda, H. & G. König (1991): "Rheological material model for the stress-crack width relation of concrete under monotonic and cyclic tension". *ACI Materials Journal,* May-June 1991, pp. 276-287.

Dugdale, D.S. (1960): "Yielding of steel sheets containing slits". *J. of Mech. Phys. Solids*, Vol. 8, pp. 100-104.

Elices, M. & J. Planas (1989): "Material models". In *Fracture Mechanics of Concrete Structures: From theory to application.* Ed. L. Elfgren, Chapman and Hall.

Evans, A.G., J.R. Clifton & E. Anderson (1976): "The fracture mechanics of mortars". *Cement and Concrete Research,* Vol. 6, pp. 538-548.

Griffith, A.A. (1921): "The phenomena of rupture and flow in solids". *Phil. Trans. Roy. Soc.,* series A221, pp. 163-198.

Gustafsson, P.J. (1985): *Fracture Mechanics Studies of Non-yielding Materials like Concrete: Modelling of Tensile Fracture and Applied Strength Analyses.* Report TVBM-1007, Doctoral thesis, Division of Building Materials, University of Lund, Sweden.

Gylltoft, K. (1983), *Fracture Mechanics Models for Fatigue in Concrete Structures.* Doctoral Thesis 1983:25D, Division of Structural Engineering, Luleå University of Technology, Sweden.

Hansen, E.A. (1990): "A visco-elastic fictitious crack model". In *Micromechanics of Failure of Quasi-brittle Materials,* eds. S.P. Shah, S.E. Swartz and M.L. Wang, Elsevier Applied Science, pp. 156-165.

Hansen, E.A. (1991): "Influence of sustained load on the fracture energy and the fracture zone of concrete". In *Fracture Processes in Concrete, Rock and Ceramics,* eds. J.G.M. von Mier , J.G. Rots & A. Bakker, 1991 RILEM, E & FN SPON, pp.825-838.

Hassanzadeh, M, A. Hillerborg & F.P. Zhou (1987): "Tests of Material Properties in Mixed Mode I and II". In *Fracture of Concrete and Rock,* Ed S. P. Shah and S. E. Swarts, pp. 353-358.

Hassanzadeh, M. (1990): "Determination of Fracture Zone Properties in Mixed Mode I and II". *Engineering Fracture Mechanics,* Vol. 35, No. 4/5, pp. 845-853, 1990.

Hellan, K. (1984): *Introduction to Fracture Mechanics.* McGraw-Hill Book Company.

Hillerborg, A., M. Modeer & P.E. Petersson (1976): "Analysis of Crack Formation and Crack Growth in Concrete by means of Fracture Mechanics and Finite Elements". *Cement and Concrete Research,* Vol. 6, pp. 773-782.

Hillerborg, A. (1986): *Compendium in Building Materials FK* (in Swedish). Division of Building Materials, University of Lund, Sweden.

Hillerborg, A. (1988): *Applications of Fracture Mechanics to Concrete.* Report TVBM-3030, Division of Building Materials, University of Lund, Sweden.

Hillerborg, A. (1989a): "Stability problems in fracture mechanics testing", In *Fracture Mechanics of Concrete and Rock. Recent developments.* Eds. S.P., Shah, E.E. Swarts and B. Barr, Elsevier Science Publishers, London/New York, 1989, pp. 369-378.

Hillerborg, A. (1989b): "The compression stress-strain curve for design of reinforced concrete beams". In *Fracture Mechanics: Application to Concrete, eds. V.C. Li and Z.P. Bazant.* SP-118, ACI, Detroit, pp. 281-294.

Hillerborg, A. (1991): "Reliance upon concrete tensile strength". In *Structural Concrete.* IABSE Colloquium, Stuttgart. pp. 589-604.

Hsu, T.R. & Z.H. Zhai (1984): "A finite element algorithm for creep crack growth". *Engineering Fracture Mechanics,* Vol. 20, No. 3, pp. 521-533.

Husak, A.D. & E.M. Krokosky (1971): "Static fatigue of hydrated cement concrete". *J. of the American Concrete Institute,* Vol. 68, pp. 263-271.

Illston, J.M. (1965): "The Creep of Concrete Under Uniaxial Tension", *Magazine of Concrete Research,* Vol. 17, No. 51, pp. 77-84.

Irwin, G.R. (1958): "Fracture". In *Encyclopedia of Physics,* Vol. 6, Spinger-Verlag, Berlin, pp. 551-590.

Janskowski, L.J. & D.J. Stys (1990): "Formation of the fracture process zone in concrete". *Engineering Fracture Mechanics,* Vol. 36, No. 2, pp. 245-253, 1990.

Jenq, Y.S. & S.P. Shah (1985a): "A fracture toughness criterion for concrete".

Engineering Fracture Mechanics, Vol. 21, No. 5, pp. 1055-1069, 1985.

Jenq, Y.S. & S.P. Shah (1985b), "Two-parameter fracture model for concrete". *Journal of Engineering Mechanics,* Vol. 111, No. 10, Oct. 1985, pp.1227-1241.

Kaplan, M.F. (1961): "Crack propagation and the fracture of concrete". *J. of the American Concrete Institute,* Vol. 58, pp. 591-609.

Karihaloo, B.L. & P. Nallathambi (1989a): "An improved effective crack model for the determination of fracture toughness of concrete". *Cement and Concrete Research,* Vol. 19, pp.603-610.

Karihaloo, B.L. & P. Nallathambi (1989b): "Fracture toughness of plain concrete from three-point bend specimens". *RILEM, Materials and Structures,* Vol. 22, pp. 185-193.

Karsan, I.D. & J.O. Jirsa (1969): "Behaviour of Concrete under compressive loadings". *J. of Structural Division, ASCE,* Vol. 95, No. ST12, Dec. 1969, pp. 2543-2563.

Kyokong, B., J.K. Frederick & J.B. Stephen (1986): "Fracture behaviour of adhesive joints in poplar". *Wood and Fiber Science,* Vol. 18, No. 4, pp.499-525.

Körmeling, H.A. (1986): *Strain Rate and Temperature Behaviour of Steel Fibre Concrete in Tension.* Doctoral Thesis, Delft University of Technology.

Li, V.C. & Z.P. Bazant (1989), *Fracture Mechanics: Application to Concrete,* SP-118, ACI, Detroit, 1989.

Liu, Z.G., S.E. Swartz, K.K. HU & Y.C. Kan (1989): "Time-dependent response and fracture of plain concrete beams". In *Fracture Mechanics of Concrete and Rock. Recent developments.* (eds. S.P., Shah, E.E. Swarts and B. Barr), Elsevier Science Publishers, London/New York, 1989, pp. 577-586.

Mindess S. (1984): "Rate of loading effects on the fracture of cementitious materials", In *Application of Fracture Mechanics to Cementitious Composites,* NATO-ARW Sept. 4-7 1984, Ed. S.P. Shah, Northwestern University, U.S.A., pp. 617-636.

Mindess, S. (1990): "Fracture process zone detection". In *Fracture Mechanics of Concrete: test method*. Draft of the report prepared by the RILEM Technical committee 89-FMT.

Mindess, S., J.S. Nadeau & J.M. Hay (1974): "Effects of different curing conditions on slow crack growth in cement paste". *Cement and Concrete Research*, Vol. 4, pp. 953-965.

Modeer, M. (1979): *A Fracture Mechanics Approach to Failure Analysis of Concrete Materials*. Report TVBM-1001, Doctoral Thesis, Division of Building Materials, University of Lund, Sweden.

Modeer, M. (1989): "Modelling of time-dependent behaviour". In *Fracture Mechanics of Concrete Structures: From theory to application*, ed. L. Elfgren, Chapman and Hall.

Nadeau, J.S., S. Mindess & J.M. Hav (1974): "Slow crack growth in cement paste". *Journal of the American Ceramic Society*, Vol. 57, pp. 51-54.

Nadeau, J.S., R. Bennett & E.R. Fuller (1982): "An explanation for the rate-of-loading and the duration-of-load effects in wood in terms of fracture mechanics". *Journal of Material Science*, Vol. 17, pp. 2831-2840.

Neville, A.M. (1970): *Creep of Concrete: Plain, reinforced, and Prestressed*. North-Holland Publishing Company-Amsterdam.

Nielsen, A. (1972): *Rheology of Building Materials*. Doctoral thesis, D6:1972. Svensk Byggtjänst, Stockholm, Sweden.

Nishibayashi, S. (1978): "Tensile creep of concrete". In *Proc. RILEM Coll. Creep of Concrete*, Leeds 1978, contribution No. 13.

Owen, D.R.J. & E. Hinton (1980): *Finite Element in Plasticity*. Pineridge Press Limited, Swansea, U.K.

Petersson, P.E. & P.J. Gustafsson (1980): "A model for calculation of crack growth in concrete-like materials". In *Numerical methods in Fracture Mechanics*, pp. 707-719. Pineridge Press, Swansen, U.K.

Petersson, P.E. (1981): *Crack Growth and Development of fracture Zones in Plain Concrete and Similar Materials.* Report TVBM-1006, Doctoral Thesis, Division of Building Materials, University of Lund, Sweden.

Raiss, M.E., J.W. Dougill & J.B. Newman (1990): "Development of fracture process zone in concrete". *Magazine of Concrete research,* Dec. 1990, Vol. 42, No. 153, pp. 193-202.

Ratanalert, S. & M. Wecharatana (1990): "Evaluation of existing fracture models in concrete". In *Fracture Mechanics: Application to Concrete, eds V.C. Li and Z.P. Bazant.* SP-118, ACI, Detroit, pp. 113-146.

Reinhardt, H.W. & H.W.A Cornelissen (1985): "Sustained tensile tests on concrete". *Baustoffe '85,* Bauverlag, Wiesbaden, pp. 162-167.

Reinhardt, H.W. (1990): "Loading rate, temperature, and humidity effects". In *Fracture Mechanics of Concrete: test method.* Draft of the report prepared by the RILEM Technical committee 89-FMT.

Rice, J.R. (1968): "Path independent integral and approximate analysis of strain concentration by notches and cracks". *J. of Applied Mechanics, Transactions, ASME,* Vol. 35, pp. 379-386.

Rolfe, S.T. & J.M. Barsom (1977): *Fracture and Fatigue Control in Structures, application of fracture mechanics.* Prentice-Hall, Inc., EnglewoodCliffs, New Jersey.

Rossi, P. (1991): "A physical phenomenon which can explain the mechanical behaviour of concrete under high strain rates". *RILEM, Materiaux et Constructions,* Vol. 24, pp. 422-424.

Rossi, P. & C. Boulay (1990): "Influence of free water in concrete on the cracking process". *Magazine of Concrete research,* Sept. 1990, Vol. 42, No. 152, pp. 143-146.

Shah, S.P. & S. Chandra (1970): "Fracture of concrete subjected to cyclic and sustained loading". *J. of the American Concrete Institute,* Vol. 67, pp. 816-825.

Shkoukan, H.T. (1989): "Behaviour of concrete under concentric and eccentric sustained tensile loading". In *Annual Journal on Concrete and Concrete Structures,* Darmstadt Concrete, Vol. 4, pp. 223-234.

Shkoukan, H.T. & J. Walraven (1991): "Sustained tensile strength of concrete". In *Structural Concrete.* IABSE Colloquium, Stuttgart. pp. 725-729.

Sluys, L.J. & R. De Borst (1991): "Rate-dependent modelling of concrete fracture". Heron, Vol. 36, No.2, pp. 3-15.

Tait, R.B. & G.C. Garrett (1986): "A fracture mechanics evaluation of static and fatigue crack growth in cement mortar". In *Fracture Toughness and Fracture Energy of Concrete.* Ed. by F.H. Wittmann, Elsevier Science Publishers B.V., Amsterdam. **Thelandersson, S.** (1987): *Notes on Linear Viscoelasticity.* Report TVSM-3009, Division of Structural Mechanics, University of Lund, Sweden.

Vinkeloe, R. (1962): "Prufverfahren Zurermittlung des Dynamischen Elastizitätsmodulus von Betonprismen", *Tonindustrie Zeitun,* Vol. 86, pp. 272-276.

Von Mier, J.G.M. (1990): "Internal crack detection in single edge notched concrete plates subjected to uniform boundary displacement". In *Micromechanics of Failure of Quasi-brittle Materials,* eds. S.P. Shah, S.E. Swartz and M.L. Wang, Elsevier Applied Science, pp. 33-42.

Von Mier, J.G.M. & E. Schlangen (1989): "On the stability of softening systems". In *Fracture Mechanics of Concrete and Rock. Recent developments, e*ds. S.P., Shah, E.E. Swarts & B. Barr, Elsevier Science Publishers, London/New York, 1989, pp. 387-396.

Wittmann, F.H. (1984): "Influence of time on crack formation and failure of concrete". In *Application of Fracture Mechanics to Cementitious Composites,* NATO-ARW Sept. 4-7 1984, Ed. S.P. Shah, Northwestern University, U.*S.A., pp. 593-615.*

Wittmann, F.H., P.E. Roelfstra, H. Mihashi, Yiun-yuang Huang, Xinhua Zhang & N. Nomura (1987), "Influence of age of loading, water-cement ratio and rate of loading on fracture energy of concrete". *RILEM, Materials and Structures,* 1987, Vol. 20, pp. 103-110.

Zhou, F.P. (1988): *Some Aspects of Tensile Fracture Behaviour and Structural Response of Cementitious Materials.* Report TVBM-1008, Licentiate Thesis, Div. of Building Materials, University of Lund, Sweden.

Zhou, F.P. (1990): "Analysis of time-dependent fracture in concrete". In *Nordic Concrete Research,* Trondheim 1990, pp. 262-263.

Zhou, F.P. (1992): "Numerical modelling of creep fracture in concrete". Prelimary accepted for presentation in the second international conference on Computer Aided Asseeement and Control: Localized Damage, 1-3 July 1992, Southampton, UK.

Zhou, F.P. & A. Hillerborg (1992): "Time-dependent crack growth and failure in concrete: testing and modelling". Accepted for presentation in the international conference on Fracture Mechanics of Concrete structures, 2-5 June 1992, Breckenridge, USA.

Time-dependent Crack Growth

and Fracture in Concrete

Fan Ping Zhou

Doctoral Thesis, Report TVBM-1011

Lund, Sweden, 1992